

X-RAY DIFFRACTION AND ESR STUDIES ON
AMORPHOUS MELANIN

A Thesis

Presented to

the Department of Physics

University of Houston

In Partial Fulfillment

of the Requirements for the Degree

Doctor of Philosophy in Physics

by

Shiu-Shin Chio

June 1977

X-RAY DIFFRACTION AND ESR STUDIES ON
AMORPHOUS MELANIN

An Abstract of a Thesis
Presented to
The Department of Physics
University of Houston

In Partial Fulfillment
of the Requirements for the Degree
Doctor of Philosophy in Physics

by
Shiu-Shin Chio

June 1977

I. Abstract

By using X-ray diffraction and ESR (electron spin resonance) techniques, some physical properties of synthetic melanin, such as intrinsic local atomic structure, structure of adsorbed water and stable free radical content and the influence of water on these free radicals, were studied in detail. Using the corrected X-ray intensities of wet and dry samples, the difference intensity (wet-dry), which refers to the structure of the adsorbed water, appears roughly similar to bulk liquid water for the part that can be desorbed at 100°C. The remaining, or more tightly bound water, which comes off at 150°C and higher, seems similar to amorphous ice. Both $\text{Cu}_{\text{K}\alpha}$ and $\text{Ag}_{\text{K}\alpha}$ radiations were used to obtain the intensity data of a 150°C dried melanin sample. A model study of the intrinsic local atomic structure of dry melanin suggests a 'best' or most possible structure model, which has its $i(K)$, the interference function, fit most successfully to the measured $i(K)$ over the entire range from $K = 1.5 \text{ \AA}^{-1}$ to $K = 19 \text{ \AA}^{-1}$. This model fit consisted of an array of planar connected monomers of from 4-8 members per layer with three layers stacked at about the graphite spacing of 3.4 \AA and included some disorder of layer orientations, such as rotations and shifting

with respect to each other, and also a (maximum) 0.02\AA random tilting of the oxygen and nitrogen side atoms. This supergroup or 'paracrystalline' array is then assumed to represent a well-correlated piece of the fully connected 3-D melanin polymer.

The ESR study shows a spin density and ESR line-width which increase with heating and pumping, and decrease with readsorbing water in a somewhat reversible fashion. Heating at 150°C and higher which drives out the small amount of more tightly bound water, caused the major increase of the ESR signal. Readsorption of water can not quench the entire ESR signal, but rather causes the signal to decrease slowly and to approach its original equilibrium value. The reversible part of the ESR signal, the difference ESR intensity of (dry-wet), was found to be quenched by water in a manner resembling a 2nd order rate process. The temperature dependence of the ESR intensities of both dry and wet samples shows that the paramagnetism follows the Curie Law with the dry sample having a greater slope. Changes of relaxation time due to water were relatively small.

Considering the information we have obtained here, it seems that melanin is a random polymer composed of stacked-layer groups, has a relative large granule size, with trapped free radicals and bound water. The bound water that diffuses

(or penetrates) into part (but not all) of the melanin granule induces free radicals to 'pair off' within that region. This 'macroscopic' melanin model which describes the free radical properties and also the influence of water on these radicals is expected to be associated with the biological functions of melanin.

II. Acknowledgements

I would like to thank my thesis advisors, Professor S. C. Moss and Professor M. Eisner for their support and guidance throughout the course of this work. In addition I would like to thank the following people: Dr. J. E. McGinness of the University of Texas System Cancer Center for supplying the L-dopa melanin samples; Dr. W. W. Wendlandt for allowing me to use his DSC and TG analyzers, and also his post-doctoral assistant and student for their help in the operation of the equipment; Dr. L. Y. Lee for providing the sample presser and for many useful suggestions on electronic techniques; Dr. T. H. Metzger for discussions on X-ray data analysis; and the machine shop workers for their assistance in setting up the X-ray equipment.

Thanks also go to those of my good friends: Dr. J. H. Chang, organic chemisist, Dr. W. L. Jeng, oceanographic biologist, and Dr. M. H. Hung, MD, for many valuable discussions on the melanin chemistry and biology; Mr. C. C. Hsu for his kind help on the IR measurements; and Mr. C. Y. Chai for his early help on my beginning laboratory experiments.

Support for this entire program came from the Robert A. Welch Foundation at the University of Houston. I gratefully acknowledge and thank the Welch Foundation not only for research support but for my own fellowship in graduate school.

Most of all, I do not have sufficient words to thank my wife, Pung-Ying, for her consistent understanding, support and concern, and also my parents for their love and for taking care of our daughter during this most difficult period of our life.

III. Table of Contents

	<u>Page</u>
I. Abstract	4
II. Acknowledgements	7
III. Table of Contents	9
IV. List of Figures	11
V. List of Tables	14
CHAPTER ONE Introduction	15
CHAPTER TWO Survey of the Literature on Melanin	18
CHAPTER THREE X-ray Diffraction Study	27
1. Introduction	27
2. Analysis of the X-ray diffraction data from amorphous materials	28
3. Experiments	31
4. Data analysis and results	38
5. Discussion	58
6. Summary and conclusions	64
CHAPTER FOUR Model Calculation Study	66
1. Introduction	66
2. Methods	67
3. Results	71
4. Discussion	85
5. Summary and conclusions	88

	<u>Page</u>
CHAPTER FIVE Electron Spin Resonance Study	90
1. Introduction	90
2. Materials and Methods	91
3. ESR studies of Wet and Dry Melanins	95
4. Dependence of ESR signal on amount of water in sample	104
5. Temperature dependence of ESR signal	106
6. Kinetics of water readsorption process	109
7. Summary of results	113
8. Macro-structure model of a melanin granule	114
CHAPTER SIX Conclusion	119
References	121
Appendix A	124
Appendix B	125

IV. List of Figures

Figure	<u>Page</u>
1. The Raper-Mason Pathway of Melanin Synthesis .	20
2. Modified Raper-Mason Pathway	21
3. Geometry of the X-ray diffraction and the block diagram of the detecting system	34
4. Bent and Ground Monochromator for Cu _{Kα} radiation	35
5. The Focusing geometry for a vertically bent monochromator	36
6. X-ray diffraction pattern (uncorrected) of L-dopa melanin	41
7. Ag-radiation data and the overall correction .	46
8.(a-b) Finally corrected Cu- and Ag-radiation data	47
9. X-ray diffraction data of the L-dopa melanin sample	50
10.(a-b) i(k) of Cu- and Ag-data	51
11. i(k) of L-dopa melanin	53
12. X-ray diffraction patterns of wet and dry samples	55
13.(a-b) Difference intensities and percentage errors .	56
14. Comparison of the difference intensity (original-100°C) to the intensity of liquid water	61
15. Comparison of the Difference intensity (100°C-150°C) to the intensity of amorphous solid water	62

Figure	<u>Page</u>
16.	Comparison of the difference intensity (wetted-150° C) to the intensities of liquid water and amorphous ice 63
17.a	Melanin monomers 68
17.b	Picture of the constructed 8-monomer layer model 70
18.	Calculated $i(k)$ of parallel stacking of one-monomer layers in same orientation 72
19.(a-e)	Calculated $i(k)$ of three one-monomer layers with disorders 74
20.	Calculated $i(k)$ of single planar layer models 79
21.	$i(k)$ of three 8-monomer layers stacked 80
22.	$i(k)$ of three 4-monomer layers stacked with tilting disorder 82
23.	Effect of randomly tilting side atoms on the calculated $i(k)$ 83
24.(a-b)	Comparison of measured $i(k)$ to our 'best' model 84;86
25.(a-b)	Effect of heating on the weight and ESR signals 98
26.	Dependence of ESR signal and weight loss on heating temperature 105
27.	Temperature dependence of ESR 108
28.	Decay of ESR signal as a function of time 111
29.	ESR difference intensity (Dry-Wet) vs. time . 112
30.	Macro-structure model of a melanin granule . . 115
B-1	Test of the inhomogeneous broadening of melanin ESR signals 129

Figure	<u>Page</u>
B-2	Inhomogeneous saturation curve for L-dopa melanin 132

V. List of Tables

	<u>Page</u>
I. Densities and Thickness of X-ray Diffraction Samples.	33
II. x in the $(C_8NHO_2) \cdot xH_2O$ of melanin samples. . . .	40
III. Line widths, T_1 and spin densities of wet and dry melanins.	101

CHAPTER ONE

INTRODUCTION

Melanins usually refer to those black or brown organic substances, pigments, normally found in living objects as in hair, skin, eyes, seeds, in the brain or liver and in tumors, as well as synthesized from the oxidation of phenolic compounds, such as DOPA (dihydroxyphenylalanine), catechol, 5,6-dihydroxyindole, and so forth. The black color of melanin indicates strong light absorption which is perhaps the only obvious function of melanins in biological systems. However the functions of melanins in the liver and the brain as well as the presence of them in tumors are still not understood. Chemical analysis has been found especially difficult because of the insolubility of melanin and only some possible pathways and monomer types have been identified. The general amorphous and free radical properties have been known for some time. A variety of physical studies have shown that both natural and synthetic melanins have similar features in IR, ESR spectra and in the X-ray diffraction patterns. However unambiguous structural information is still hard to obtain because of their insolubility, strong light absorption, noncrystallization and ease of moisture uptake.

It is well known that melanins in the ambient state, equilibrated with the atmosphere, contain a high percentage of water. In our saturated diethyl-amine melanin sample, for example, the water content amounted to as much as 50 percent of its dry weight. Studies of the influences of water on the physical properties in melanin are as important as in other biological materials. Studying the influence of water on the semiconductivity in melanin, Powell and Rosenberg^{(1) (2)}, and also McGinness⁽³⁾ reported that the conductivity of melanin increases exponentially with the increase of water content and tends to saturate when the water content is high. By using the non-contact u.h.f. (ultra high frequency) method Trukhan⁽⁴⁾ found the photo-conductivity of melanin also rises exponentially with increase of water content. In the ESR study of Blois et. al.⁽⁵⁾, they reported the influence of water on the ESR signal of melanin, but no further work was done in their experiment because of the difficulty in controlling water content. Studying the structure of melanin by X-ray diffraction, Thathachari^{(6) (7) (8)} found that amorphous melanin contains a random stacking of the planar monomers. But the contribution of the scattering intensity from the adsorbed water was neglected, as was the lateral extent of the structure.

In this work we concentrate our studies especially on the influence of water on the free radical and structural properties of melanin. The intrinsic, dry melanin, structure was also studied in detail.

This thesis includes two major experiments, X-ray diffraction and ESR. Chapter two presents a selected literature survey on melanin. The X-ray diffraction experiment and model study of the local atomic structure are given in Chapter three and four respectively. ESR studies are given in Chapter five. Chapter six presents a summary of our conclusions.

CHAPTER TWO

SURVEY OF THE LITERATURE ON MELANIN

Melanins ($\mu\acute{\epsilon}\lambda\alpha\rho$ = black), the brown or black biological pigmentation, are quite widespread in the animal and vegetable kingdoms. Nicolaus⁽⁹⁾ first tried to classify them into eumelanins ($\epsilon\acute{\nu}$ = good), paeomelanins ($\varphi\alpha$; $\acute{\omicron}\rho$ = dusky) and allomelanins ($\alpha\lambda\lambda\omicron\rho$ = other) according to their original sources and colors. For example, the eumelanins and phaeomelanins are found in the animal kingdom, phaeomelanins referring to those pigments whose color varies from brown to yellow and eumelanins referring to black pigments. The allomelanins occur in plants such as mushrooms and single organisms such as bacteria. Some related synthetic pigments are known, for example as tyrosine-melanin, dopa-melanin, 5,6-dihydroxindole-melanin, catechol-melanin, etc., are named in accord with their starting materials.

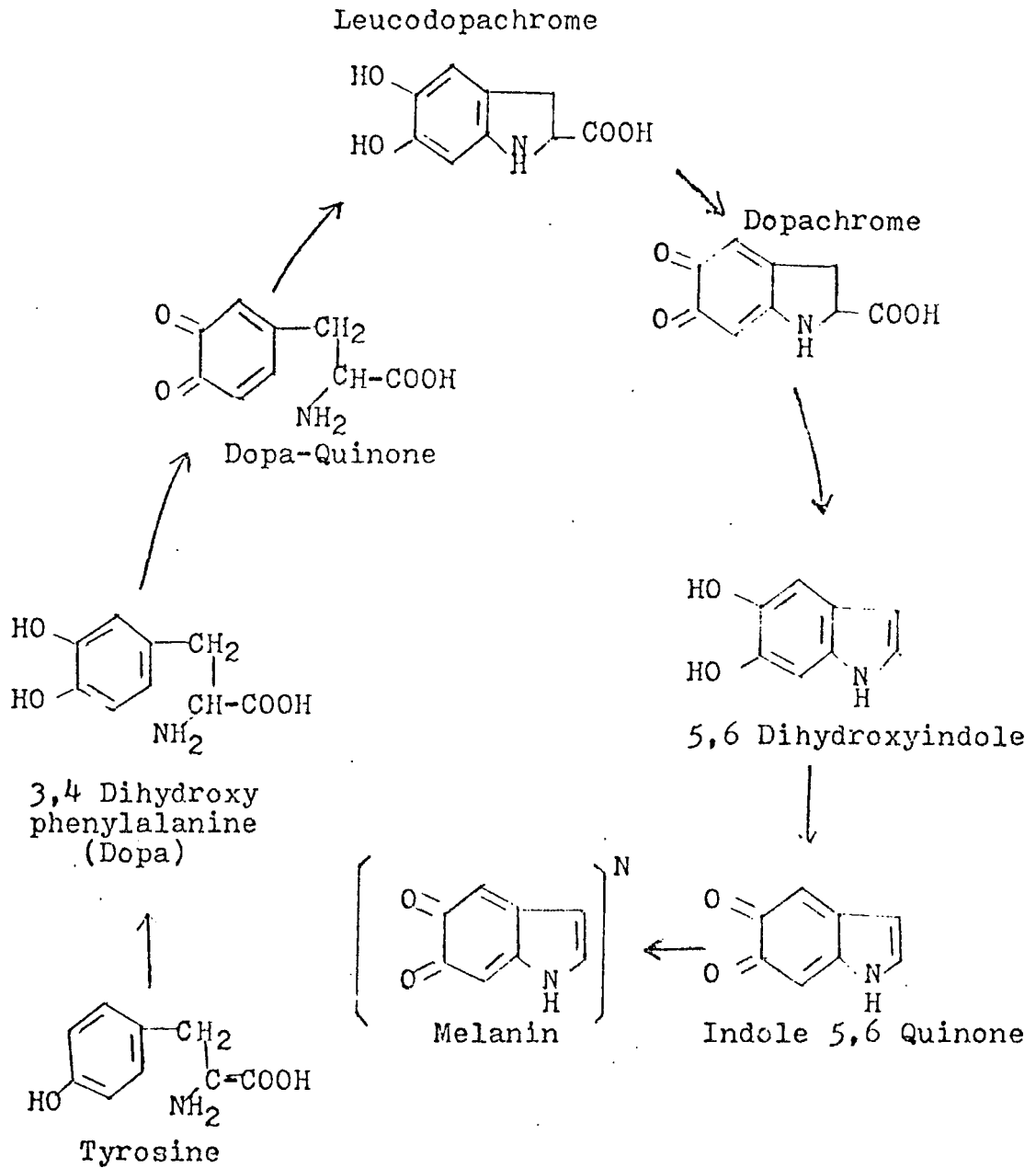
In general, these black pigments are considered to be insoluble amorphous bio-polymers, of high molecular weight, formed by oxidation of phenolic compounds. Because of their chemical insolubility and noncrystalline nature, melanins are difficult to study and the period from 1856 to 1930 is characterized by Nicolaus as the first period in the development of melanin chemistry - a period of frustration, in the attempt to identify the possible precursors and enzyme

systems that were capable of causing the oxidative polymerization. This period terminated with Raper's fundamental work⁽¹⁰⁾⁻⁽¹⁴⁾ on the identification of the compounds of melanin formation. On the basis of the findings of Raper and the spectrophotometric measurements, Mason⁽¹⁵⁾⁽¹⁶⁾ then proposed the scheme presented in Fig. 1 to describe the possible pathway of melanin synthesis. This is known as the Raper-Mason scheme of melanogenesis which has many supporters. The Raper-Mason scheme was further modified by Blois⁽¹⁷⁾ to include semiquinone free radical intermediates, which were found by Wertz et. al.⁽¹⁸⁾. Who identified at least five kinds of semiquinones in their ESR study on the alkaline oxidation of dopa and the multiplicity of reaction pathways. Fig. 2 shows this modified scheme.

In the second period - a period of uncertainty, which is where we are now according to Nicolaus, more modern experimental techniques have been applied to study both physical and chemical properties of melanins. Attempts have been made to correlate these later results with biological mechanisms. The developments of this period will be described below.

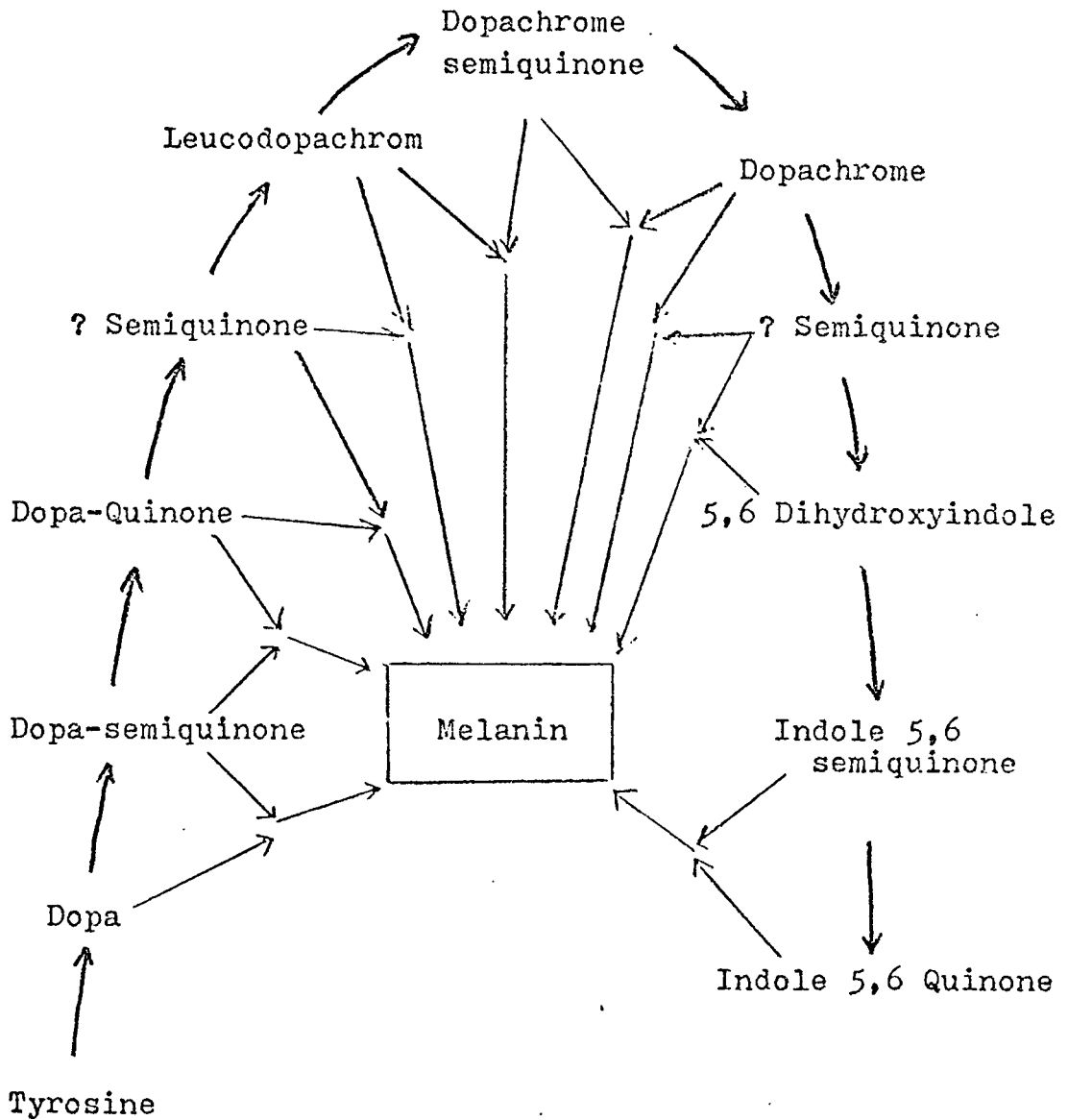
The free radical property of natural melanins was first reported by Commoner et. al.⁽¹⁹⁾ using an ESR technique. They showed that the free radicals in melanin polymers were

Fig. 1



(Fig. 1) The Raper-Mason pathway of melanin synthesis

Fig. 2



(Fig. 2) The Raper-Mason pathway modified to show the probable semiquinone free radical intermediates and the multiplicity of reaction pathways.

generated during ring condensation and became trapped and stabilized in the polymer lattice. Later, Mason et al.⁽²⁰⁾ determined the ESR property of some other melanins, such as 3,4-dihydroxyphenylalanine, sepia ink, human hair etc., and they also noted that the ESR signal increases after exposure to ultra-violet light. They then proposed that melanin might act, in some organisms, as a biological electron exchange polymer. At the same time, Longuet-Higgins⁽²¹⁾ suggested a one-dimensional semiconductor model in order to explain the paramagnetism of melanin. This was later shown incorrect by Blois et. al.⁽¹⁷⁾ because the temperature dependent paramagnetism of melanin followed the Curie law. In the earlier paper⁽⁵⁾, more detailed studies and further discussion on the ESR absorption lines, g-values, relaxation times, spin density, temperature dependence and the effect of Cu^{++} ions were reported. The fact that the ESR signal is quenched by paramagnetic ions, such as Cu^{++} , Zn^{++} , Ni^{++} , etc., was recently shown by Sarna et. al.⁽²²⁾ to be an effect of magnetic coupling of two interacting spins of different kinds⁽²³⁾, ion and melanin, rather than a chemical interaction of the type assumed by Blois et. al. The influence of moisture on the ESR signal of melanin was also mentioned in Blois' paper, and was assumed simply to be due

to the variation of relaxation times. No further work has been done presumably because of the variability in the moisture control in their experiments. (Our earlier study on this moisture dependent ESR signal showed that the effect of hydration in melanin was somewhat reversible⁽²⁴⁾.)

Studying the effects of pH on the ESR at Q band (35 GHz), Grady et. al.⁽²⁵⁾ found changes in the ESR spectra with pH in which the g-value shift was assumed to be due to the increase of unpaired electron density on oxygen, while the g-value anisotropy was attributed to the delocalization of electrons over the heterocyclic nitrogen atoms.

The optical and infrared absorption spectra of melanins were also reported by Blois et. al.⁽⁵⁾ to be quite different from those of charcoal and graphite. However similarities were found among all melanins, natural and synthetic. As for the electrical transport properties of melanin, the dc resistivity was reported to be in the range of 5×10^{10} Ohm-cm by Potts et. al.⁽²⁶⁾, while by Thathachari, a value of about 4.4×10^6 Ohm-cm at 100 volts was obtained. According to McGinness' recent measurements on an L-dopa melanin sample⁽³⁾, the resistivity drops in a nearly exponential way from about 10^{12} Ohm-cm down to 10^5 when the water content in the sample increases to about 15 percent of its dry weight and then saturates while more water is absorbed. The differences

between Potts et. al. and Thathachari may therefore be due to joule heating of the Potts' sample with consequent loss of moisture. This hydration dependent resistivity was earlier reported by Powell and Rosenberg⁽²⁾ in their studies of the semi-conductivities of melanin, proteins and nucleic acids. By doing a solid state electrolysis measurement, they concluded that melanin is a 'mixed' semiconductor with protonic to electronic ratio of 65 : 35 which does not change over a hydration range of 10 to 35 percent. This ratio 65 : 35 cannot, of course, explain the enormous change of 10^7 ⁽³⁾ that occurs on drying (removing protons). A dc electrical field induced breakdown, switching, in the melanin with lower resistivity, wet state, was reported by McGinness et. al.⁽²⁷⁾ Further study on the switching phenomenon was reported by Culp et. al.⁽²⁸⁾ in which, again, adsorbed water may play an important role as the switching takes place due to joule heating in the switched region. Results of the photo-conductivity measurements on the hydrated and dehydrated melanin samples were reported by Trukhan et. al.⁽⁴⁾

The first report of the X-ray diffraction patterns of melanin samples was given by Spiegel-Adolf and Henny⁽²⁹⁾ in 1939. They studied and compared the diffuse rings on film recorded diffraction patterns of natural and synthetic melanins such as sepia and human tumor melanins on the one

hand and tyrosine, phenylalanine and tryptophan melanins on the other. More detailed studies on this diffuse X-ray diffraction pattern using modern X-ray equipment have been done by Thathachari et. al.⁽⁶⁾ They carefully studied the presence, shape and position of the first major diffuse peak of the melanin diffraction pattern. They pointed out that the planar monomeric melanin units, such as catechol and indole quinone, have a strong tendency to form a random stacking, similar to that in disordered carbon samples⁽³⁰⁾, which could give rise to the shape and position of this diffuse peak. Fitting the remainder of the diffraction pattern was less successful.

Chemical studies of the structure of melanins by degradative methods and chromatographic analysis⁽³¹⁾⁻⁽³³⁾ as well as by an isotopic tracer method⁽³⁴⁾, suggested that melanins are not homopolymers of indole quinone only, but are co-polymers of considerable complexity with several types of bonds being involved such as -C-C-C-, -C-O-C-, -C-O-O-C-, etc. As shown in Fig. 1, all essential 'indole' type units, such as indole-5,6-quinone, 5,6-dihydroxyindole, dopachrome, leucodopachrome and 5,6-nihydroxyindole-2-carboxylic acid, and even dopa may constitute the co-polymer.

"We are now still in the second period" said Nicolaus, "but we hope that the ever increasing interest in the

biological and physico-chemical properties of melanins will lead us into the third period - a period of elucidation - very soon."

CHAPTER THREE

X-RAY DIFFRACTION STUDY

1. Introduction

In this experiment, both $\text{Cu}_{K\alpha}$ and $\text{Ag}_{K\alpha}$ radiations were used to obtain the diffraction patterns of melanin samples. In order to have better focussing, monochromators of the horizontally and vertically bent types were designed and made for the Cu and Ag radiations, respectively. An automatic recording system with step-scanning, counting and printing was set up to increase the accuracy.

Since melanins always contain water when prepared, samples in wet and dry states were both considered and examined by X-rays. The difference between the corrected dry and wet intensities was taken and compared to the intensities of liquid and amorphous (solid) water. The intensity of a dry melanin sample was assumed to relate to the intrinsic structure of the melanin. Further analysis was done on this intrinsic intensity data to get the intrinsic curve of $i(k)$, the interference function of melanin. The procedures of the data analysis that include the corrections and normalization leading to the final results of the $i(k)$ are given and discussed in this chapter.

2. Analysis of the X-ray diffraction data from amorphous materials

As described in the Warren's book⁽³⁵⁾, the coherent scattering intensity expressed in electron units, I_{eu} , from any array of atoms, the scattering centers, is related to the distribution of these atoms by the following double sum:

$$I_{eu} = \sum_m \sum_n f_m f_n e^{(2\pi i/\lambda)(\vec{s} - \vec{s}_0) \cdot \vec{r}_{mn}}$$

where

f_i = scattering factor of atom i .

\vec{s} , \vec{s}_0 = scattering vectors of diffracted and incident beams respectively.

\vec{r}_{mn} = position vector of atom m relative to atom n .

By considering this array of atoms as a rigid body taking with equal probability all orientations in space, the average unmodified intensity is then given as

$$I_{eu} = \sum_m \sum_n f_m f_n \frac{\sin k r_{mn}}{k r_{mn}}$$

where, $k = 4\pi \sin \theta / \lambda$, 2θ is the scattering angle between \vec{s} and \vec{s}_0 . This equation is often called the Debye scattering equation.

For scattering from a real amorphous (or liquid) sample, a general treatment is usually applied by introducing a density function $\rho_m(r_{nm})$, such that $\rho_m(r_{nm}) dV_n$ is the number

of atom centers in the volume element dV_n at the position r_{nm} relative to atom m , and by neglecting the small angle intensity contribution to give the usual amorphous scattering expression.

If only one kind of atom is present then spherical averaging allows the expression to reduce to the usual form as:

$$i(k) = \frac{I_{eu}/N - f^2}{f^2} = \int_0^{\infty} 4\pi r^2 [\rho(r) - \rho_a] \frac{\sin kr}{kr} dr$$

or

$$k i(k) = 4\pi \int_0^{\infty} r [\rho(r) - \rho_a] \sin kr dr$$

where, $i(k)$ = the reduced intensity, is usually known as the interference function.

$\rho(r) = \langle \rho_m(r_{nm}) \rangle$, the average is over all $\rho_m(r)$ within the sample that are at a displacement r from an atom.

I'_{eu}/N = intensity per atom with the small angle term omitted.

For a system with more than one kind of atom, although an exact method that leads to the pair distribution solution has been developed by Finbak and reported by Warren⁽³⁵⁾, in the

case of melanin, an approximate method is more convenient and suitable to analyse the diffraction data. This method involves defining:

$\sum_{uc} f_m, \sum_{uc} Z_m$ = sum of the scattering factors and atomic number over the atoms within a convenient unit of composition, uc.

$K_m = f_m/f_e$, the effective electron numbers.

$f_e = (\sum_{uc} f_m)/(\sum_{uc} Z_m)$, the average scattering factor per electron.

N_{uc} = number of uc in the sample.

The equivalent Fourier expression becomes

$$i(k) = \frac{I_{eu}/N_{uc} - \sum_{uc} f_m^2}{f_e^2} = \int_0^{\infty} 4\pi r^2 \sum_{uc} K_m [\rho_m(r) - \rho_e] \frac{\sin kr}{kr} dr$$

or

$$k i(k) = 4\pi \int_0^{\infty} \sum_{uc} K_m [\rho_m(r) - \rho_e] \frac{\sin kr}{kr} dr$$

where $\rho_e = \frac{N_{uc}}{V} \sum_{uc} Z_m$, the average electron density. By

inverting the Fourier integral, one may obtain the reduced radial distribution function (RDF), $G(r)$:

$$G(r) = 4\pi \sum_{uc} K_m r [\rho_m(r) - \rho_e] = \int_0^{\infty} k i(k) \sin kr dr$$

Since I'_{eu} can be obtained both from experiment by correcting the measured intensity for such effects as absorption, polarization, Compton and multiple scattering, etc., as well as from the numerical calculation of a known model using the Debye scattering equation. The correcting details will be given in the following section. It is then possible to study the atomic structure of the amorphous material by comparing either $i(k)$ or $G(r)$ for the measured and calculated values.

3. Experiments

(1) Samples: Two kinds of synthetic melanins were studied: the tyrosine melanin purchased from the Sigma Chemical Company and the auto-oxidative L-dopa melanin (with about .25% diethyl-amine impurity) supplied by the University of Texas System Cancer Center. About one gram of original powdered melanin was pressed, by a hydrolic presser, up to about 20000 lbs pressure for about three hours. A final cylindrically shaped sample of one inch diameter was obtained for this X-ray diffraction study. The thicknesses and the densities of our L-dopa and tyrosine samples are given in Table I. After examination by X-rays, these original samples were heated in rough vacuum for about four hours at 100°C (tyrosine) and 150°C (L-dopa). The dry samples were again weighted and examined by X-rays. The tyrosine sample was

further heated at 150°C in rough vacuum for 4 hours and examined by X-rays. Measured densities of these dry samples are also given in Table I. The dry (150°C) tyrosine sample was observed partially to recover its weight while left in air for about one day. This recovered density was measured to be 1.28 g/c.c., and the sample was also examined by X-rays for investigation into the nature of the recovered water.

(2) Equipment: Fig. 3 shows the geometry of the X-ray diffraction and also the block diagram of the detecting systems used in this measurement. The diffractometer and the X-ray housing were designed to be movable on a metal table in order to meet the requirement of using both $\text{Cu}_{k\alpha}$ and $\text{Ag}_{k\alpha}$ radiations. A hot air blower was used to keep the dry sample dry but was not used for wet samples.

In order to get more intensities for the $\text{Cu}_{k\alpha}$ and $\text{Ag}_{k\alpha}$ radiations, two types of monochromator were used. For the Cu case, horizontal monochromator was made. A 1" x 1" LiF single crystal with (200) surface was cut and polished to have thickness of 16 mil, then was bent, at about 1100°F, and ground, at room temperature, to give the final feature as shown in Fig. 4^{(36) (37)}. For the Ag radiation, a LiF crystal singly bent in the vertical direction, of thickness 8 mil was made according to the method described by Chipman⁽³⁸⁾ and Warren⁽³⁹⁾. Fig 5 shows the focussing geometry of such a vertically bent monochromator.

Table I

Densities and Thicknesses of X-ray Diffraction Samples

Sample	Thickness		Density (g/c.c.)	
	(cm)	original	100° dry	150° dry
L-dopa	.13	1.29	---	1.12
Tyrosine	.16	1.58	1.36	1.19

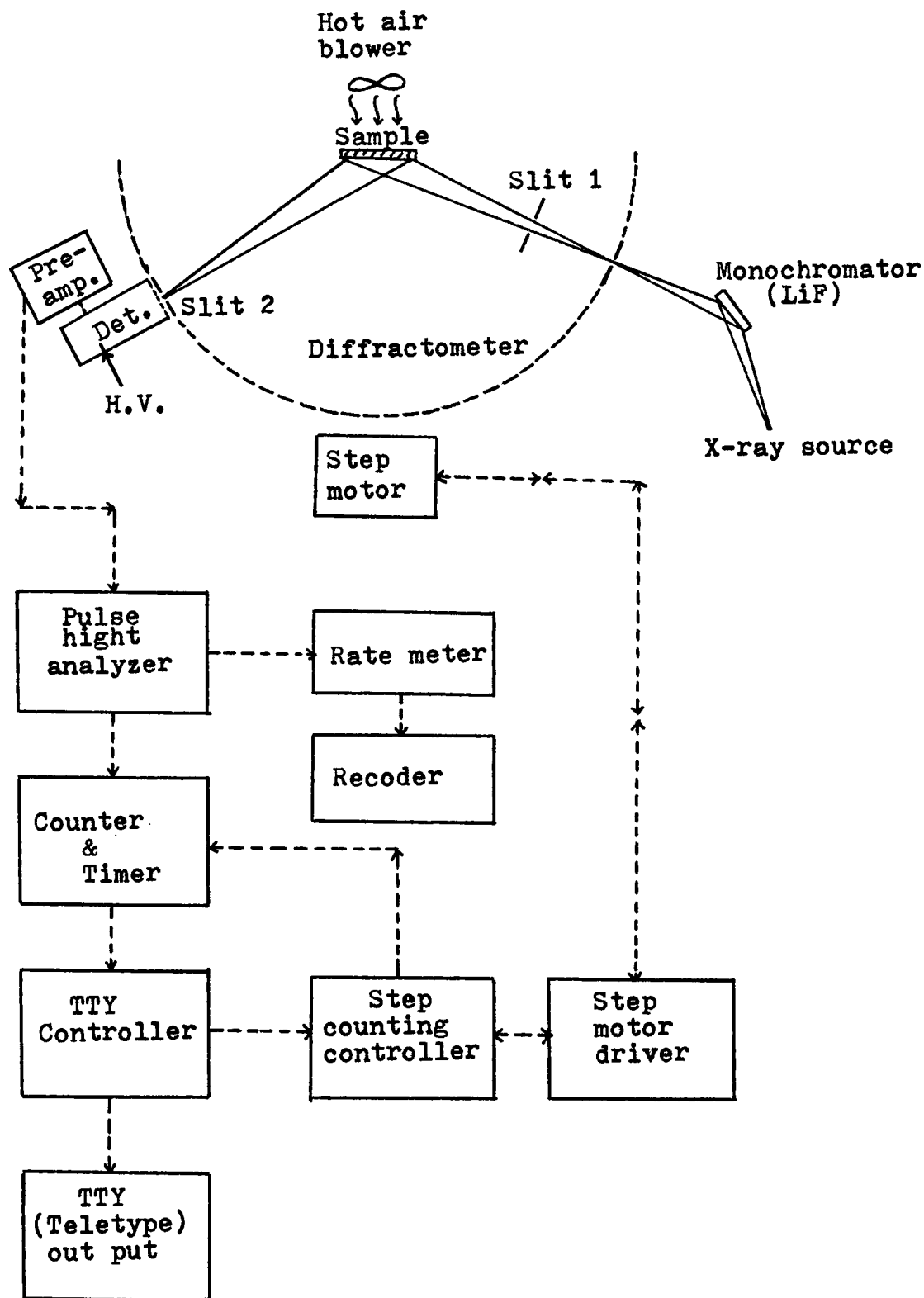


(Fig. 3) Geometry of the X-ray diffraction and the block diagram of the detecting system.

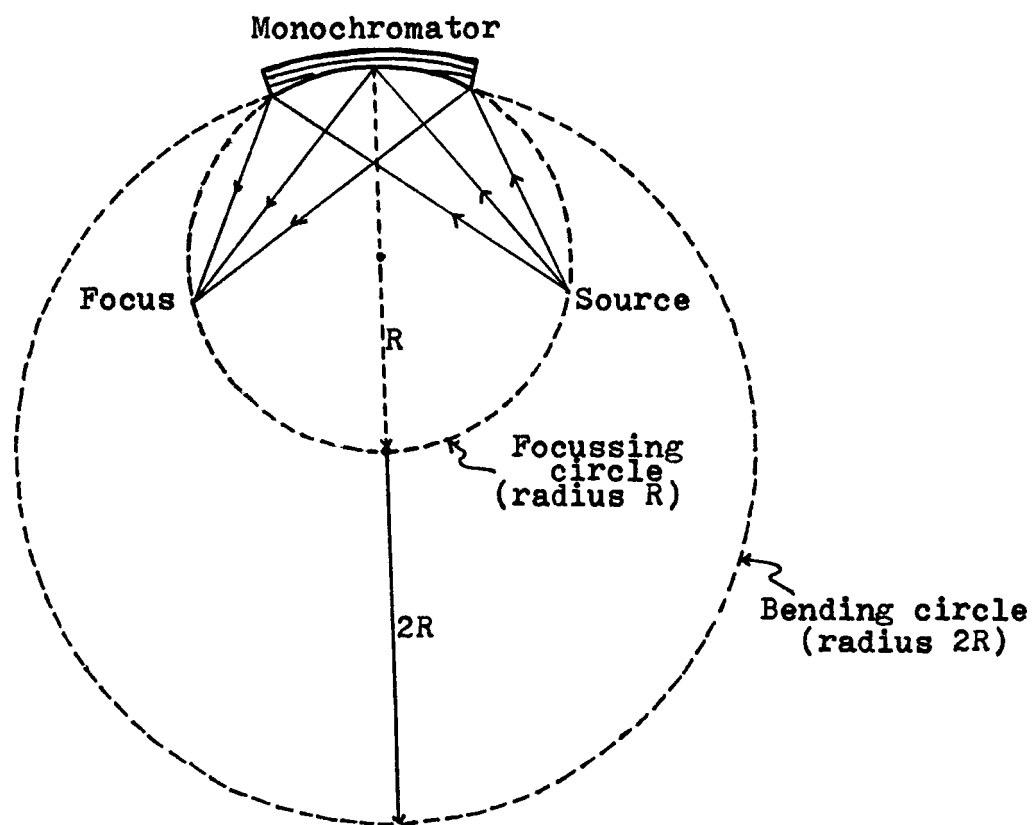


(Fig. 4) Bent and ground monochromator
(For $\text{Cu}_{K\alpha}$ radiation)

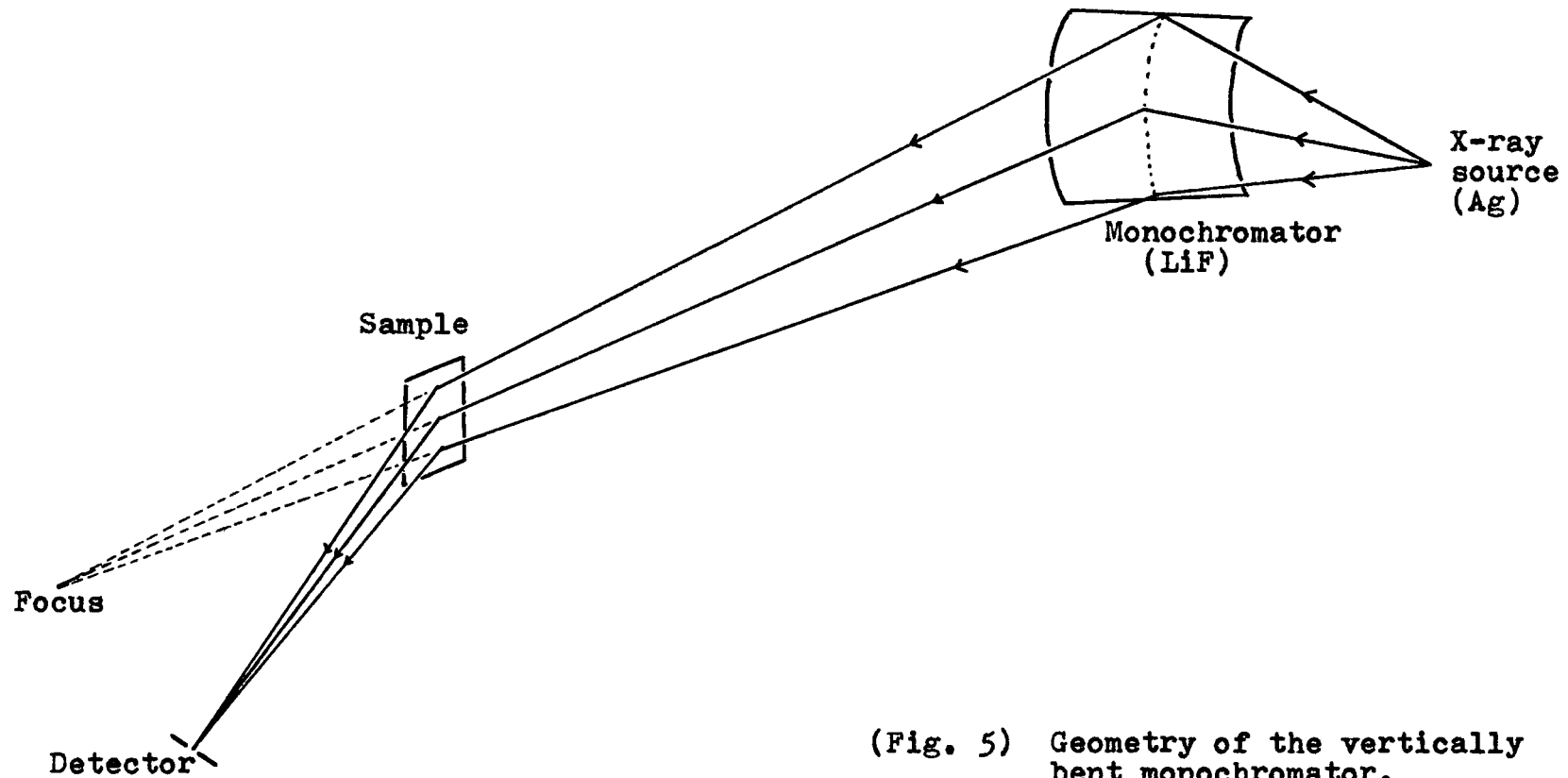


(Fig. 5) Geometry of the vertically bent monochromator.

(3) Alignment: By using a standard GE alignment kit, the center of X-ray tube, sample holder and receiving slit were levelled. With the monochromator, the reflected X-ray beam was adjusted through the center of sample holder and the receiving slit at $2\theta = 0^\circ$. This adjustment was finished by putting a thin wire at the center of the sample holder and with the help of a fluorescent screen, the diffractometer was moved such that the wire remains always in the center of the primary beam for all rotation angles. Then, with the wire in place, the receiving slit was narrowed to $.05^\circ$ and the primary beam was scanned with the counter in order to establish the zero of 2θ . The final alignment was further checked by scanning several peaks from a silicon powder standard disk. All peaks were within $.09^\circ$ in 2θ of the calculated values, which was considered satisfactory for measuring amorphous patterns.

(4) Operations: Both Cu and Ag X-ray tubes were operated at 40 KV and 20 ma. Slit 1, as shown in Fig. 3, was used to have an incident beam divergence of about $.8^\circ$ so that the samples intercept the whole beam at all angles. The receiving slit, slit 2, was used to have a 2θ opening of about 1° . For Cu data, counting-measurements were taken every $.5^\circ$ for every 100 seconds on the range of 2θ from 6°

to 140° . In the case of the Ag data, time-measurements were taken for every 10,000 counts on the range of 2θ from 4° to 120° .

4. Data analysis and the results

The X-ray diffraction data from original wet samples, dried samples and re-wetted samples were all collected. An analysis that corrects and normalizes the intensity to give the reduced intensity was carried out for the 150°C heated dry sample only. Other intensity data were then compared to this normalized dry data to give the difference intensities. The procedures of data analysis and the results of the tyrosine and L-dopa melanin samples are given below. Unless specifically noted as L-dopa, results given in this chapter refer to the tyrosine melanin supplied by Sigma Chemical Company.

Two assumptions were found necessary for this data analysis. First, the 150°C heated dry melanin sample was assumed to have a unit of composition of the indole 5,6 quinone, C_8NHO_2 . Secondly, we assumed that the weight difference between the wet and dry samples was due to the water content only (and not, for example, to loss of actual melanin). Furthermore, from the weight ratio of the wet and the 150°C dry sample, we then figured the number of H_2O molecules in the unit of

composition of the wet melanin, $(C_8NHO_2) \cdot xH_2O$. The corresponding values of x of the wet samples are given in Table II. The rewetted sample which has density of 1.28 g/c.c. have $x = 1.0$.

(1) Analysis of the data on the 150°C dry sample to give the intrinsic structure of melanin:

It is well known that the diffraction intensity pattern of an amorphous material contains only several continuous diffuse or broad peaks. But, since the data from the L-dopa melanin sample has some sharp (extraneous) peaks in its intensity pattern, as shown in Fig. 6, a smooth curve was drawn, as shown also in the Fig. 6, to represent the intensity from the amorphous portion of the sample. The smoothed intensity curve was then used for the data analysis. The extraneous structure was attributed to crystallized impurities such as salts taken up during preparation.

The amorphous intensity in electron units per unit of composition, I'_{eu}/N_{uc} , was obtained by correcting the measured intensity, I_m , for several factors as described below:

$$\frac{I'_{eu}}{N_{uc}} = \frac{\pi}{PA} (I_m - B) - (C.M.)_{uc} - (M.S.)_{uc} + (OVERALL CORRECTION)$$

Table II

x in the $(C_8NHO_2) \cdot xH_2O$ of melanin samples

Sample	original	100°C	150°C
L-dopa	1.2	---	0
Tyrosin	3.3	1.4	0

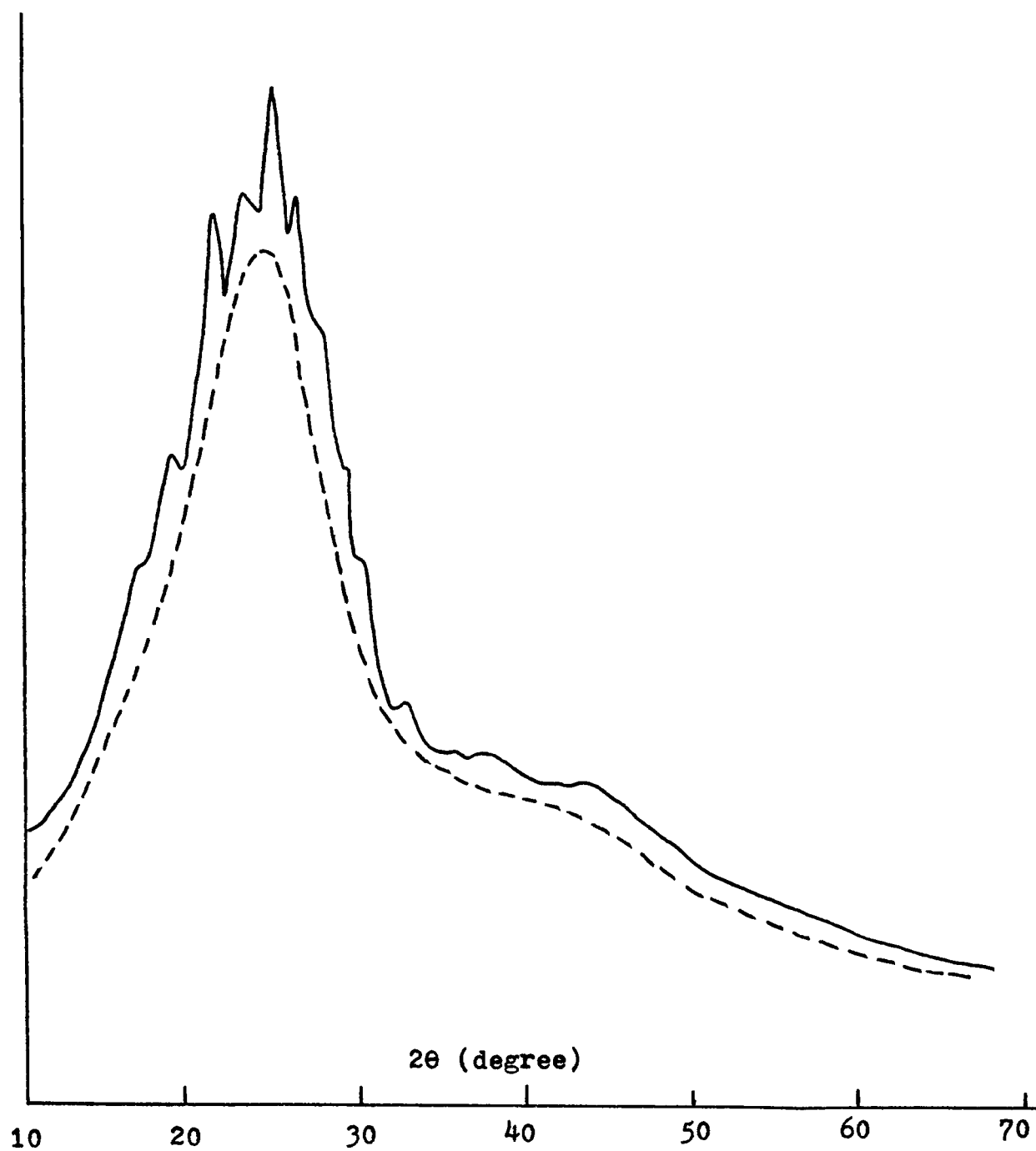


(Fig. 6) Observed intensity(solid-curve) and the smoothed curve(dash) of dry L-dopa melanin sample.

where,

a) B = background due to air scattering and very weak angular independent sources such as cosmic rays, electronic noise, etc. In our case, only air scattering was considered. A fraction of $\frac{1}{2}$ was used for the measured air scattering since the detector system recorded air scattering about twice as much volume with the sample removed as with the sample in place.

After the correction for background, because a comparatively wide receiving slit, 3 mm, was used in data collecting, a deconvolution correction was thought to be necessary. An approximation suggested by Warren⁽⁴⁰⁾ of the slit function as a rectangular pulse function was used. The true function, $g(x)$, is related to the measured function, $f(x)$, and the slit width, $2d$, by the following equation

$$g(x) = \frac{4}{3} f(x) - \frac{f(x-d) + f(x+d)}{6}$$

b) P = Polarization factor: For a primary beam which has been reflected from a monochromator at $2\theta_M$, $P = (1 + \cos^2 2\theta_M \cos^2 2\theta) / (1 + \cos^2 2\theta_M)$. In this experiment, for radiation reflected from the (200) planes of a LiF monochromator crystal, $(2\theta_M)_{\text{Cu}_{K\alpha}} = 45^\circ$, and $(2\theta_M)_{\text{Ag}_{K\alpha}} = 16^\circ$.

c) A = absorption correction which corrects the intensity to what it would be for an infinitely absorbing sample. The Milberg⁽⁴¹⁾ correction was used in the form

$$A = \left(1 - \frac{I}{2\mu a \cos 2\theta}\right) \left(1 - e^{-2\mu t \cos \theta}\right) + \frac{2t \cos \theta}{a} e^{-2\mu t \cos \theta}$$

where, a is the breadth of the beam, t is the thickness of the sample, and μ is the linear absorption coefficient of the sample. By using the equation $I = I_0 e^{-\mu t}$, the linear absorption coefficients of the samples are measured for both Cu and Ag radiations. The measured values are $\mu_{\text{Cu}} = 20 \text{ cm}^{-1}$ for the tyrosine sample, 8.6 cm^{-1} for the L-dopa sample, and $\mu_{\text{Ag}} = 1. \text{ cm}^{-1}$ for the tyrosine sample.

d) $(\text{C.M.})_{\text{uc}}$ = Compton-modified correction. The Compton-modified intensity in electron units per unit of composition was calculated by using $(\text{C.M.})_{\text{uc}} = R \sum_{\text{uc}} Y(k)$, where $R = (\lambda / (\lambda + 0.04852 \sin^2 \theta))^{3.5}$, the Breit-Dirac recoil factor, and $Y(k)$ are the tabulated values given in the International Tables.

e) $(\text{M.S.})_{\text{uc}}$ = Multiple scattering correction. Here only the second-order multiple scattering was considered. The ratio of the second-order to the first-order intensity, $I(2)/I(1)$, were obtained by using the equation given by Mozzi and Warren⁽⁴²⁾.

f) n = Normalization constant. Before the corrections of (C.M.) and (M.S.), the partially corrected intensity must be converted to the unit of eu/uc. In order to do this, a normalization constant had to be used to match the measured total intensity with the calculated total independent intensity in the high k region where the oscillation of the total intensity is small. The total independent scattering curve, $IS(k)$, was calculated using the relation:

$$IS(k) \equiv \sum_{uc} [f_m^2 + (C.M.)_{uc} + (M.S.)_{uc}]$$

$$= \sum_{uc} f_m^2(k) [1 + MS(k)] + (C.M.)_{uc}$$

where $\sum_{uc} f_m^2(k)$ was calculated by using the scattering factors for C, N and O atoms which were computed Doyle and Turner⁽⁴³⁾ including anomalous dispersion. Details are given in Appendix A; $MS(k) = \frac{I(2)}{I(1)}$. For the case of Ag-radiation, since it is possible to obtain the intensity information at k as high as 19 \AA^{-1} , this requirement of independent scattering was satisfied. The normalization for the Ag data was then performed by fitting the diffraction curve to the total independent scattering on the interval $15 \leq k \leq 19$. However for the Cu data, since the maximum value of k was only 7.8 \AA^{-1} , the diffraction curve did not converge to the independent scattering curve at this value. Therefore a modified Norman⁽⁴⁴⁾ method was employed:

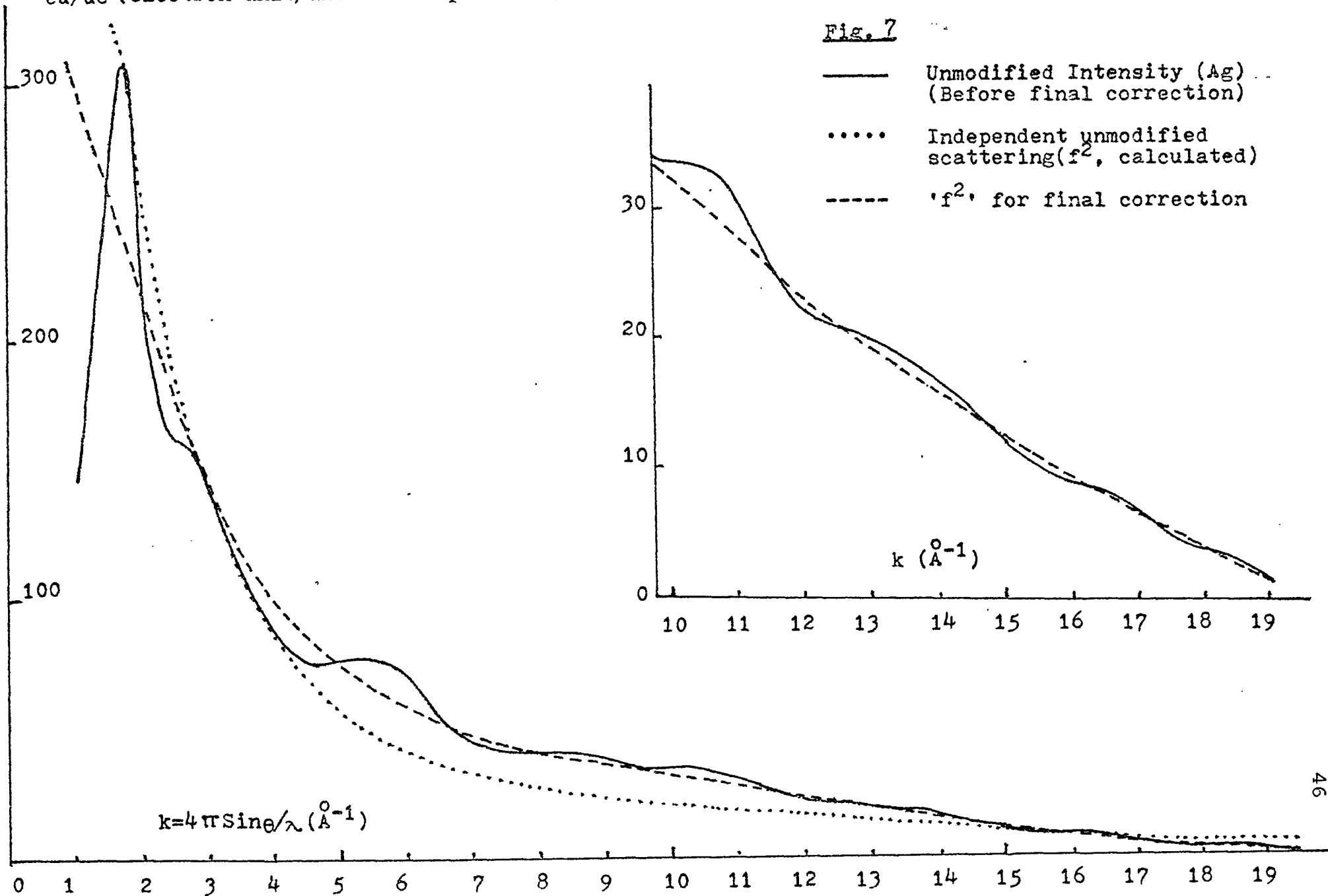
$$\begin{aligned}
 n \cdot \int_0^{k_m} \frac{k^2 e^{-\alpha^2 k^2}}{f_e^2} \left(\frac{I_m - B}{PA} \right) dk \\
 = \int_0^{k_m} \frac{k^2 e^{-\alpha^2 k^2}}{f_e^2} IS(k) dk - 2\pi^2 \rho_e \sum_{uc} Z_m
 \end{aligned}$$

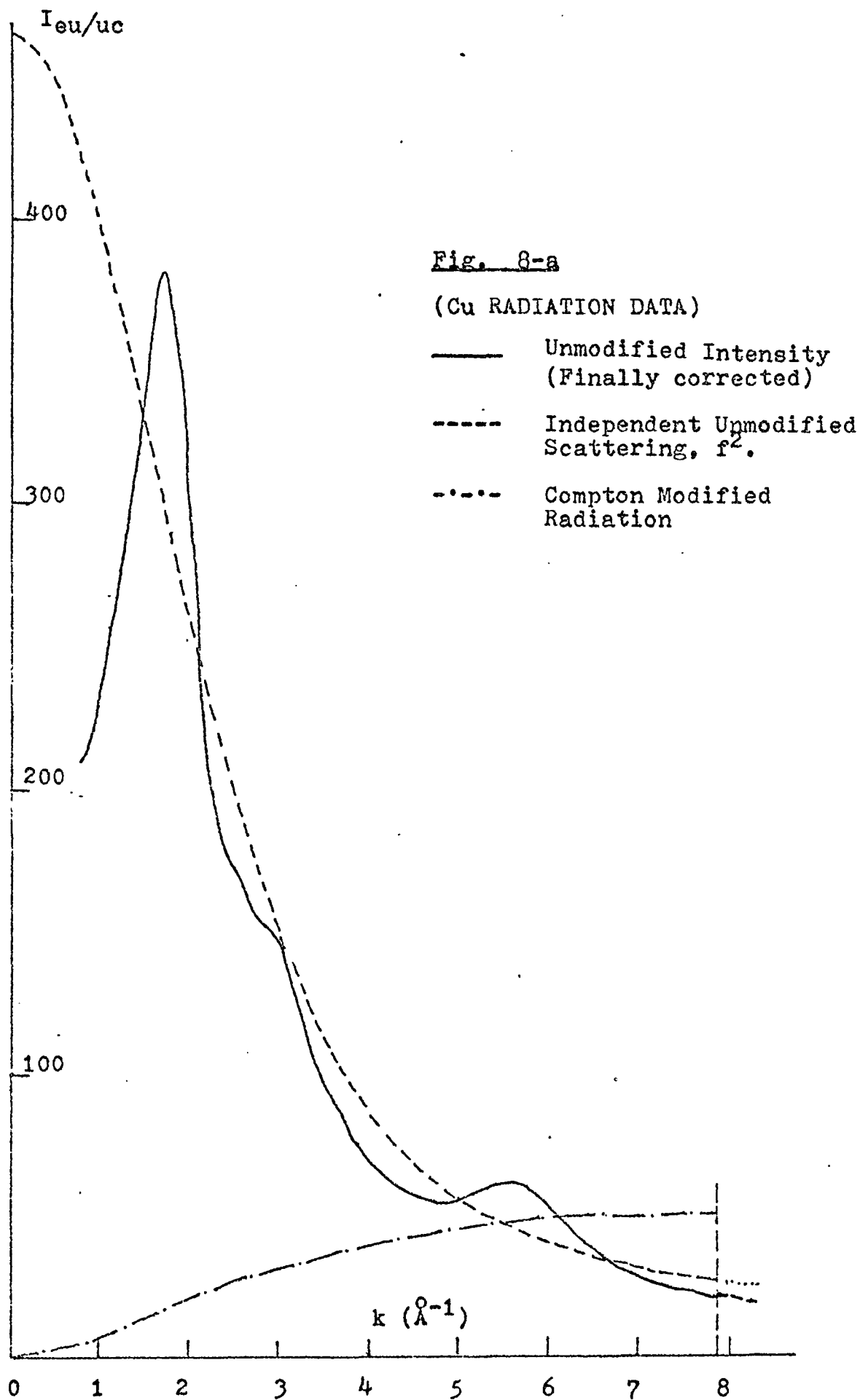
where, $\rho_e = \frac{N_{uc}}{V} \sum_{uc} Z_j$, is the average electron density; $IS(k)$ = total independent scattering curve; f_e = the effective scattering factor as been defined before; and a rather strong convergence factor with $\alpha^2 k^2 = 4$ was used since the integrands involve k^2 . After the partially corrected diffraction curve $I''(k)$ was normalized to eu/uc , the corrections for Compton and Multiple Scattering made to obtain $I'(k)$ using $I'(k) = [I''(k)/(1 + Ms(k))] - (C.M.)_{u.c.}$.

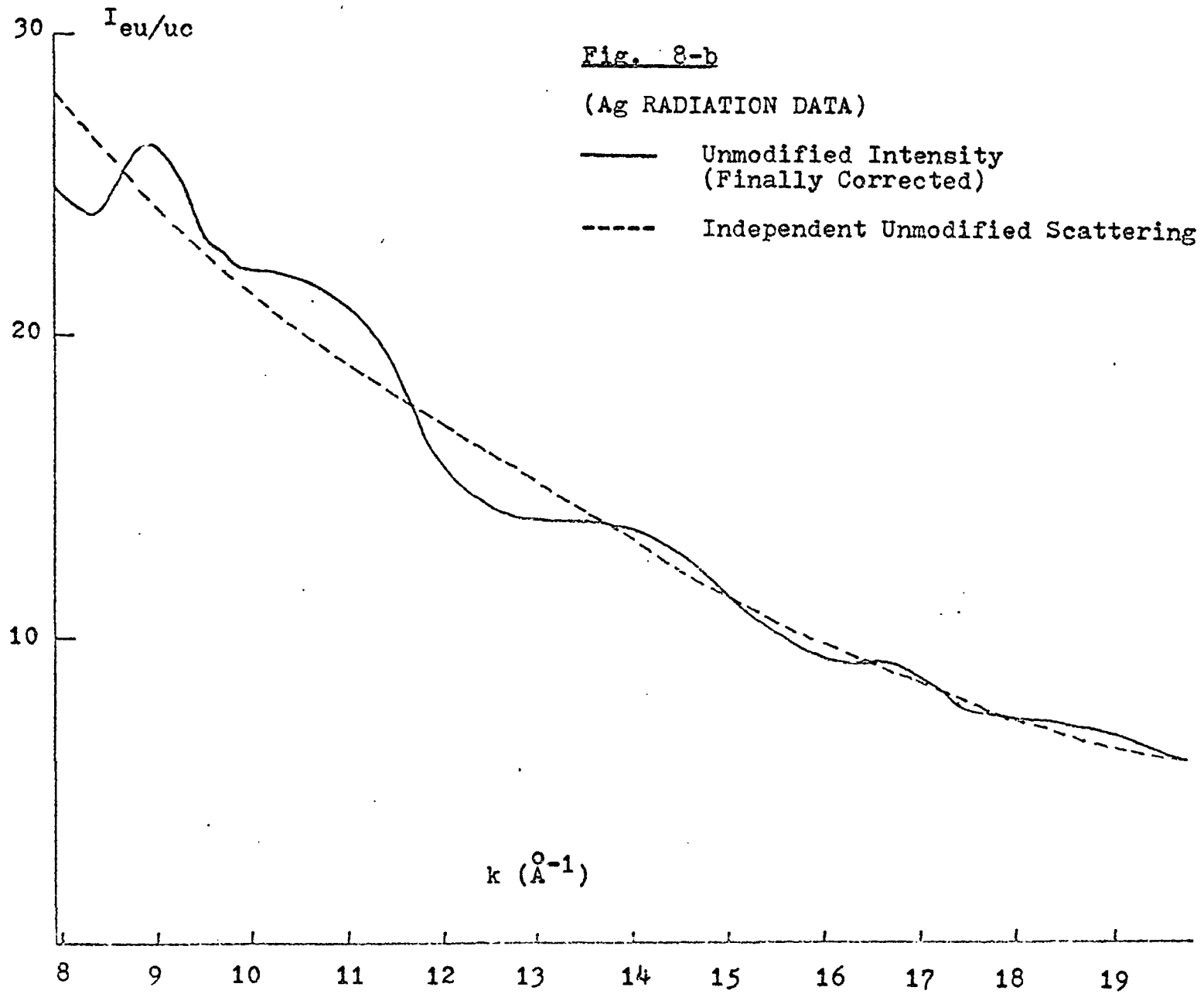
g) Over-all Correction: After normalization and correction for C.M. and M.S., it was found necessary to do further visible correction for the tyrosine melanin samples, but not necessary for the L-dopa sample. Since the normalized intensity curve, $I'_{eu/uc}$, did not oscillate always through the calculated independent unmodified scattering, $\sum_{uc} f_m^2$, a smooth curve was then drawn to go through the oscillating intensity curve for this final correction. Fig. 7 shows the over-all correction for the Ag data on the tyrosine sample.

The final X-ray diffraction intensity curve for the 150°C heated dry tyrosine melanin sample is given in Fig. 8, where

$I_{eu/uc}$ (electron unit/unit of composition)







the Cu-data for $k = 1$ to $k = 7.8 \text{ \AA}^{-1}$ and the Ag-data for $k = 7.8$ to 19 . were used. Fig. 9 shows the normalized total intensity for the dry L-dopa melanin sample, and the calculated Compton modified and the independent unmodified scattering of the indole 5,6 quinone.

Finally, the interference function, $i(k)$, of the dry tyrosine sample was obtained and given in Fig. 10, where Fig. 10-a is the Cu-data, and Fig 10-b is the combination of the Cu- and Ag-data. The $i(k)$ of the L-dopa melanin samples, dry and wet, are given in Fig. 11.

All computations were done using the UNIVAC 1108 computer at the University of Houston Computing Center. The Fortran programs were mostly written by the author with the help of the 'Computer Programs for Radial Distribution Analyses of X-ray and Electron Diffraction Data' given by A. L. Renninger and R. Kaplow⁽⁴⁵⁾.

(2) Analysis of the data of wet samples to give the difference intensities:

The measured intensities of the wet samples were corrected for background, polarization and absorption. The corrected total intensities were then converted to the electron units per unit of composition of their own, as shown in Table II, by using the already normalized dry melanin data as a standard, and the relation given in the Warren's book:

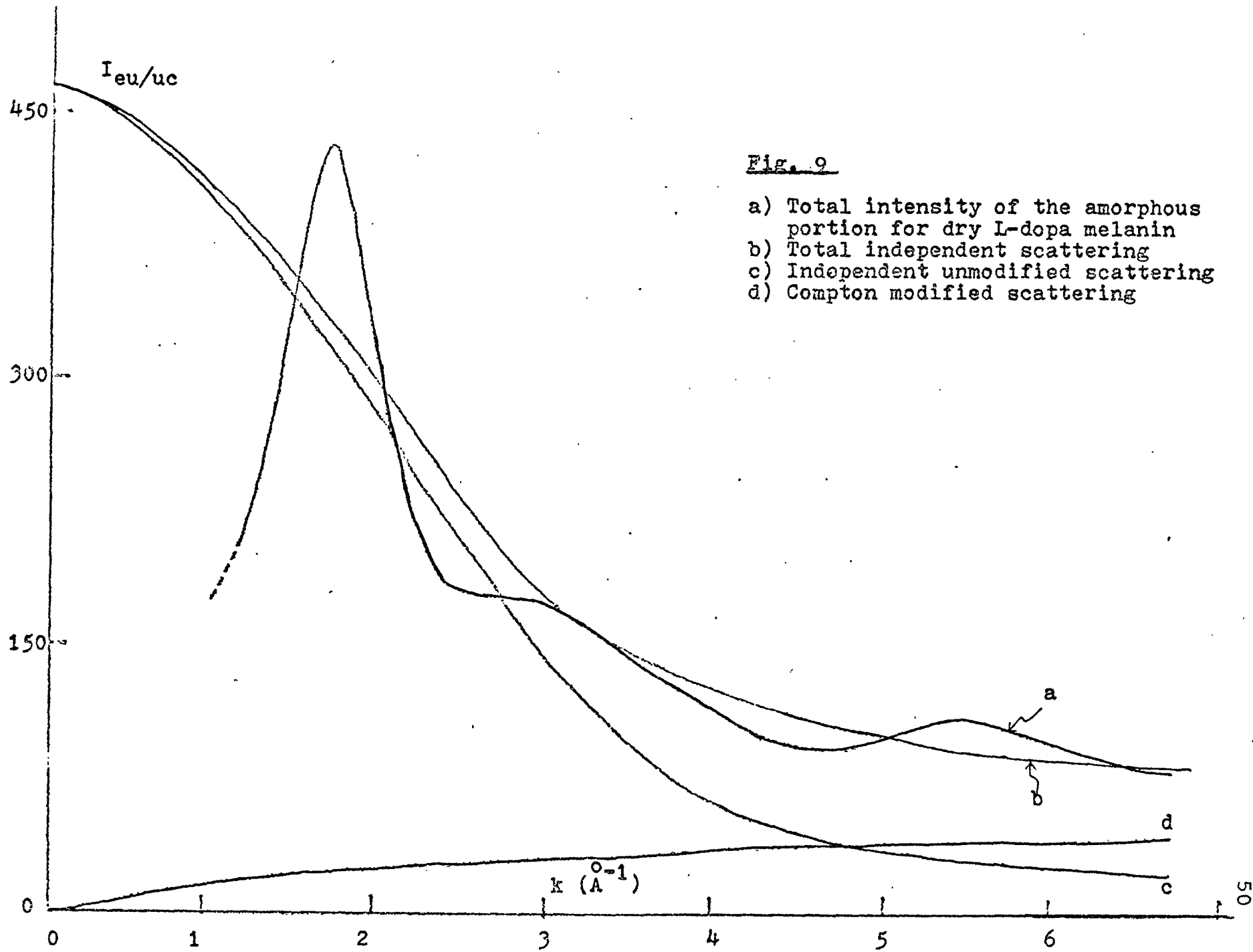
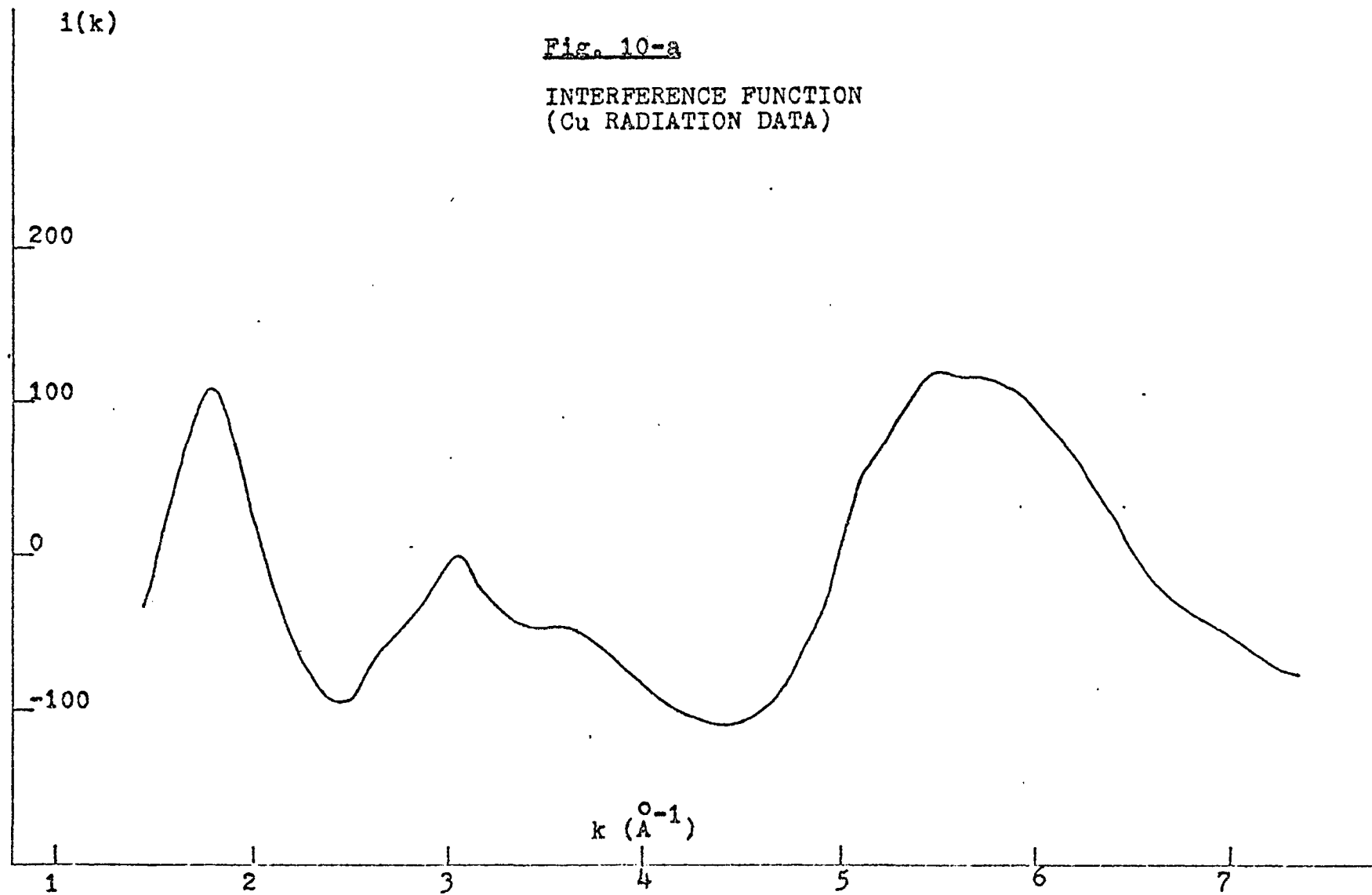
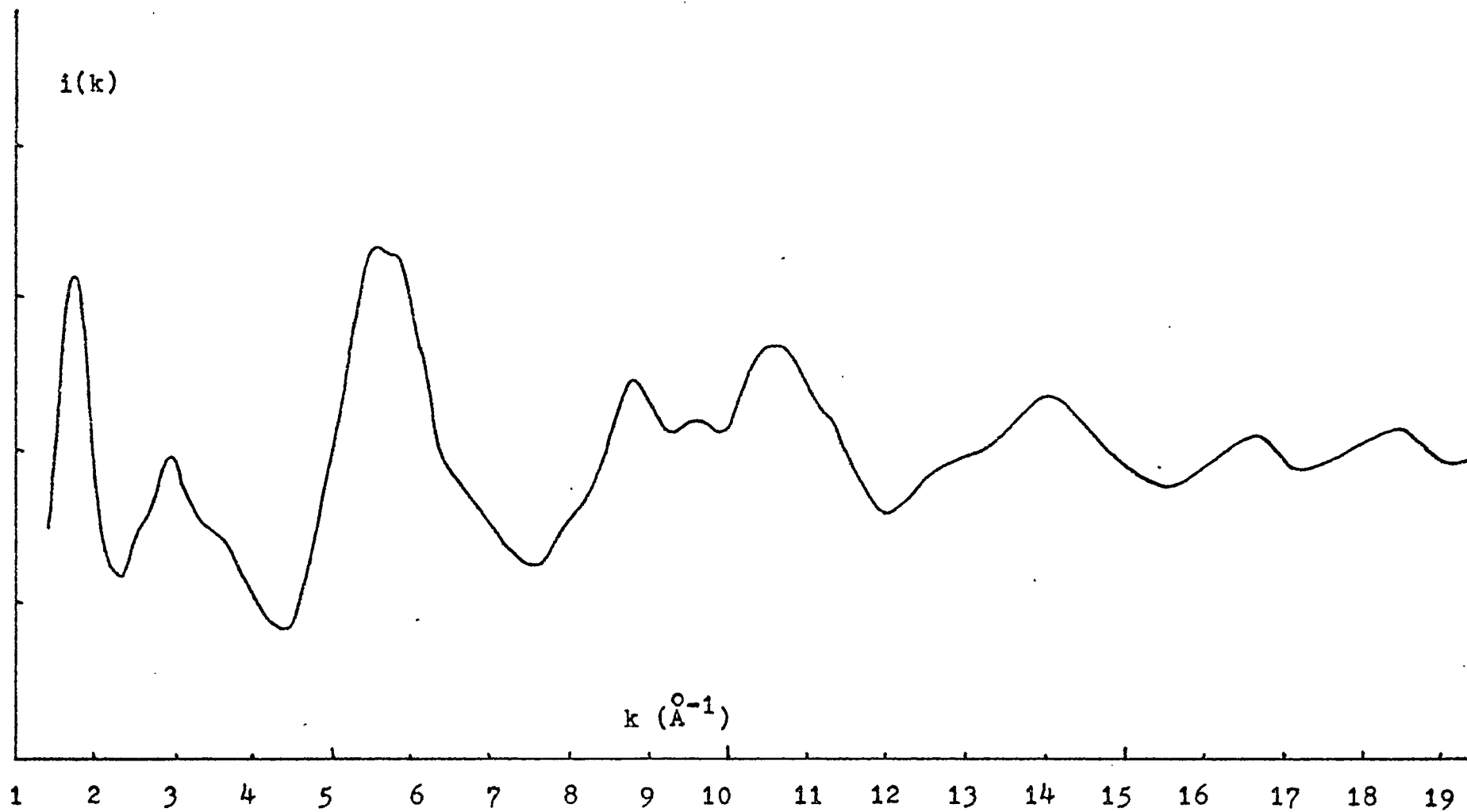


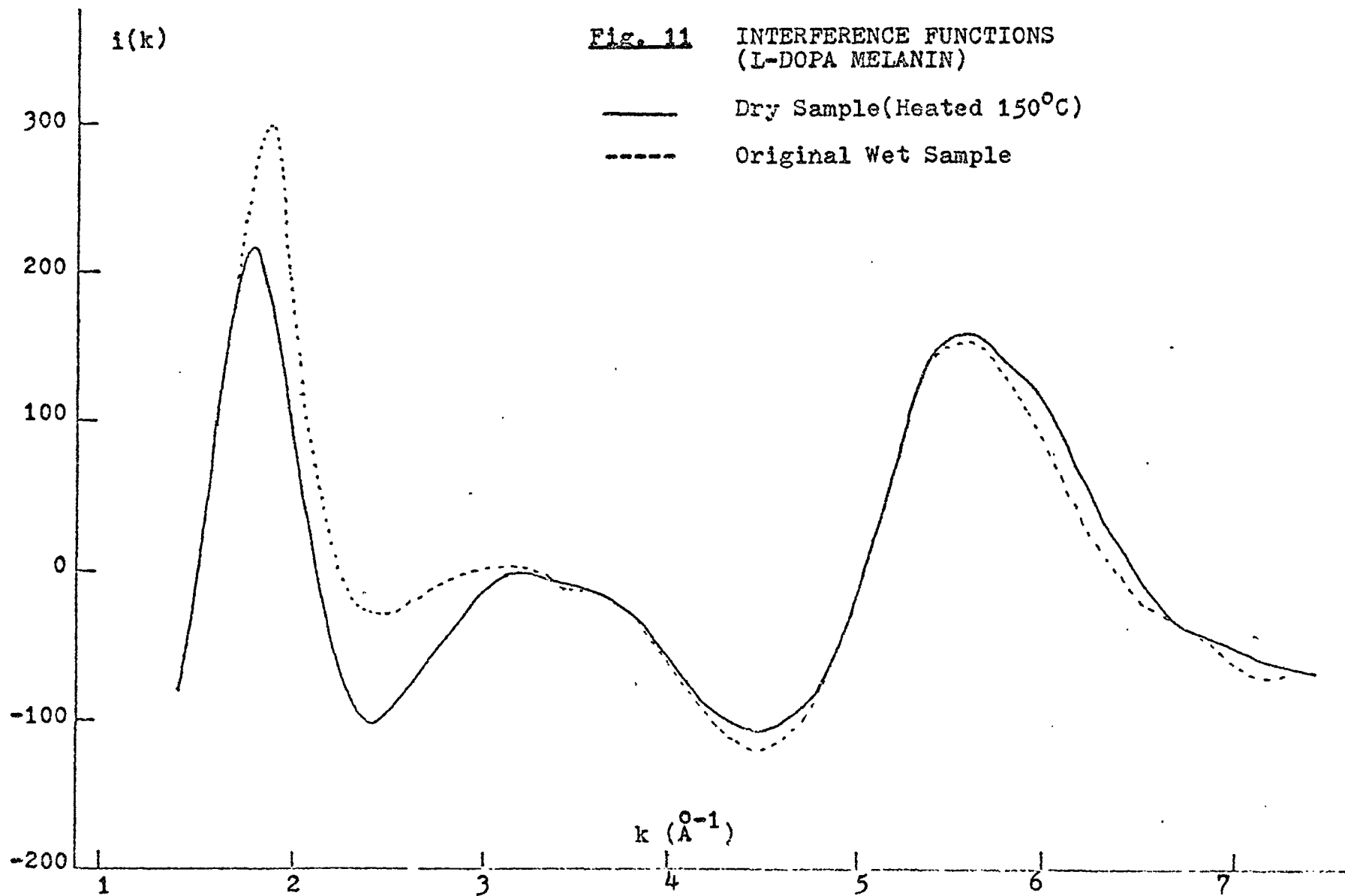
Fig. 9

- a) Total intensity of the amorphous portion for dry L-dopa melanin
- b) Total independent scattering
- c) Independent unmodified scattering
- d) Compton modified scattering





(Fig. 10-b) Interference function (Cu and Ag radiation data)



$$I'_m \sim I_{eu/uc} \cdot \frac{M'}{2\mu'} \quad \text{and}$$

$$\frac{M'}{2\mu'} = \frac{L}{2 \sum_{uc} (\mu'_m A)}$$

where,

I'_m = measured intensity corrected for background, polarization and absorption.

$I_{eu/uc}$ = Total intensity in eu/uc.

M' = number of uc per unit volume.

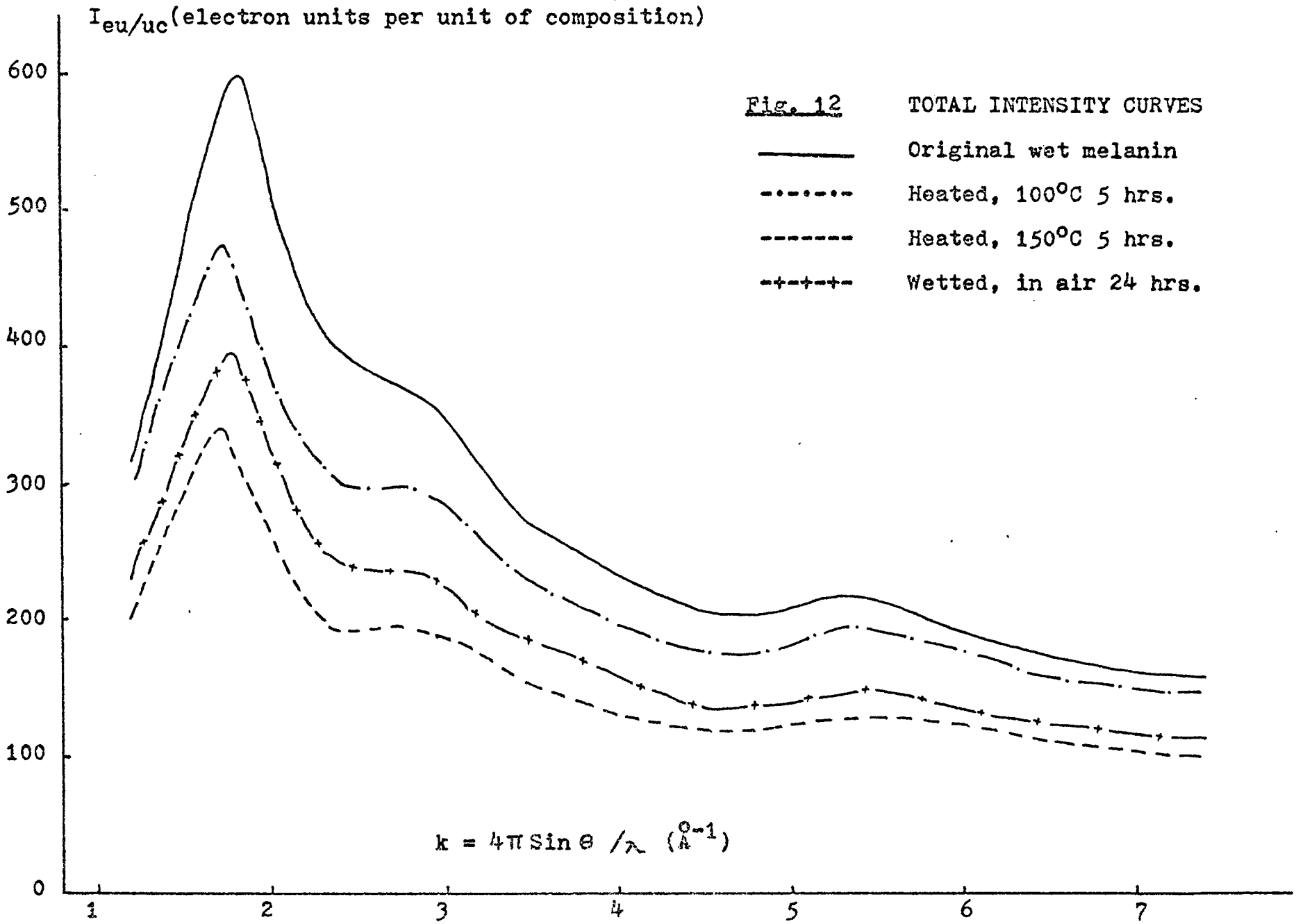
μ' = linear absorption coefficient of the sample.

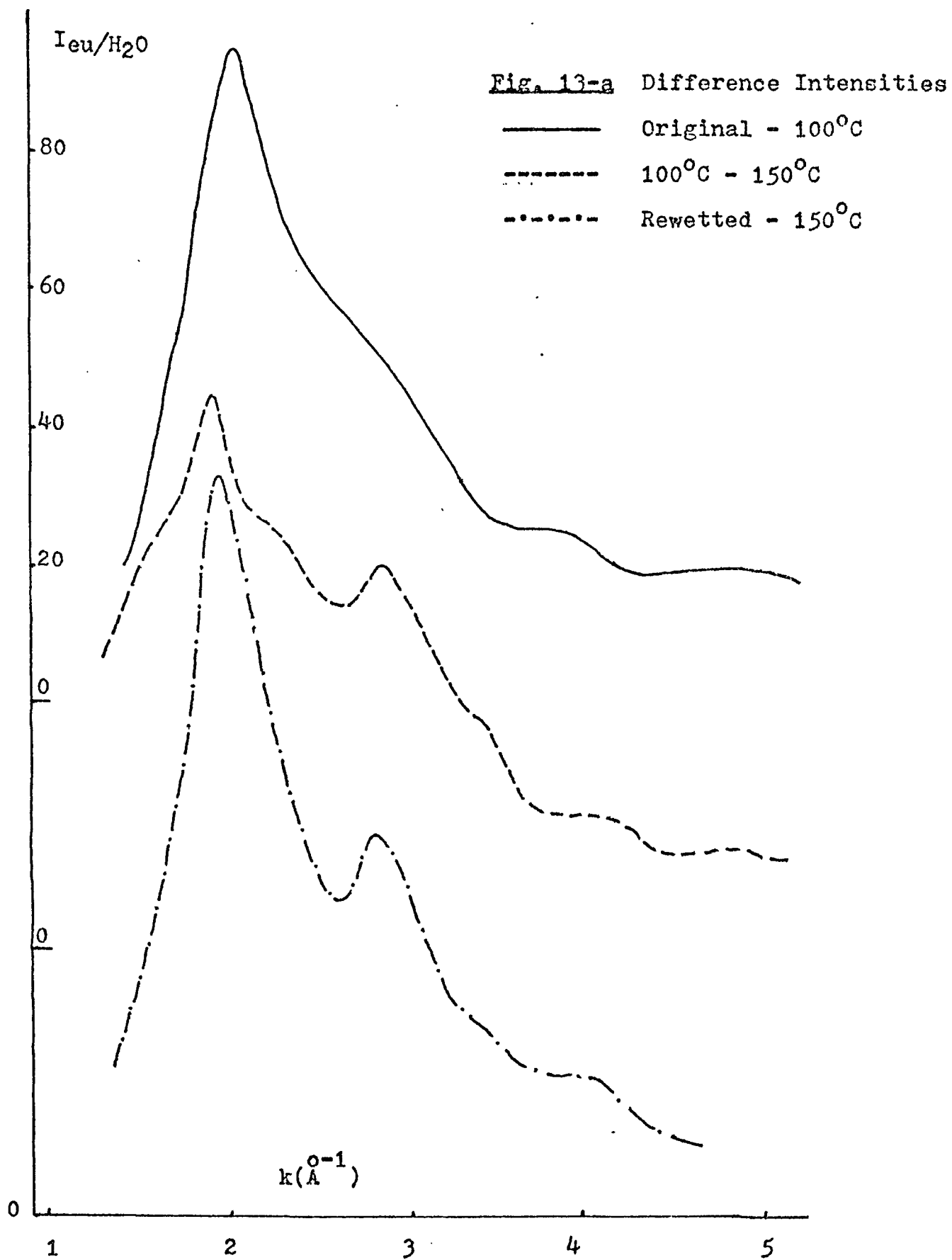
μ'_m = mass absorption coefficient.

A = atomic weight.

L = Avogadro number.

The results of the total intensity curves for the tyrosine sample in different states of hydration levels are given in Fig. 12. By taking the intensity differences between the original and the 100°C dry data, the 100°C and 150°C data and the 150°C and the moistened data, and dividing by the differences of the number of H₂O molecules in their composition, ($x_1 - x_2$), the difference intensities in electron units per H₂O were obtained and shown in Fig. 13-a. Fig. 13-b gives





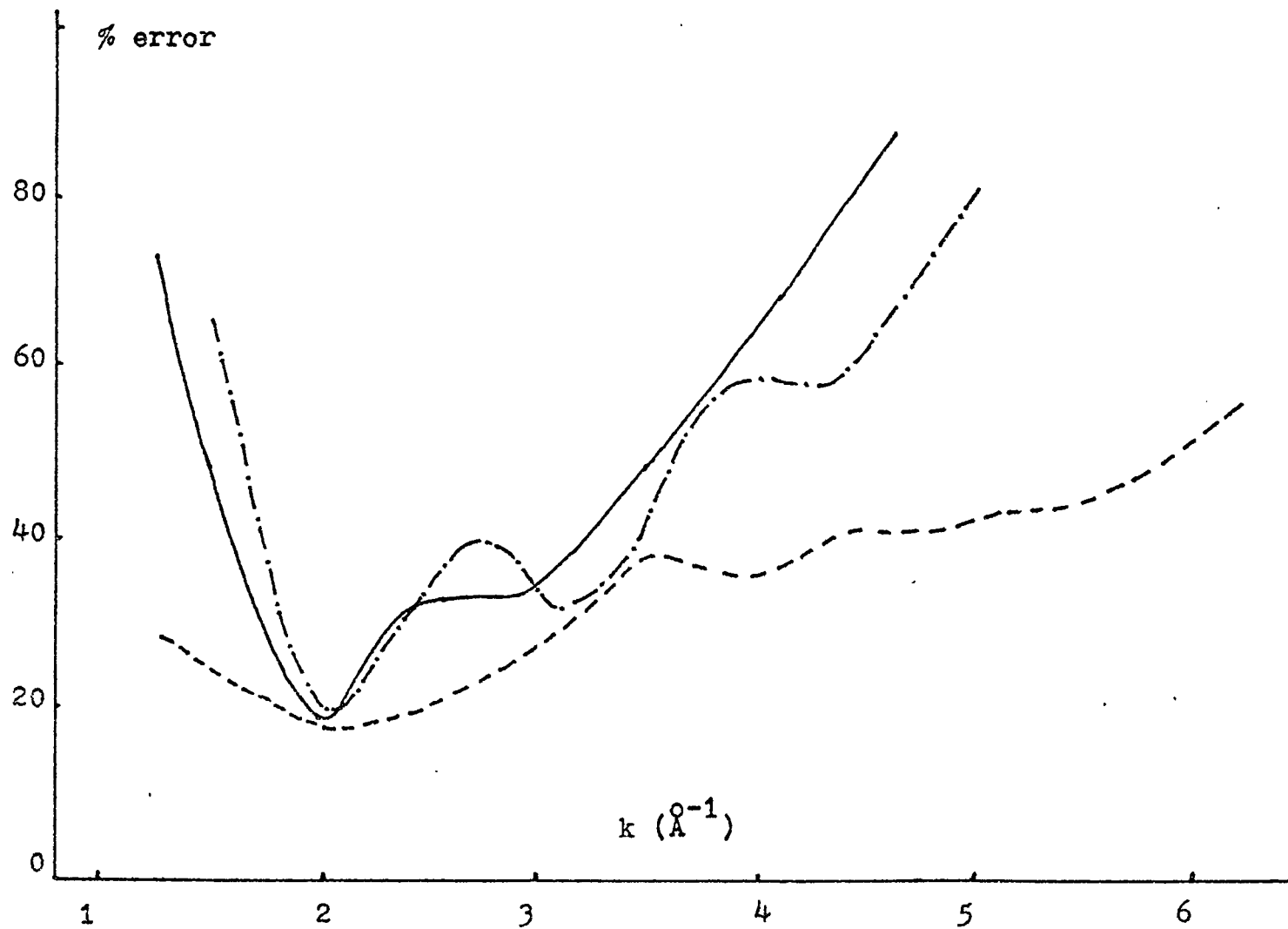


(Fig. 13-b) Percentage errors of the difference intensities of Fig. 13-a.

the percentage errors of the difference intensities of the Fig. 13-a, where the percentage error was estimated by comparing the difference counts between the original measured intensities of the two samples to the higher counting error, the square root, of the measured intensities by using the following relation:

$$\% \text{ error} = \frac{(I_{m>})^{\frac{1}{2}}}{(I_{m>} - I_{m<})} \cdot 100 \%$$

where, $I_{m>}$ is the measured intensity (wet or dry) which has larger value than the other measured intensity $I_{m<}$ (dry or wet).

5. Discussion

In the experiments, X-ray tubes were turned on and set at the operation conditions, preheated for about one hour and not turned off until the final data was collected. During operation, the stability of the system was checked by examining the scattering intensity of a lucite plate at its first diffuse peak position of $2\theta = 14.5^\circ$. The measured intensity fluctuation was found to be less than 3% during the data collection period. The background due to cosmic ray and electronic noise was measured every 20° throughout the

experimental region. It was found to be less than two counts per 100 seconds and has been neglected for the data analysis.

In this experiment, since the energy window of the pulse height analyzer was selected at 0.4 volts, compared with the average pulse height of $\text{Ag}_{\text{K}\alpha}$ of 4 volts, the lower limit comes about 1104 eV below the average $\text{Ag}_{\text{K}\alpha}$ energy of 22125 eV, which in turn corresponds to a wavelength increase of $\Delta\lambda \approx 0.029 \text{ \AA}$. However, the Compton shift of wavelength at 100° 2θ is $(\Delta\lambda)_c = 0.04852 \sin^2\theta \approx 0.029 \text{ (\AA)}$. Compton intensity measured at 2θ greater than 100° is increasingly cut off by this lower limit on the analyzer. This could be one of the major reasons causing the corrected coherent scattering intensity to drop down lower than the independent scattering in the higher k region for the Ag-data as shown in Fig. 7. Although this defect was cured by the final over-all correction, the reason for correcting the low k data seems still strongly dependent on some unknown and uncertain items, such as the higher order multiple scattering, the assumption of the unit of composition of melanin and the uncertain amount of water content in the sample. However, the correction was noted not to be necessary for the L-dopa sample which was found to have a measured linear absorption coefficient of only about $\frac{1}{2}$ of the tyrosine melanin sample.

The tyrosine sample may have a higher measured linear absorption coefficient than L-dopa if its small particle size gives increased small angle scattering outside the slit, and lowers the detected intensity in what is assumed to be I (transmitted). This is the first indication that tyrosine does indeed have a smaller effective particle size than L-dopa and we will return to this point in discussing the spin resonance results. The multiple scattering of higher than second order may be also important for the tyrosine sample.

As far as the difference intensities are concerned, since the errors are high as shown in Fig. 13-b, they are only qualitatively important for the study of the water in melanin. In Fig. 14, the difference intensity curve of the original - 100°C is compared to the intensity of the liquid water at 20°C, that was obtained by Narten⁽⁴⁶⁾. There are some similarities between them, namely the first peak and the following shoulder. However the other two curves, the difference intensities of 100°C - 150°C and of the wetted - 150°C, show a second peak which was assumed to relate to the second peak of amorphous solid water obtained by Boutron et. al.⁽⁴⁷⁾ Comparisons are given in Fig. 15 and Fig. 16. At this moment, it is necessary to point out that the difference intensities include not only the contribution of the adsorbed water but

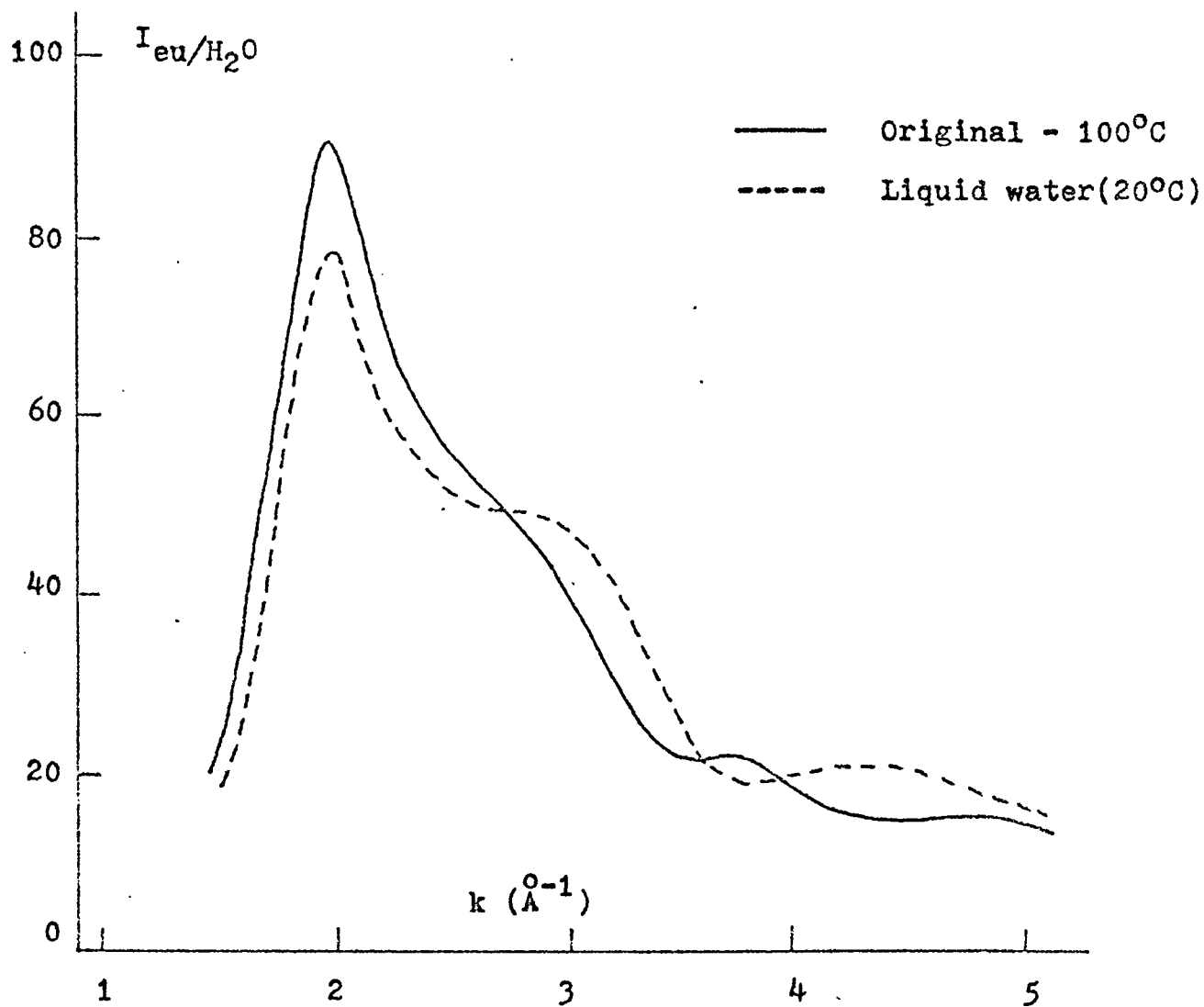


(Fig. 14) Comparison of the difference intensity to the intensity of liquid water(Narten, 1973).

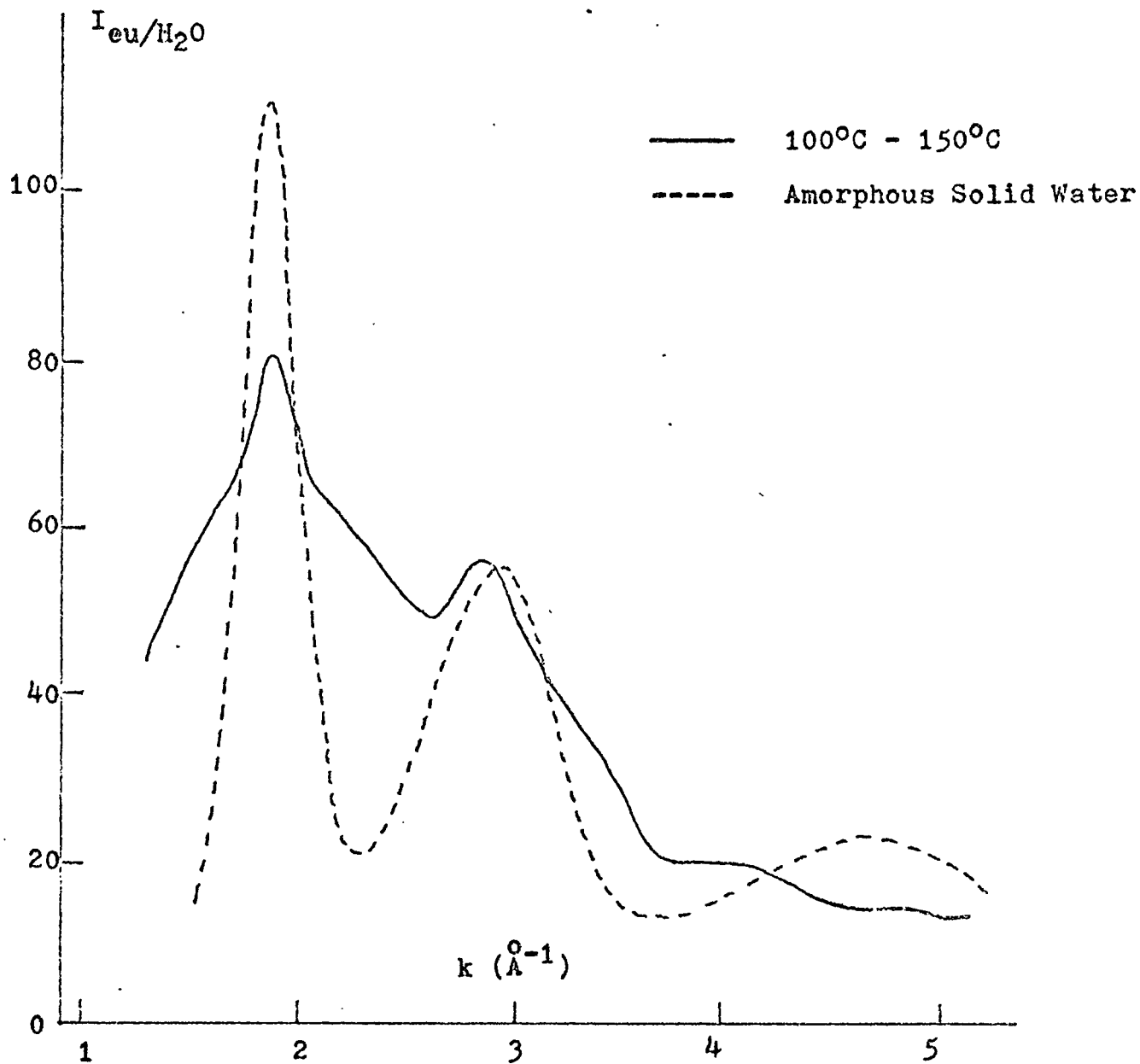


(Fig. 15) Comparison of the difference intensity to the intensity of amorphous solid water (Boutron and Alben, 1975)

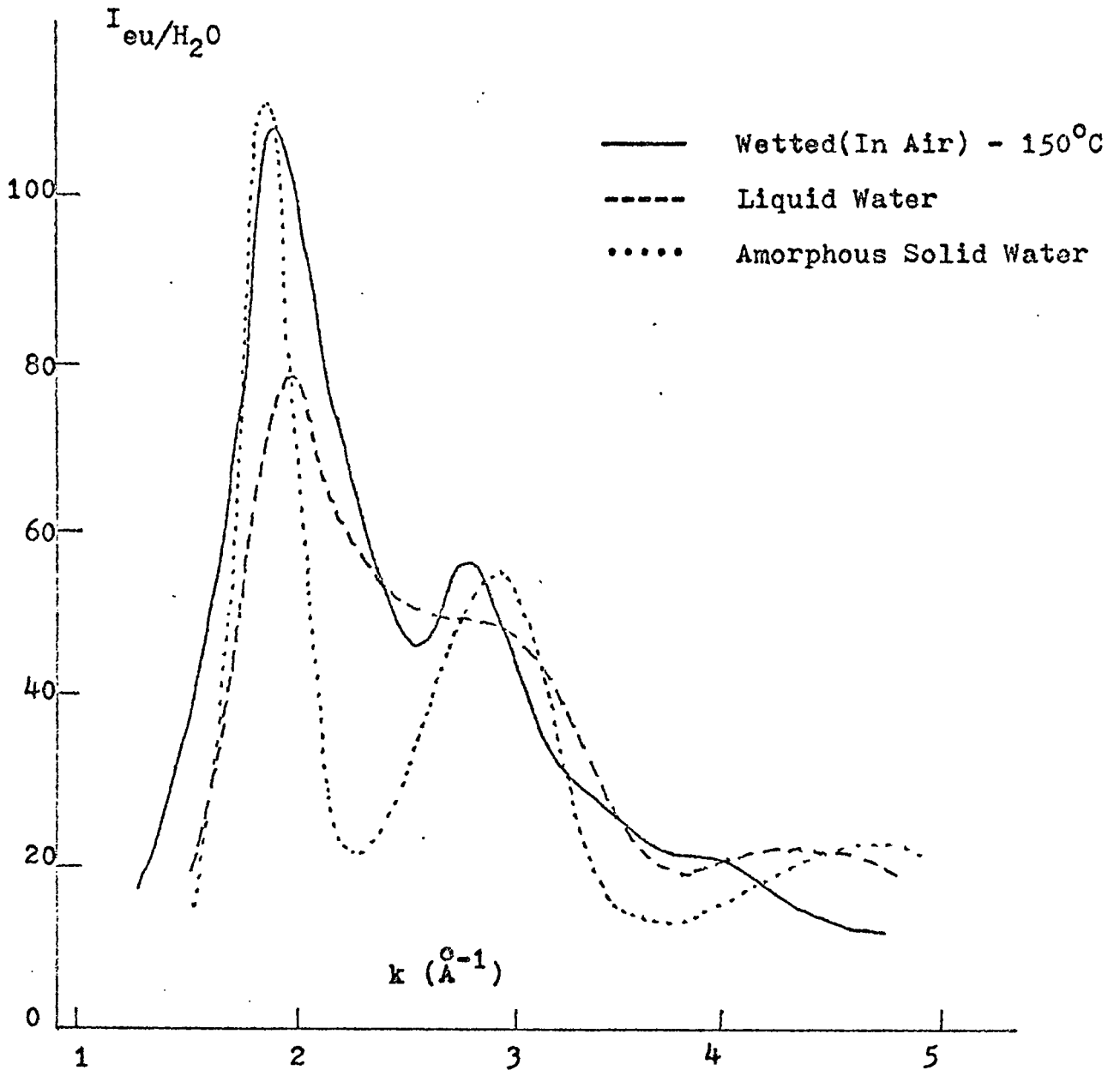


(Fig. 16) Comparison of the difference intensity to the intensities of liquid water (20°C) and amorphous solid water.

also the informations about the interaction between the water and the melanin polymers as well as the possible thermal degradation of the melanin sample. We must therefore emphasize how tentative are our conclusions about the detailed nature of the adsorbed water.

6. Summary and Conclusions

According to this study, we may conclude that:

(1) The X-ray diffraction pattern of the intrinsic, dry, melanin has no shoulder at $k \approx 2.3 \text{ \AA}^{-1}$. With water removed, the dry melanin shows a dip at $k \approx 2.3 \text{ \AA}^{-1}$ in its diffraction pattern. This is important because it proves that adsorbed water contributes the intensity of the shoulder rather than any particular characteristic of melanin itself, as was suggested by Thathachari⁽⁸⁾, and it also gives the intrinsic structure of melanin which will be studied in detail and described in the next chapter.

(2) The adsorbed water has two forms in melanin. As has been shown in Fig. 14 and Fig. 15, the difference intensity of the original - 100°C that is associated with the more easily removed water, and the difference intensity of 100°C - 150°C that is associated with the more bound water are somewhat related respectively to the two forms, liquid and amorphous solid, of water. The re-adsorbed water, Fig. 16, also shows the two possible forms.

(3) Heating at higher temperature and low vacuum causes the thermal degradation of melanin. This was assumed to be so because we were able to show that the weight of a melanin sample, kept at 240°C in rough pump vacuum, decreased exponentially vs time, and that the difference intensity of 150°C - 240°C of a tyrosine sample, once measured, behaves like the intensity of melanin itself rather than water of any form.

CHAPTER FOUR
MODEL CALCULATION STUDY

1. Introduction

To interpret the structure of an amorphous material, one usually compares the measured interference function, IF, or the radial distribution function RDF, to the calculated values of a known model. The construction of a test model is made possible by having some atomic structure information, such as bond lengths, bond angles, etc. The RDF of atoms, in general, can be obtained directly from the model and then transformed into the IF by Fourier techniques. The Debye scattering equation is such a general Fourier transformation that considers the model as a rigid body taking with equal probability, all orientations in space. In this study, since the indole 5,6 quinone monomer includes almost all information of the local atomic structure within $r \approx 7 \text{ \AA}$, it is more suitable and convenient to compare the IF rather than the RDF.

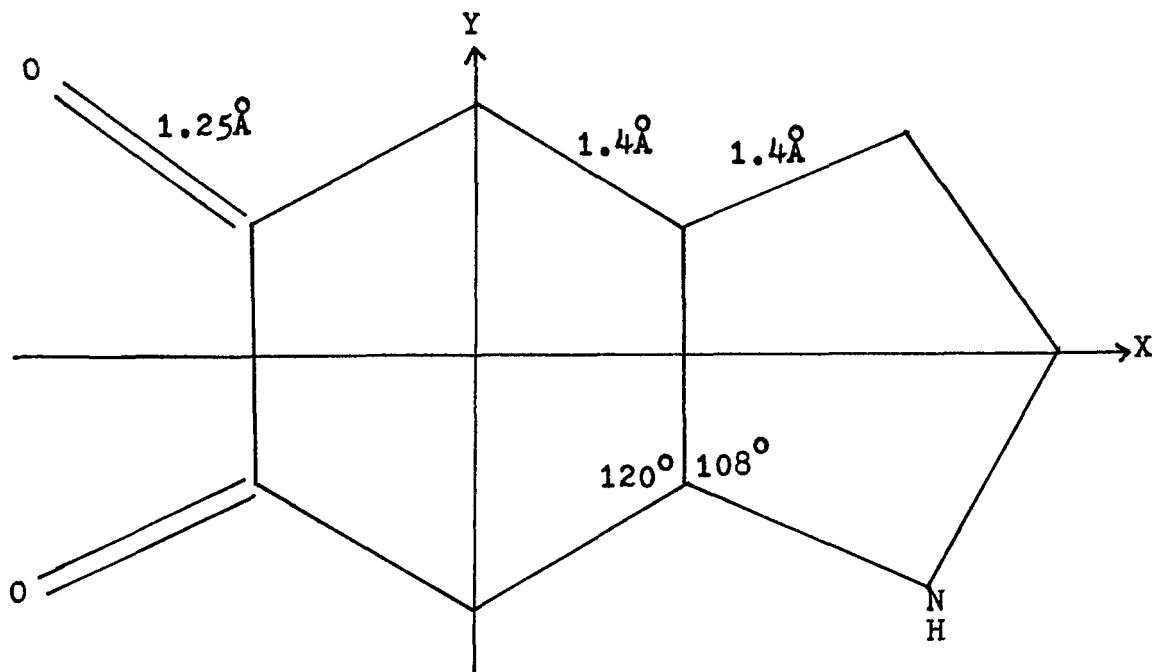
In order to match the computed and the observed IF curves, the following items were studied: a) The extension of the number of melanin monomers on a planar layer from one to four to eight; b) The increase of the stacking thickness or number of stacked layers; c) The disorder, such as

rotation, shifting and tilting, of the stacking layers; and d) further disorder induced by disturbing the oxygen and nitrogen atoms. With all of these features systematically studied, the best matching IF has been obtained and the intrinsic structure of melanin is discussed.

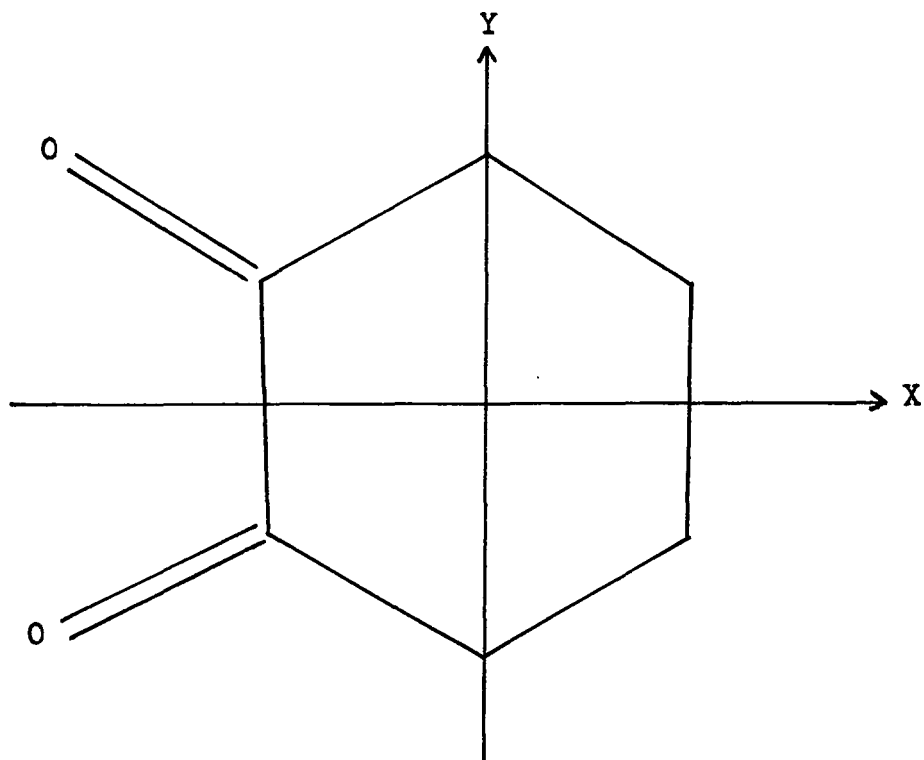
2. Methods

As shown in Fig. 17-a, the melanin monomer, indole 5,6 quinone was drawn on a paper with the bond lengths of C-C and C-N at 1.4 Å and C = O at 1.25 Å, and the bond angles as given in the figure. The coordinates of every atom were measured directly and converted to Angstrom units. After stacking similar planar layers with a 3.4 Å inter-layer spacing, the coordinates of the atoms on the second, the third, etc. layer were generated by computer. In detail, the computer generation consists of a second layer generated from the first one by introducing an inter-layer spacing of 3.4 Å and (or) one of the disorder parameters, such as rotation, shifting, etc., and then a third layer generated from the second by the same process, and then the fourth from the third, and so on. Without specification, rotations were all anticlockwise as viewed along the Z-direction; shiftings were in the positive X-direction; and tiltings were clockwise as viewed along the Y-direction. The reduced intensity

Fig. 17-a
MELANIN MONOMERS



Indole 5, 6 Quinone
(used in this work)



Catechol
(used by Thathachari)

$i(k)$ in electron units per unit of composition was then computed using the Debye scattering equation and the $i(k)$ equation given in chapter three with the calculated scattering factors.

The same method was used to calculate the $i(k)$ of the four and eight monomer models. Fig. 17-b shows the picture of the constructed 8-monomer layer, where the red bars are the C = O bonds and the positions of N atoms are indicated by short white bars. The 4-monomer layer is simple the half of the 8-monomer layer that was divided by the Y-axis. This 8-monomer layer model was constructed using the Framework Molecular Models of the Prentice-Hall Inc. Bond lengths of 1.25 inches for C = O, and 1.4 inches for C-C, C = C and C-N were measured to have less than 2% errors. The trigonal bipyramid connector (120° bond angle) was used for both 6- and 5-ring constructions which, as we shall see, introduces errors into the calculated $i(k)$ for near neighbor distances associated (presumably) with the 5-ring section. This final planar model was set over a sheet of graph paper and the position of every atom was measured.

In order to match the calculated $i(k)$ to the observed $i(k)$, the second major peak ($k \approx 5.7 \text{ \AA}^{-1}$), that refers to the peak of melanin monomers, was considered. Its area (peak height multiplied by half height width) was compared to the area of the corresponding peak of the observed $i(k)$.

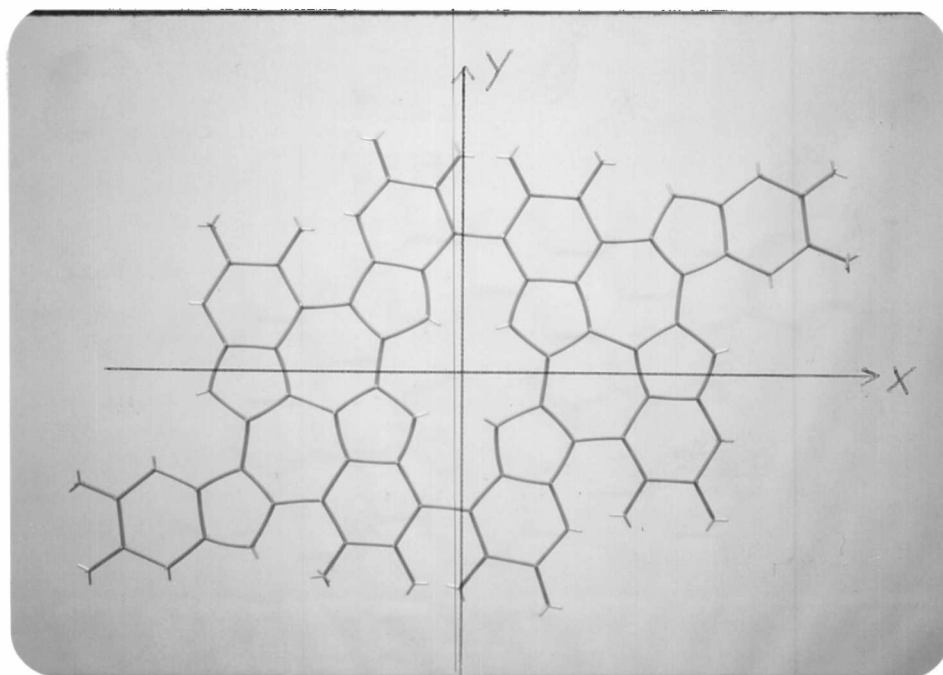


(Fig. 17-b) The eight-monomer layer model

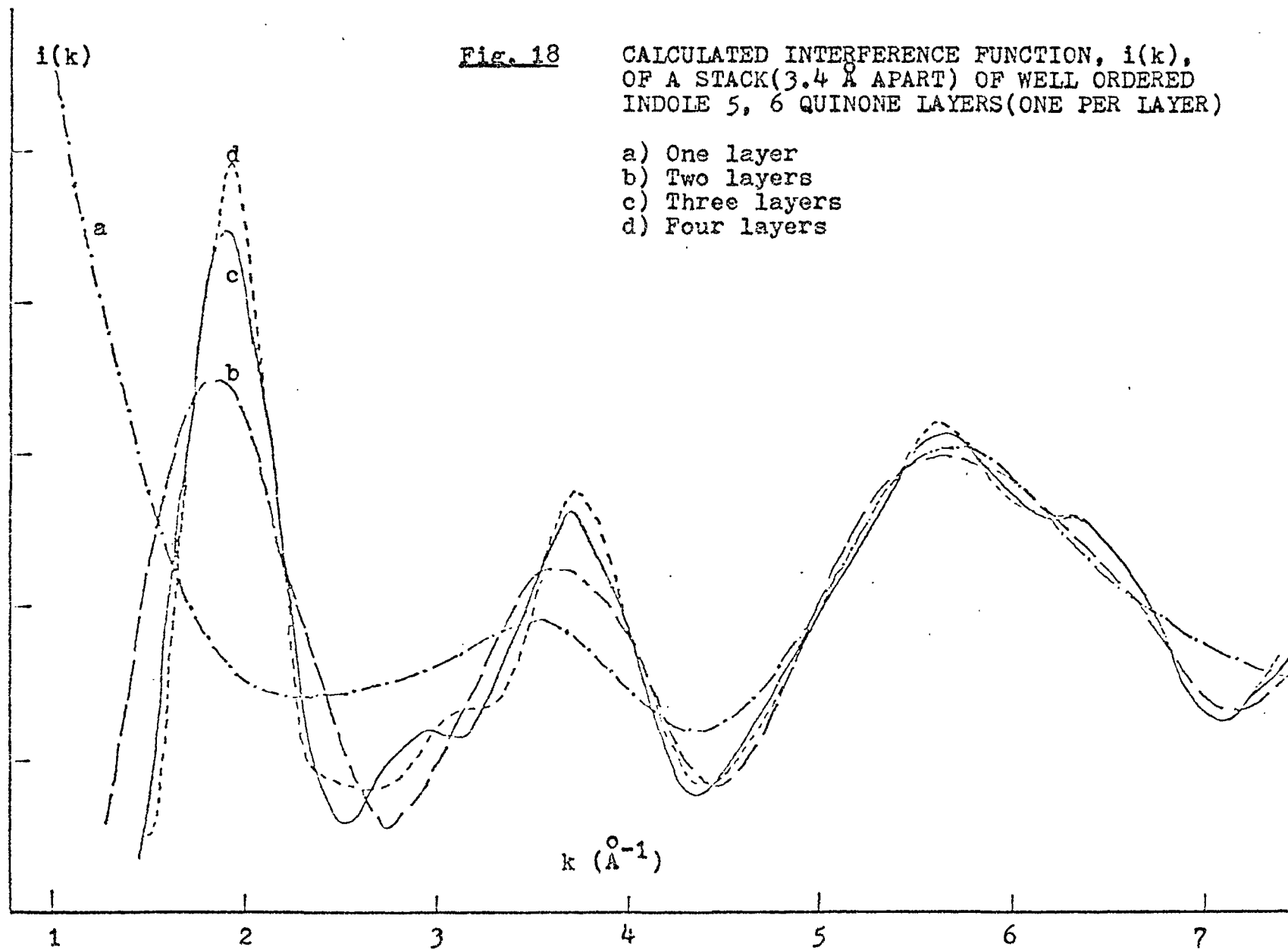
Ratio of the two areas (observed: calculated) was used to modify the computed $i(k)$ and to bring model and data into the same basis. In essence this procedure enables us to allow for a variability in the number of atoms per unit volume of sample that actually exist in the model on configurations.

3. Results

(1) Models with the 1-monomer layers:

The $i(k)$ calculations of the models with only one indole 5,6 quinone monomer per layer, Fig. 18, shows the following features: a) The $i(k)$ of a single layer, curve a, has no peak at $k \approx 2 \text{ \AA}^{-1}$, while it is the location of the first major peak observed from melanin samples. Only a small hill at $k \approx 3.5 \text{ \AA}^{-1}$ and a higher broad peak at $k \approx 5.7 \text{ \AA}^{-1}$ were obtained for this single layer model. b) Increasing the number of the stacks from two to four with all parallel layers having 3.4 \AA inter-layer spacing and same orientation, curve b to d, builds up a peak at $k \approx 2 \text{ \AA}^{-1}$, a dip at $k \approx 2.6 \text{ \AA}^{-1}$ and a peak at $k \approx 2.7 \text{ \AA}^{-1}$, and there is some change for the peak at $k \approx 5.7 \text{ \AA}^{-1}$.

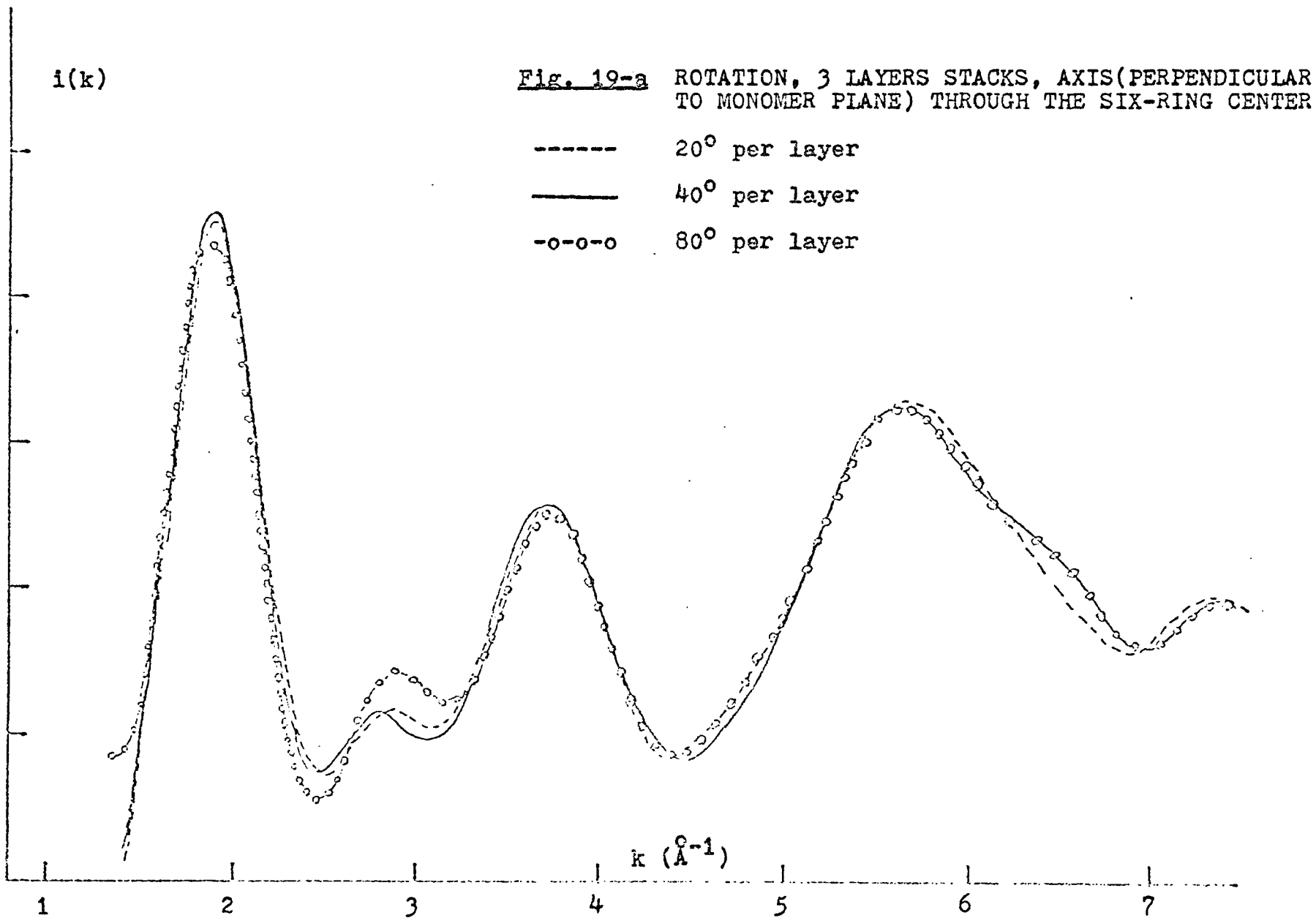
Comparing with the observed $i(k)$, the first peak of the two layer stacking model, curve b, seems too broad and has its peak position a little lower than the measured peak. The width of the first peak of curve c and d seems much better

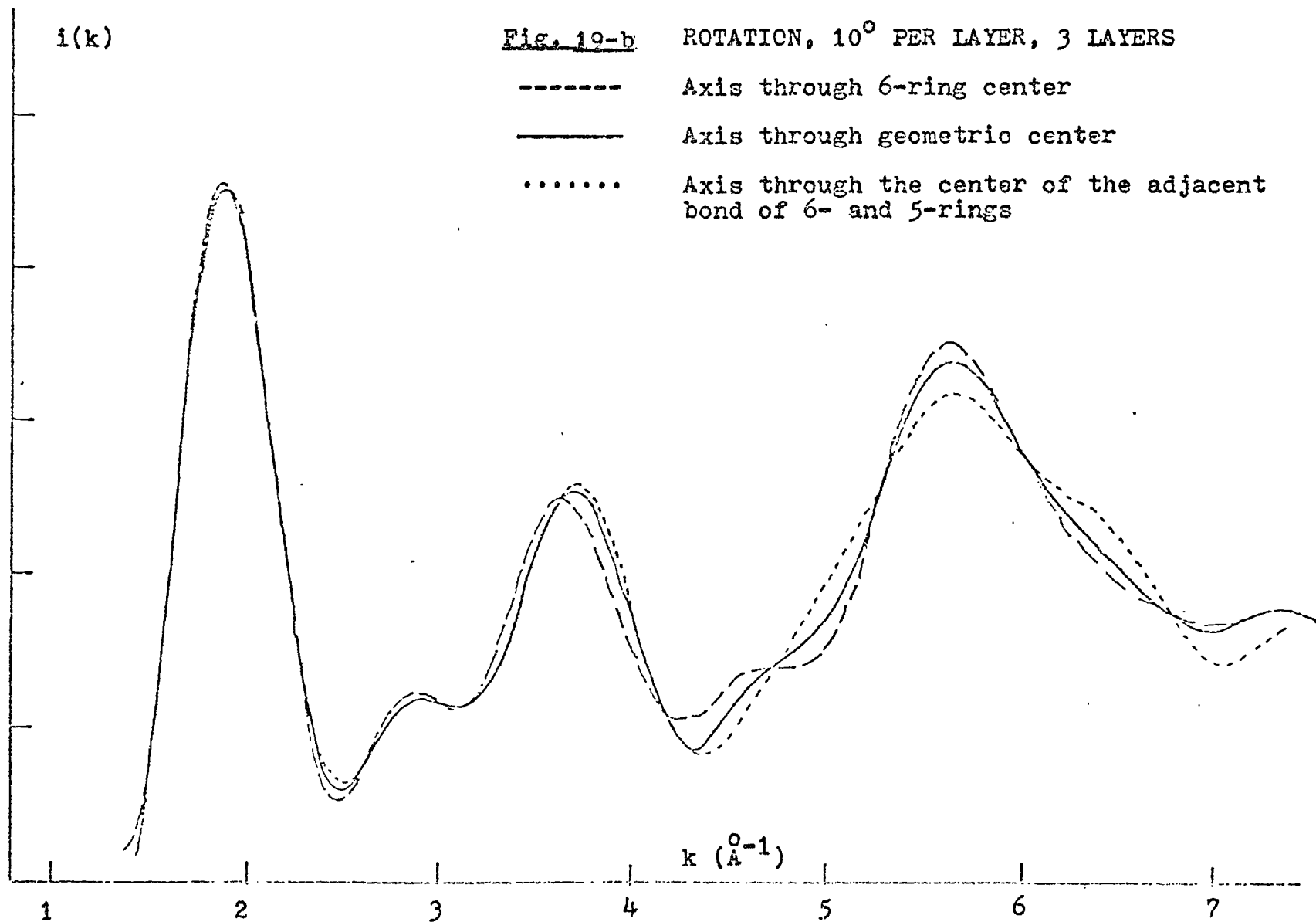


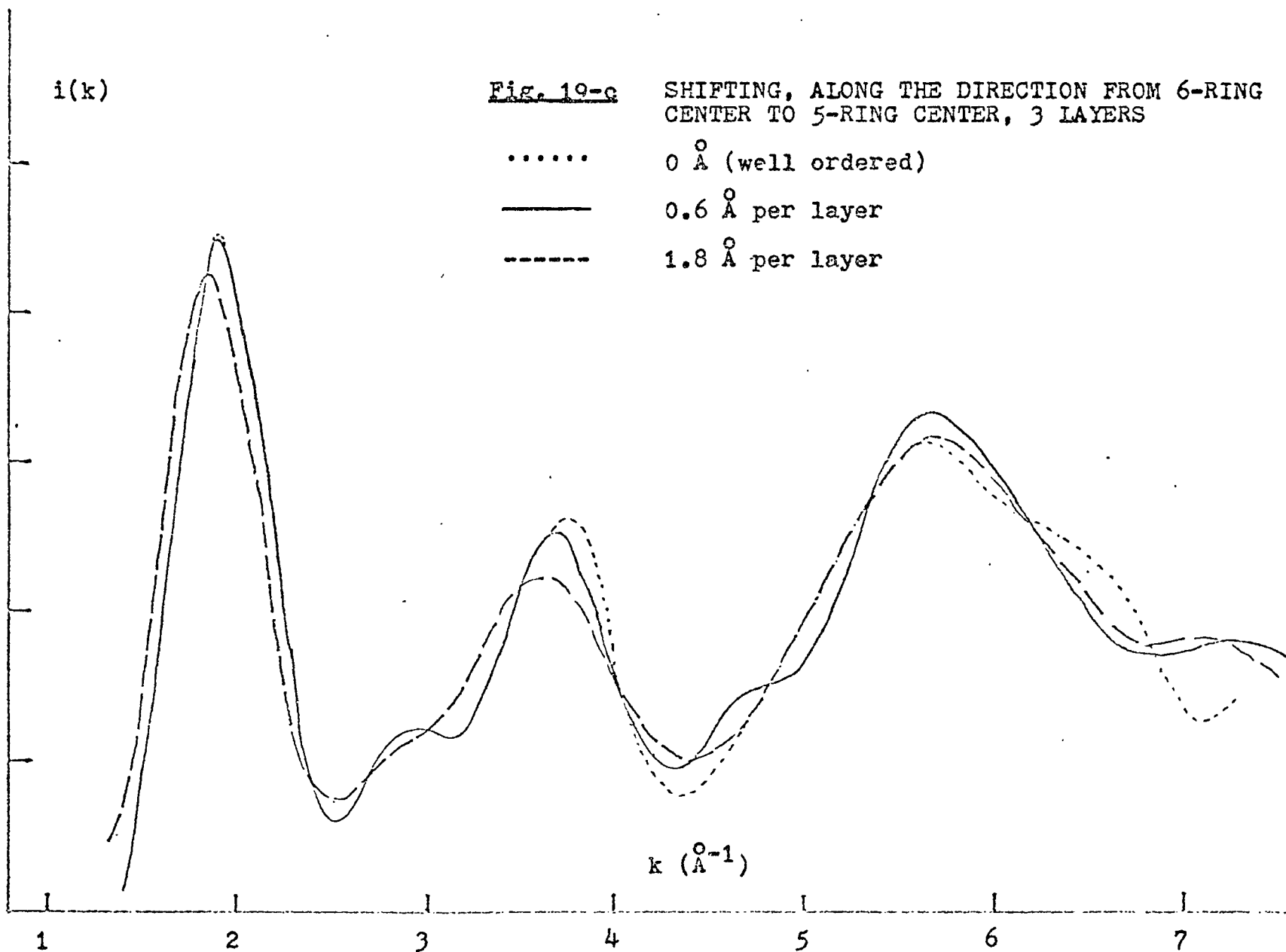
in agreement with the experimental value. Although the third peaks, at $k \approx 5.7 \text{ \AA}^{-1}$, fit well with the experimental result, the second peak $k \approx 3.7$, was not observed in the experimental $i(k)$. Instead, the observed $i(k)$ has a peak at $k \approx 3.1$ and a shoulder at $k \approx 3.6$. In order to match the calculated and observed $i(k)$ curves, the three layer stacking model was selected and some attempts to disorder the stacking orientation, such as rotation, shifting and tilting have been done. The calculated $i(k)$ of these disordered models are given in Fig. 19-a to Fig. 19-e. Unfortunately, none of these curves has a satisfactory fit for the peak at $k \approx 3.1 \text{ \AA}^{-1}$ and the shoulder at $k \approx 3.6 \text{ \AA}^{-1}$ of the observed $i(k)$.

(2) Models with the 4- and 8- monomers layers:

The failure to find a peak at $k \approx 3.1 \text{ \AA}^{-1}$ was relieved by using the 4-monomer and 8-monomer layer models. The calculated $i(k)$ of one of these layers is given in Fig. 20 in comparison with the $i(k)$ of the one-monomer layer, where we can see a peak starting to build up at $k \approx 3.1 \text{ \AA}^{-1}$ in the 4- and 8- monomer single layer. Calculating the $i(k)$ of the three stacked 8-monomer layer model, Fig. 21, even though a peak at $k \approx 3.1 \text{ \AA}^{-1}$ and a peak at $k \approx 3.7$ were obtained, shows the first $k \approx 2$ peak too high and the broader peak at $k \approx 5.8$ too sharp in comparison with the observed







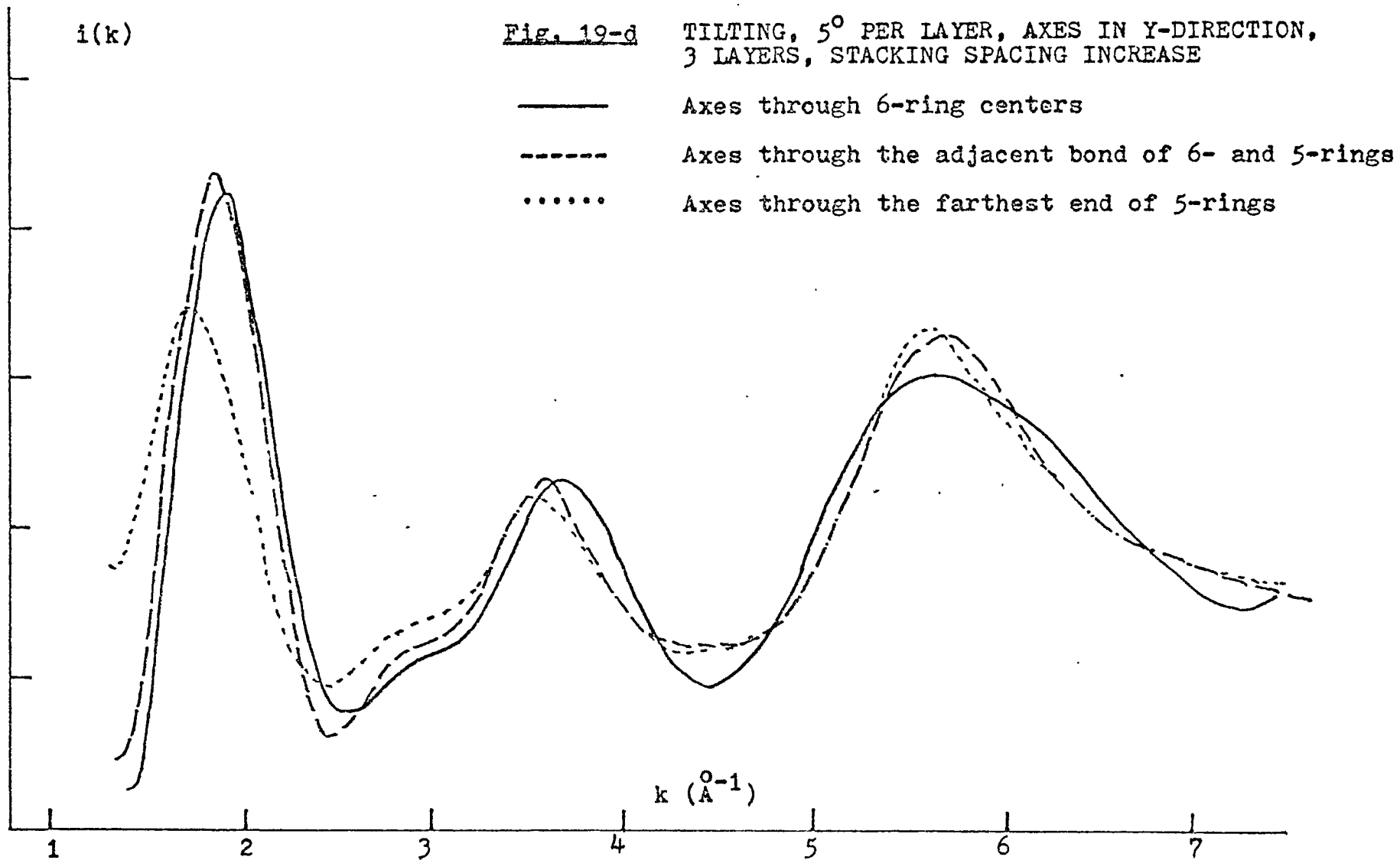
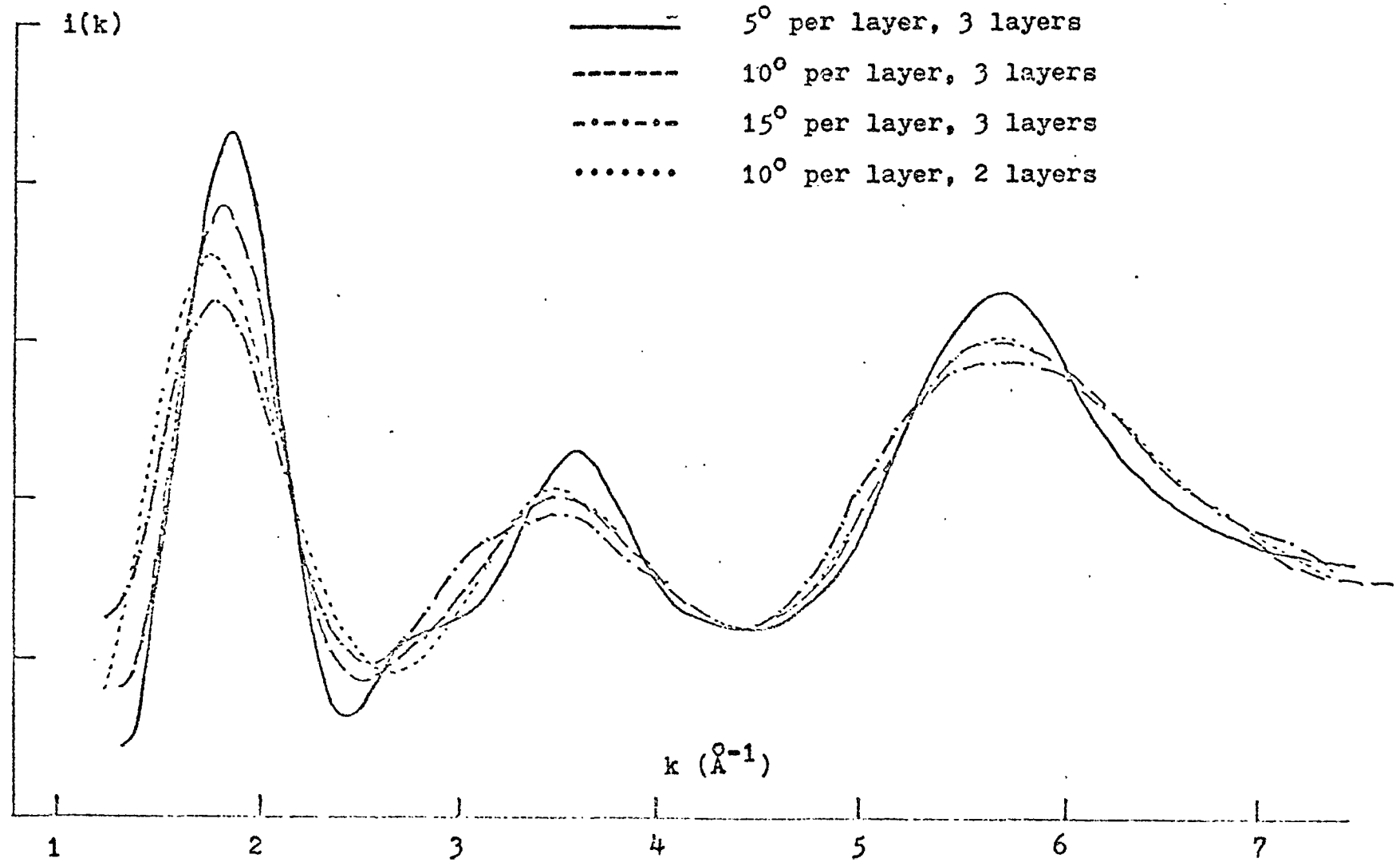


Fig. 19-e

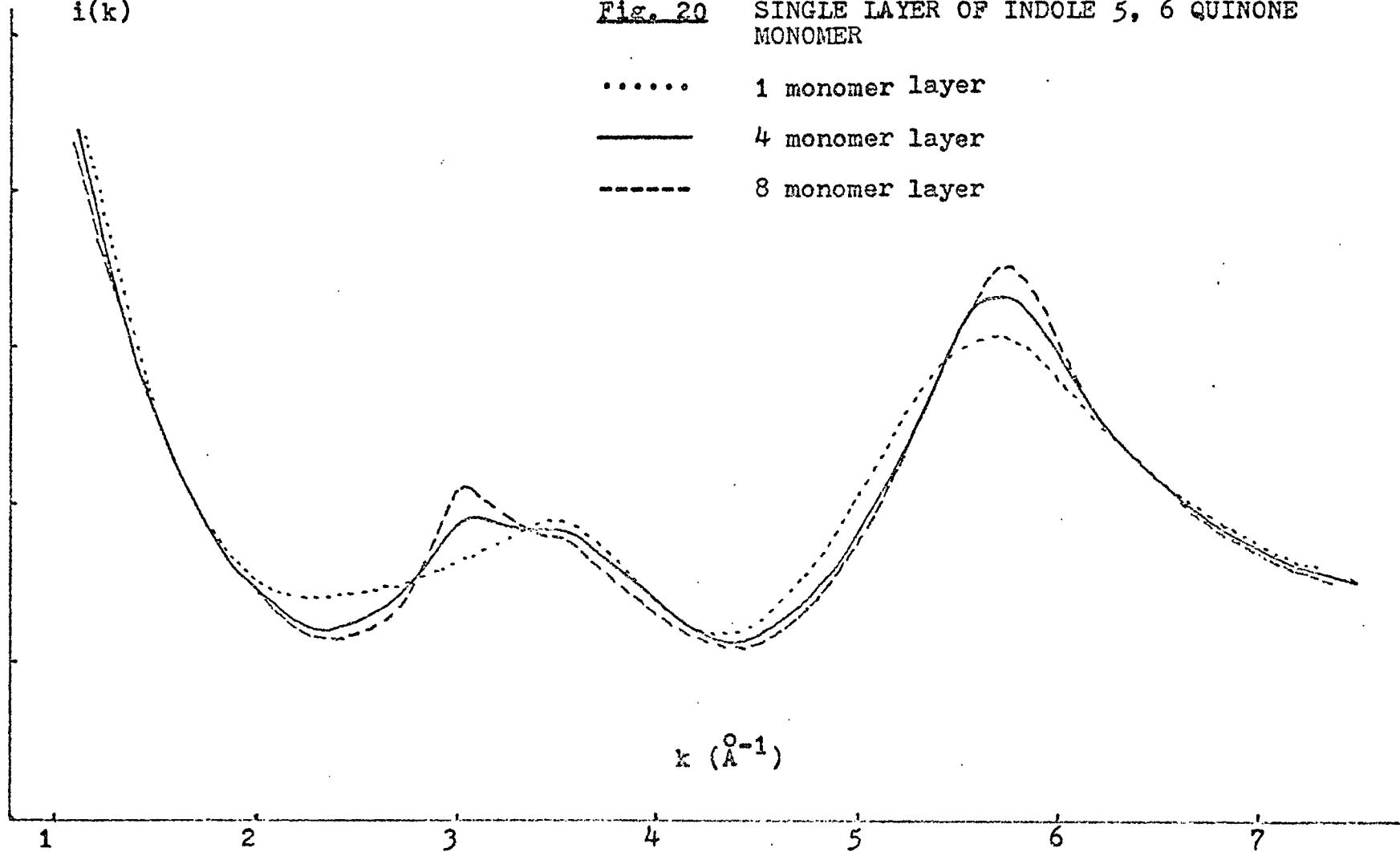
TILTING, AXES IN Y-DIRECTION THROUGH THE ADJACENT BOND OF 6 AND 5 RINGS



$i(k)$

Fig. 20 SINGLE LAYER OF INDOLE 5, 6 QUINONE MONOMER

- 1 monomer layer
- 4 monomer layer
- 8 monomer layer



$i(k)$

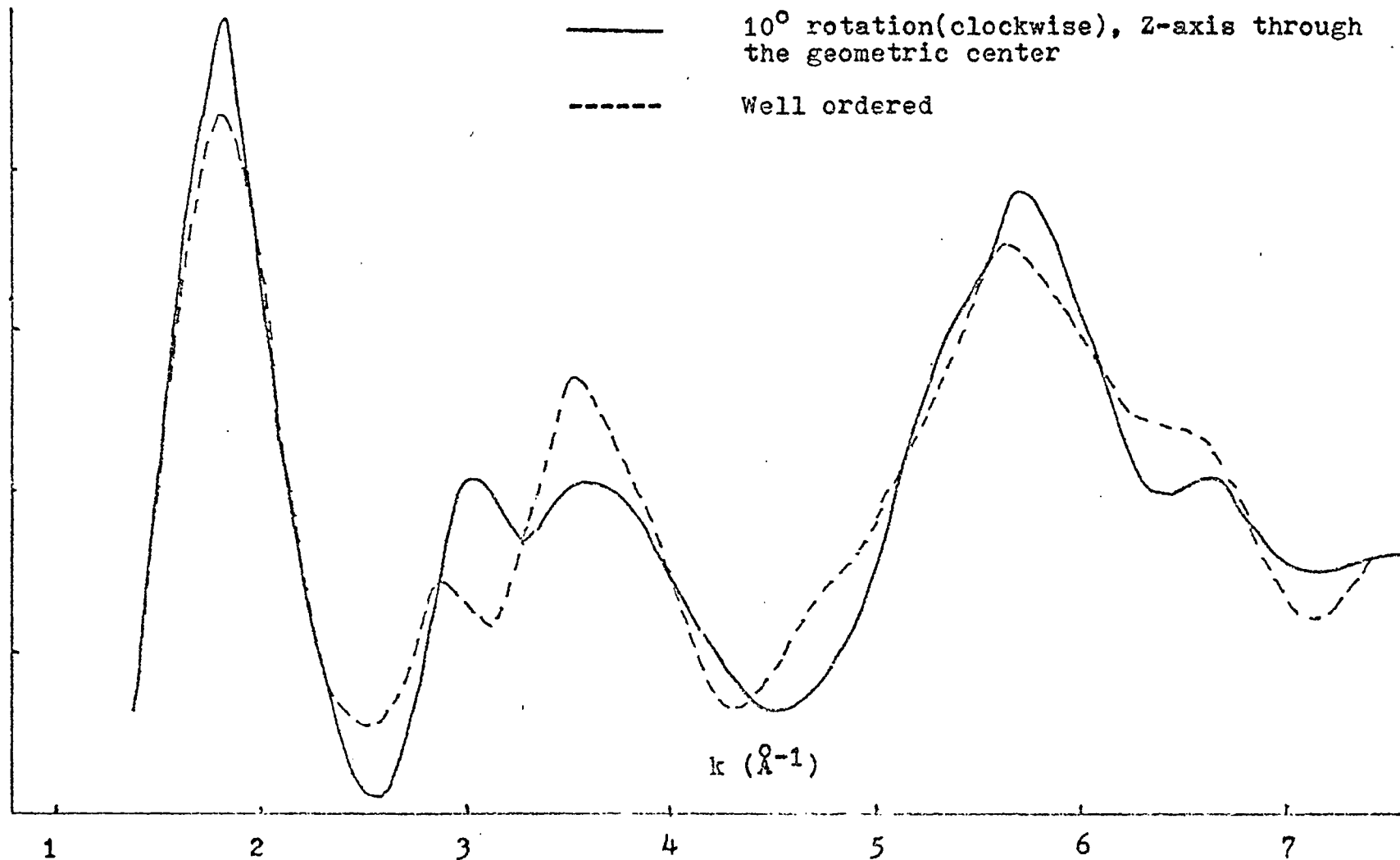
Fig. 21

STACK OF THREE 8-MONOMER LAYERS

————

10° rotation (clockwise), Z-axis through the geometric center

Well ordered



$i(k)$. Since it is known, from Townsend's ⁽⁴⁸⁾ study of the X-ray diffraction from a microcrystalline random layer structure, that the displacement (shifting) disorder would bring down the stacking peak, (the first peak) a stacking model with three of the 4-monomer layers was studied with disorders of rotation, shifting, tilting and disturbed side atoms. Tilting disorder was found to be impossible, as shown in Fig. 22, giving a worse fit to the observed $i(k)$. A combination of the rotation and shifting disorders was achieved by rotating around a perpendicular axis which has a finite distance from the axis through the geometric center of the planar layer. The final, or 'best', fitted curve of $i(k)$ was obtained from such a model of three 4-monomer layers stacked with 5° rotation around the Z-axis that goes through the geometric center of the 8-monomer layer model (Fig. 17-b) with the side atoms, oxygen and nitrogen, randomly tilted by no more than 0.02 \AA in their Z direction. Fig. 23 shows the resulting $i(k)$ curves calculated from this model with and without the side atom disorder. Randomly tilting the side atoms was noted to bring down the peak at $k \approx 3.6 \text{ \AA}^{-1}$, which gives a better fit to the observed curve. Fig. 24-a is the final fit of the calculated and measured $i(k)$ curves in the region of the Cu-radiation. Comparison of the final measured $i(k)$, Fig. 10-b, to the

$i(k)$

Fig. 22

THREE 4-MONOMER LAYERS STACKING, TILTED 4° EACH LAYER AROUND Y-AXIS

----- Tilted to increase the stack spacing

..... Tilted to decrease the stack spacing

————— Sigma Chemical supplied melanin

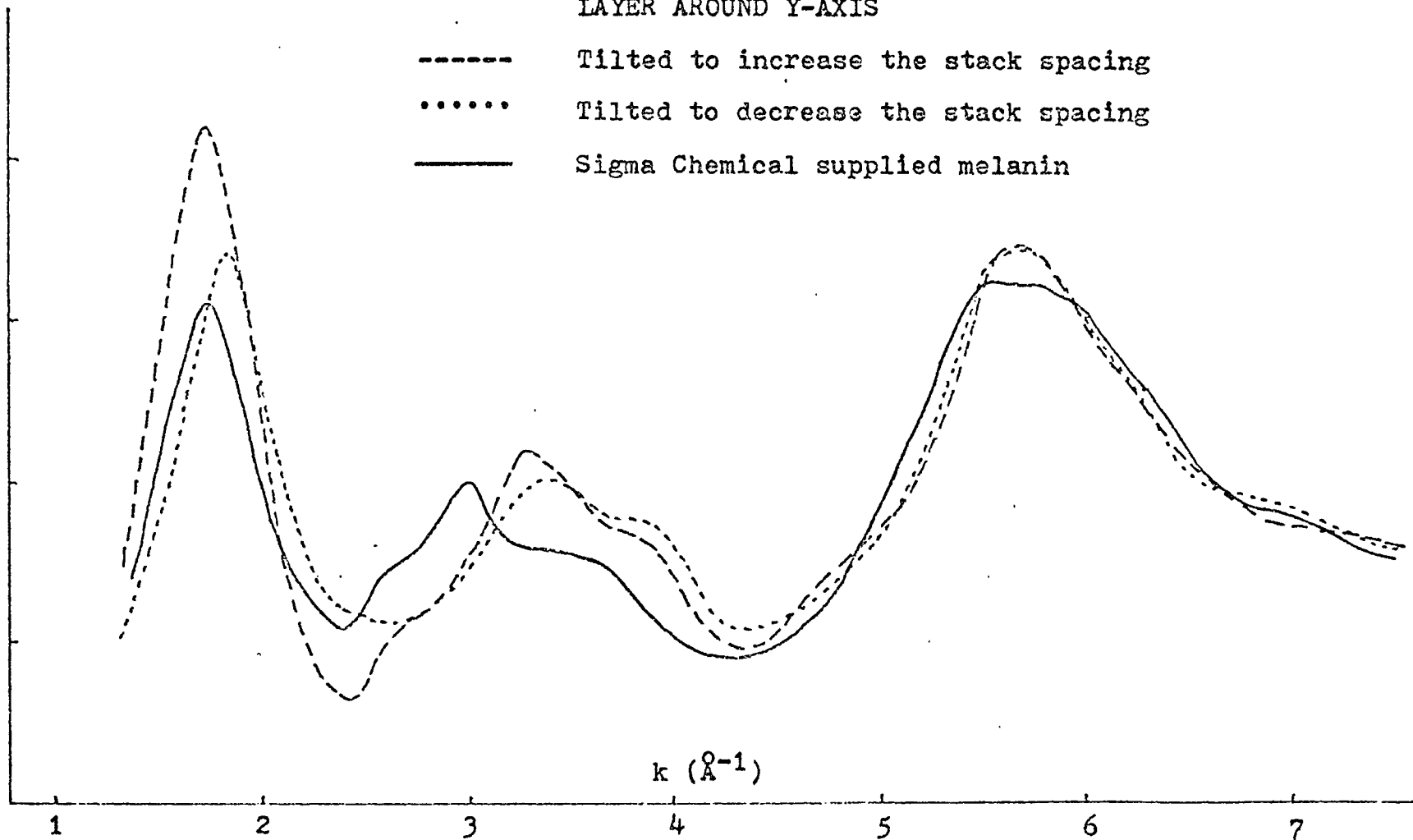


Fig. 23

STACKS OF THREE 4-MONOMER LAYERS
ROTATION 5° PER LAYER AROUND THE
AXIS IN Z-DIRECTION THROUGH (0,0)

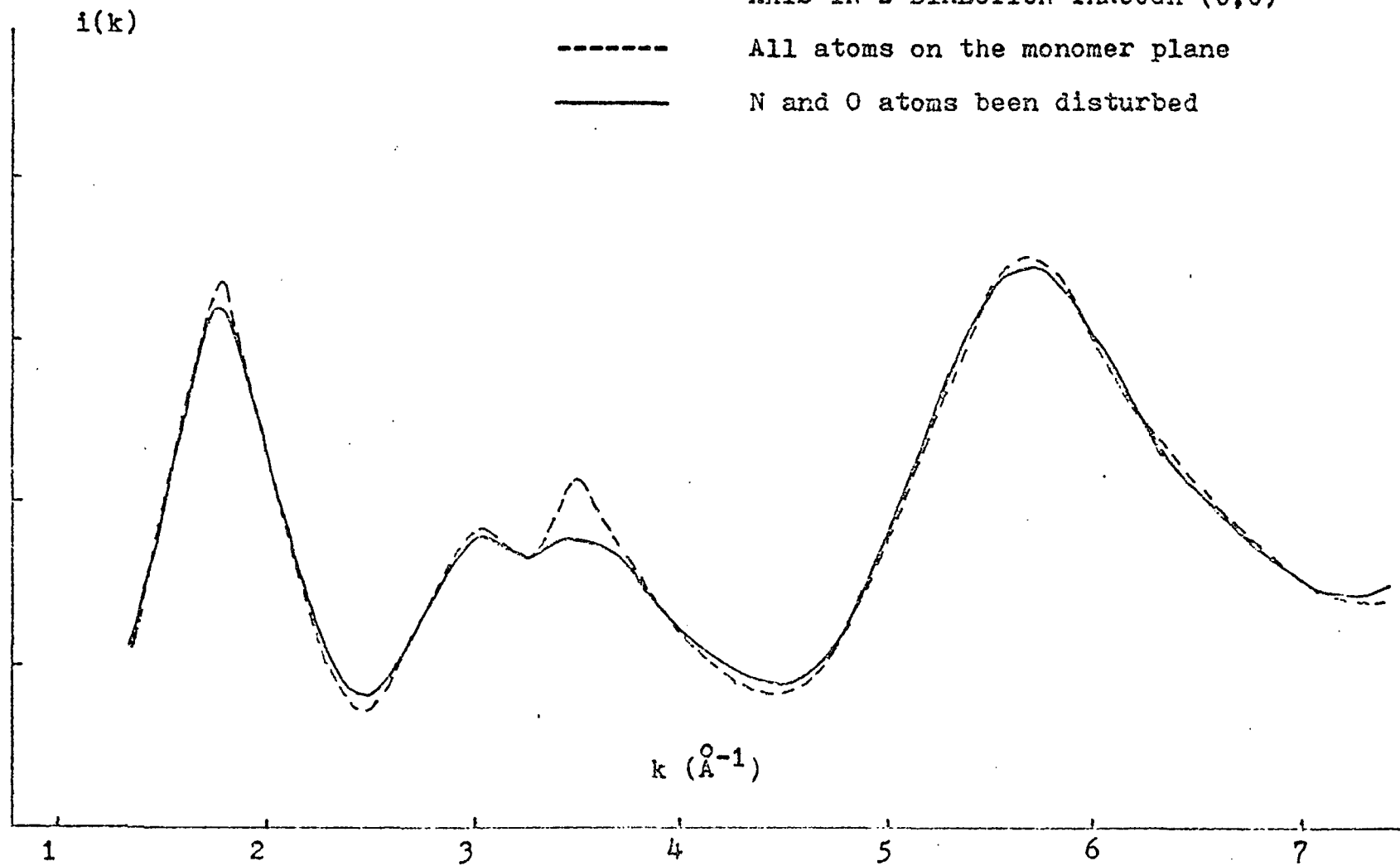
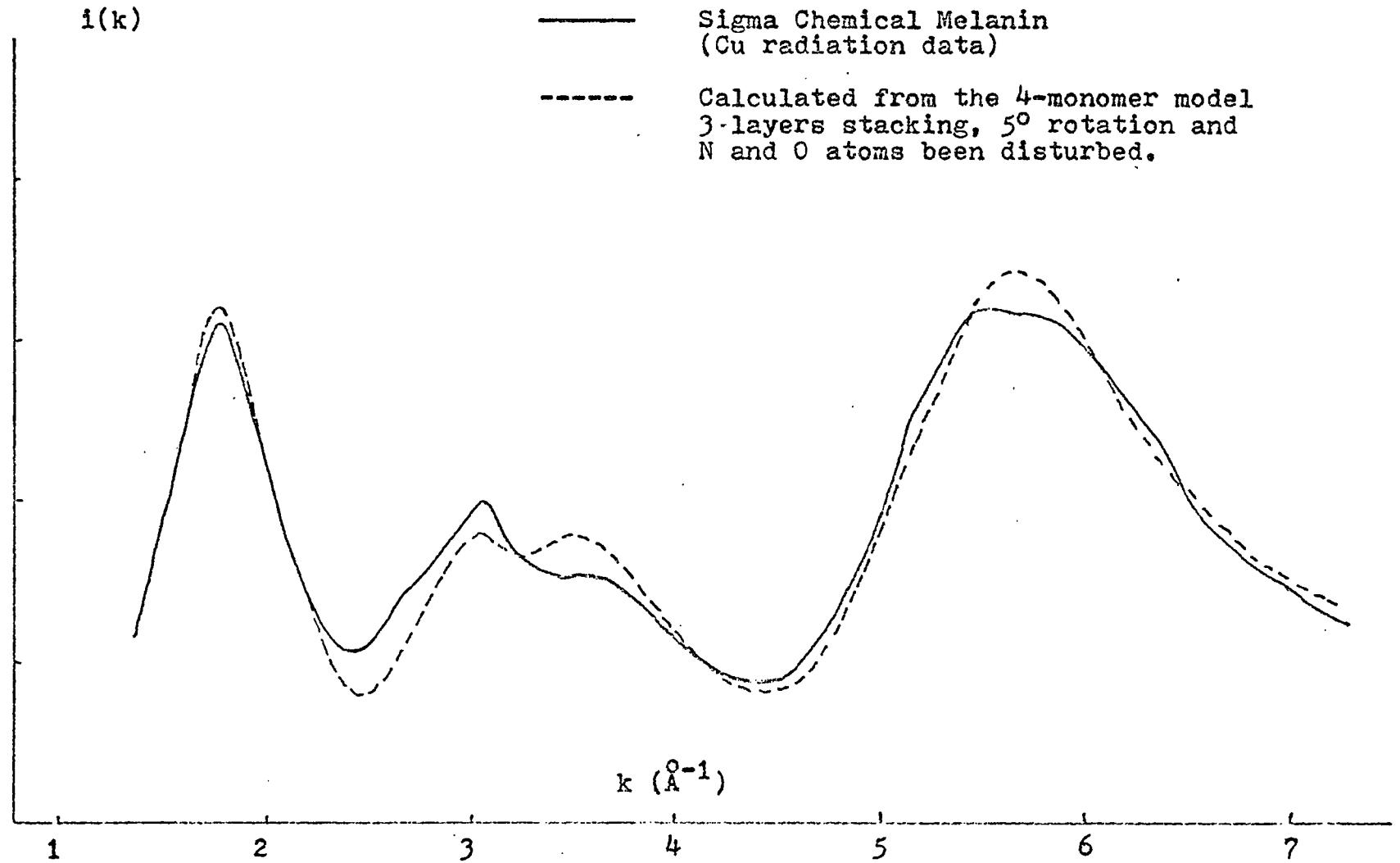


Fig. 24-a



calculated $i(k)$ up to $k = 19 \text{ \AA}^{-1}$ is given in Fig. 24-b. While the fit is not perfect the trend, as best we could explore it, seems correct - namely to bring up the peak at $\sim 3.1 \text{ \AA}^{-1}$ and bring down the peak at $\sim 3.6 \text{ \AA}^{-1}$ while preserving the height, width and position of the first (interlayer) peak. Once this fit has been more or less achieved it should be true that we now have specified the monomer and its relative organization. Therefore, the higher k region should be well fit, being more sensitive to local rather than long range features. In Fig. 24-b, this seems to be the case.

4. Discussions

Since melanin is well known as an amorphous or random polymer, and therefore there are probably no two identical melanin samples in existence, the construction of the 8- or the 4-monomer layer model, Fig. 15-b, can be based only on our best knowledge about the types of bonds in the melanin polymer which was in turn concluded from the chemical studies as described by Nicolaus in his book⁽⁹⁾. In our models, there were no -C-O-C- and -C-O-O-C- types of bond connection, since these kinds of linkage do not entirely guarantee that the next connected melanin monomer will stay in the same plane; they were therefore not used in our current study of the random stacking of planar layers. But these types of

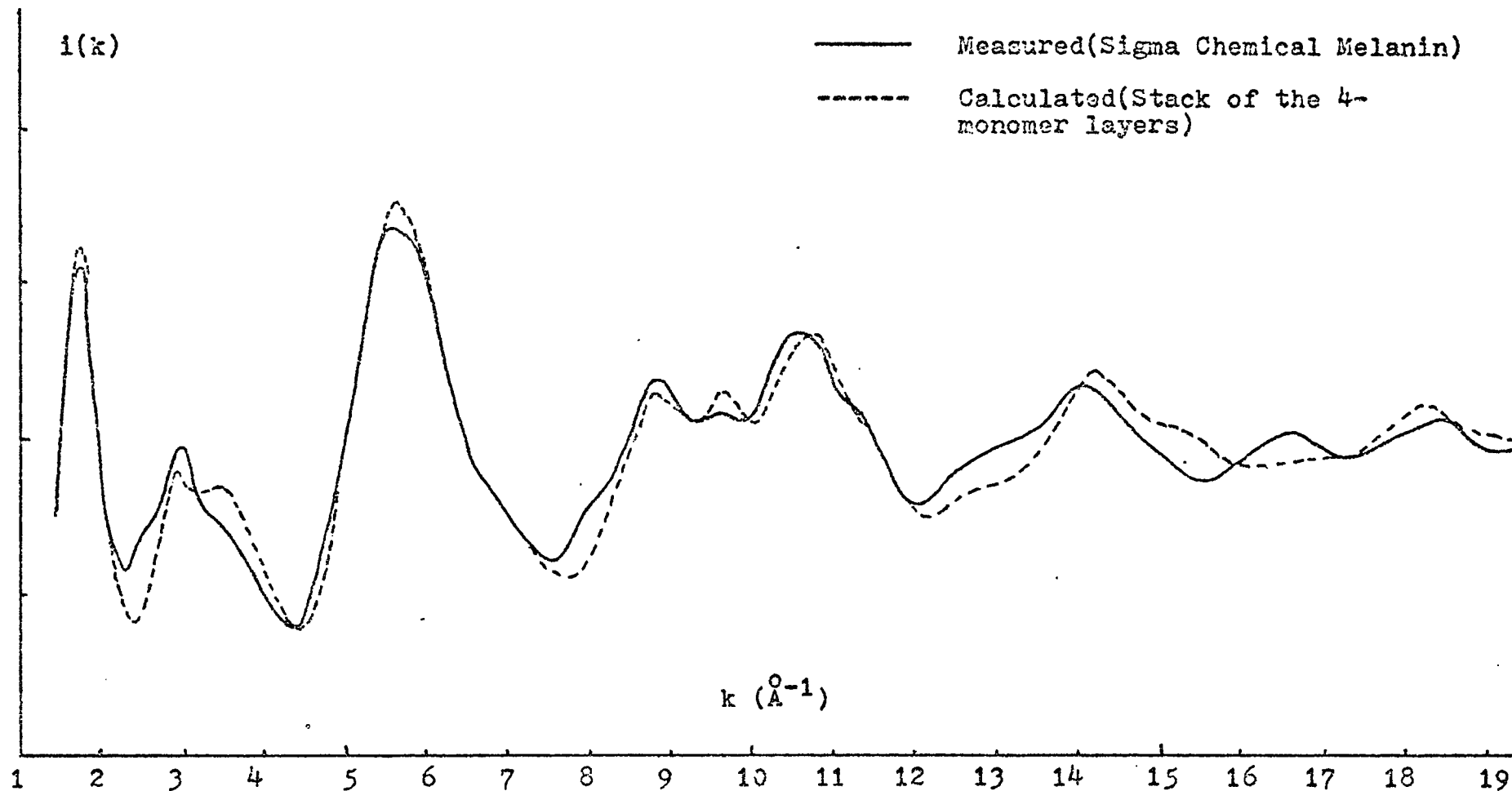


(Fig. 24-b) Comparison of the measured interference function for the Sigma Chemical supplied melanin to the calculated $i(k)$ by stacking three of the 4-indole quinone monomer layers, rotating 5° per layer around an axis in Z-direction through (0,0) and disturbing the N and O atoms by changing their Z positions not more than 0.02 Å.

bonding, as well as those possible side groups, such as -COOH and -OH, may play important roles in the formation of a real (complicated) three dimensional melanin polymer, and would be a good place to continue further study of the structure of melanin. Because of the errors in the bond-lengths, the bond-angles (especially as noted earlier for 5-rings), and accompanying distortion of the model, the interatomic distances obtained from the measured atomic positions will shift by some amount. This systematic shift probably caused the position shifts of the peaks at higher k , observed in Fig. 24-b.

As far as the layer stacking is concerned, of course there is no reason, again, to select any combination of any particular planar layer model for the 3-D connected melanin polymer. Since the stacking was expected to have an effect mainly on the first diffuse peak, the decision to use the same layer for stacking seems good enough for our current study. Because of the termination of the model being used and the unknown fraction of the planar units in the melanin sample, the ratio of the areas of the observed and the calculated $i(k)$ peaks was noted to have a lower limit of about .4 in Thathachari's study of the catechol melanin⁽⁸⁾. Similarly, in our tyrosine melanin sample, we found the second major peak ratio of about .6 was necessary for the 'best' model to match its $i(k)$ to the observed curve.

This ratio may give a general idea about the fraction of planar units in melanins, but we need more information about the composition of melanin and further studies on structure to resolve entirely the question.

5. Summary and Conclusions

From the model study, the tyrosine melanin polymer seems to have the following features in its local atomic structure: a) It contains the basic planar indole quinone type monomer. b) The planar monomeric units have a tendency to form a lamellar structure with more than one unit in the layer (4 units were used here). c) The planar layers have a tendency to form a graphite-like stacking which may extend to three or four stacking layers with random mutual orientations.

With all of these stacked and non-stacked units, and with the side groups linking together randomly, one may then propose a "most possible" structure of the amorphous melanin where the present cluster of, say, 3 stacked layers of 4 units each represents one possible piece of a large fully connected 3-D melanin polymer network. This cluster can be considered as a "paracrystalline" unit or building block with the understanding that the melanin which it represents cannot be crystallized (or even suffer grain

growth) either by heating or by pressing. It is therefore almost certainly a 3-D random polymer and not merely a quasi-crystalline substance like bulk "amorphous" carbon or the various forms of disordered graphite. We do, however, allow the possibility that the structure of melanin is locally heterogeneous with a mixture of the 3-layer units in a more random monomeric structure.

CHAPTER FIVE

ELECTRON SPIN RESONANCE STUDY

1. Introduction

Since the ESR absorption spectrum of melanin consists of a single broad structureless line, the significant information one can obtain from ESR studies of the free radical is limited to determinations of the g-value, the line width, the spin-lattice relaxation time and the free radical density. The most complete ESR study of melanins up till now has been done by Blois et. al.⁽⁵⁾ Although changes in the spectra associated with different water contents were noted, no detailed study was made of the nature of this effect. In studying the literature it became clear to us that many contradictory results could be resolved if one took into account the effect of water on the spin signal. In this work we therefore decided to study the effect of water content on the ESR signal characteristics, concentrating on the variation of line width, spin-lattice relaxation time and spin density, resulting from variation of the water content of the melanin sample. Hopefully, as a consequence of the water-effect study we may be able to better understand the effect of other physical parameters such as particle size, shape and surface, water affinity

and effects of dopants, that influence the free radical properties of melanin.

2. Materials and Methods

(1) Melanins:

The majority of the ESR studies were on synthetic melanins prepared by auto-oxidation of L-dopa. These samples were prepared by Dr. John E. McGinness of the University of Texas System Cancer Center. Along with the pure L-dopa melanin, Dr. McGinness also prepared L-dopa melanins doped with either diethylamine (DEA) or homo-cystine-thio-lactone (HCTL), two drugs of current interest for chemotherapy treatment in melanoma. Although our studies of these 'doped' melanins are by no means exhaustive, partial results have been included here since they indicate some interesting trends. Melanin supplied by Sigma Chemical, which was synthesized from tyrosine, was also studied.

(2) Control of the water content in melanin:

The as-received melanin samples had a relatively large initial water content, determined primarily by the method of preparation and their subsequent storage. We classified these untreated melanins as wet. Using a combination of vacuum dessication and heating we found that it was possible to remove a weight of water which varied from 10% to about

50% of the original total wet melanin mass. The variations in total water content of different samples is not thought to be associated with their previous storage history, but rather to be a fundamental effect due to the differences in particle size, shape, surface configuration and impurity doping. This will be discussed later.

We considered that water removed by a combination of 'pumping' and 'heating' processes would be sufficient for a qualitative study of the water effect in melanins. We first noted that pumping alone, no matter how good the vacuum, has little effect on the ESR signal, and that heating in a high vacuum (10^{-5} Torr), or in a rough vacuum (lower than 10^{-2} Torr), or even in the absence of vacuum, produced a significant effect on the ESR signal. Previous investigators observed some changes in the ESR spectra when the melanin was dried by lyophilisation as vacuum dessication, but no one appears to have used a combination of heating and vacuum dessication. Our thought was that if the water in melanin was somewhat strongly absorbed, it would require some heating to free this water. Fortunately, the melanin free radical is quite stable and is not destroyed by heating to quite high temperatures. In order to determine the high temperature limit, we examined L-dopa melanin in a

differential scanning calorimeter and found a decomposition peak at 280°C. We therefore avoided heating much above 200°C in our drying treatment. Since it was noted that a significant increase of ESR signal occurred only when samples were heated at a temperature higher than 150°C but that little additional change was noted for heating in the range 200°C to 250°C, we decided to use 200°C as our standard drying temperature. Heating at 200°C, in a rough vacuum was thought to be a reasonable way for obtaining sufficiently dry melanin samples suitable for ESR studies. This degree of heating is also thought to be necessary in order to study the effects due to the tightly bound - so called 'hard' water - observed in our X-ray diffraction study. Although it is clear that there is very little reason to study biological materials at such an elevated temperature, there may be important insights gained which relate to the biological functions of melanin from such high temperature studies.

In order to make sure that most of the water had been removed by heating the melanin under vacuum, a study of the relation between the weight loss and ESR signal as a function of the length of time that sample is held at the high temperature was performed. We will show later that it requires more than one hour of heating to reach a steady state.

Also, in order to make sure that the dry sample is maintained in an equilibrium state, we either sealed the sample under vacuum or else filled the sample tube with air which had been dried. In either case we found little change in either the ESR signal or the sample weight over time periods of the order of weeks. All samples were cooled to room temperature after sealing and unless otherwise noted, all ESR spectra were recorded with the sample at room temperature.

In order to determine whether the effects observed when water was removed could be reversed if water was allowed to be reabsorbed, experiments were performed in which water vapor was allowed to interact with the sample and the subsequent decay of the enhanced ESR signal was followed. Typically, a swab of cotton saturated with water was inserted in the top of the sample tube so that it was outside the microwave cavity and the ESR signal observed as a function of time. The samples are not in equilibrium with their surroundings, however, since the ESR scanning time (2 min.) is much smaller than the rate at which the ESR signal is quenched, this method should provide an adequate means for studying the rate of reabsorption.

(3) ESR Measurements:

All ESR measurements were made using a Varian model E-3 spectrometer (X-band, 100 KHz field modulation).

Since melanin has an unusually long spin-lattice relaxation time, some care must be taken to avoid saturation effects. Saturation effects were found down to a power level of about 4 mw. therefore, in determination of line widths and signal strengths a microwave power of 1 mw. was used in order to avoid saturation effects.

By comparing the area of the integrated ESR signal of melanin with a standard diphenyl-picryl-hydrazyl (DPPH) sample, we obtained the total spins (free radicals) contained in our melanin samples. Observation of the ESR signal as a function of microwave power permits the determination of the spin-lattice relaxation time, T_1 . Details of the T_2^* method of Castner⁽⁵⁰⁾, which was employed here, are presented in Appendix B.

3. ESR Studies of Wet and Dry Melanins

Dry samples, as has been noted before, are prepared by holding the sample at a temperature of 200°C for about one hour while it is being maintained under a rough vacuum. The dried sample is sealed and allowed to cool back to room temperature. What we call wet samples are those samples

which have been hydrated by being allowed to reach equilibrium while being exposed for long periods (weeks) to moist air. Unfortunately the time taken to reach final equilibrium may be very long, so that we cannot be sure of the exact state of hydration. However, there is comparatively little change in water sensitive properties after a certain minimum amount of water has been absorbed, so that it was not considered important to standardize wet samples with precision.

It is interesting to study the relation between the amount of water released from the sample and the temperature to which the sample has been heated. The results of one experiment are illustrated in Fig. 25 (a and b). A sample was heated in an oven held first at 100°C , and after each five minute heating interval, the sample was removed from the oven, cooled, and its weight and ESR spectrum measured. The increase in the weight loss and ESR spectrum intensity tend to level off after the sample has been kept at 100°C for a total time of 90 minutes. The oven temperature was next raised to 150°C and the experiment was repeated using the sample which had previously been equilibrated at 100°C . The second branches of the curves in Fig. 25 illustrate the growth of the weight loss and the ESR signal in this phase of the experiment. Finally, the oven temperature was raised to 200°C and the experiment repeated once more; the

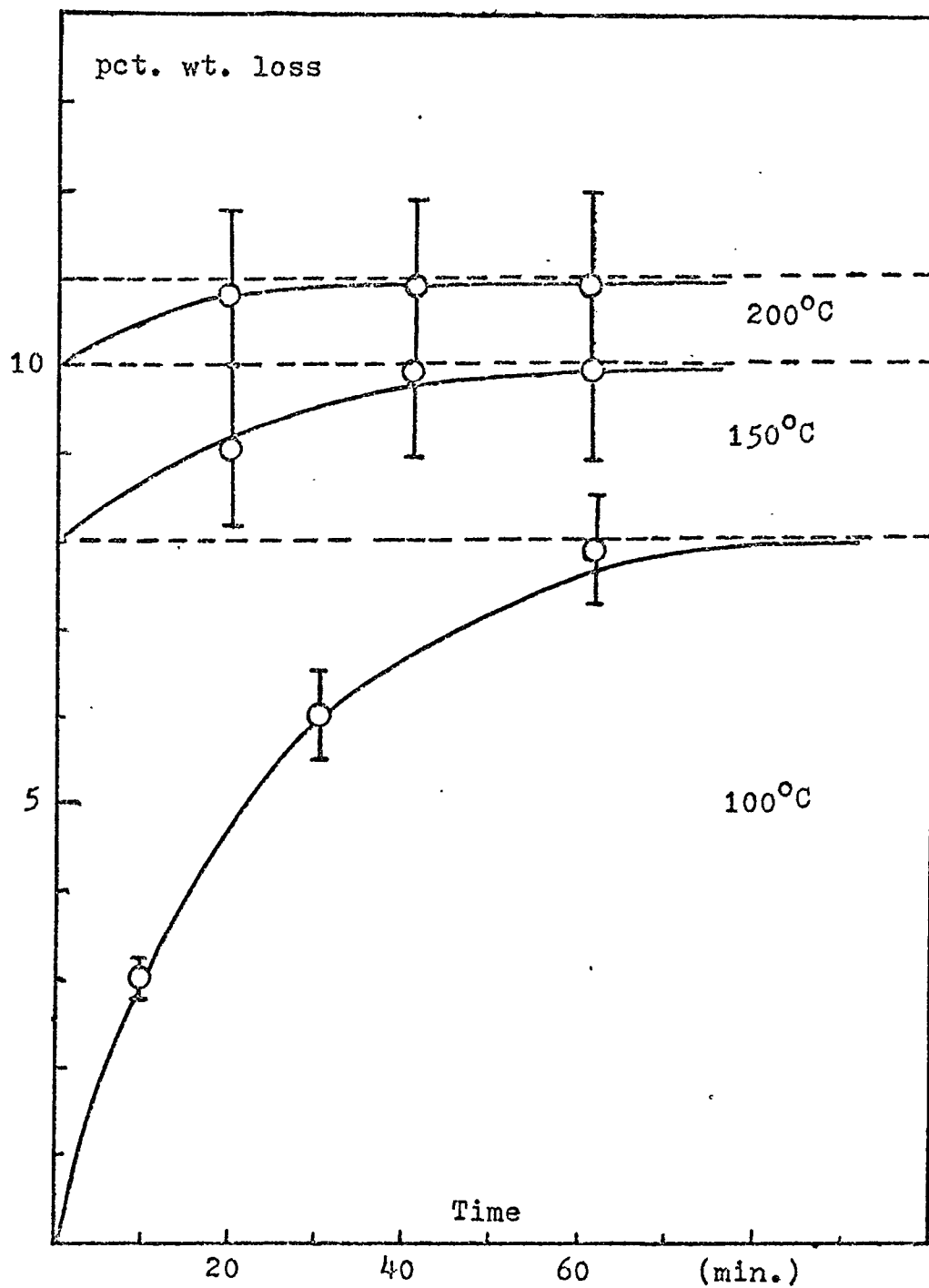


(Fig. 25-a) Percent weight loss of an L-dopa melanin sample vs. total time of heating at 100°C, 150°C and 200°C.

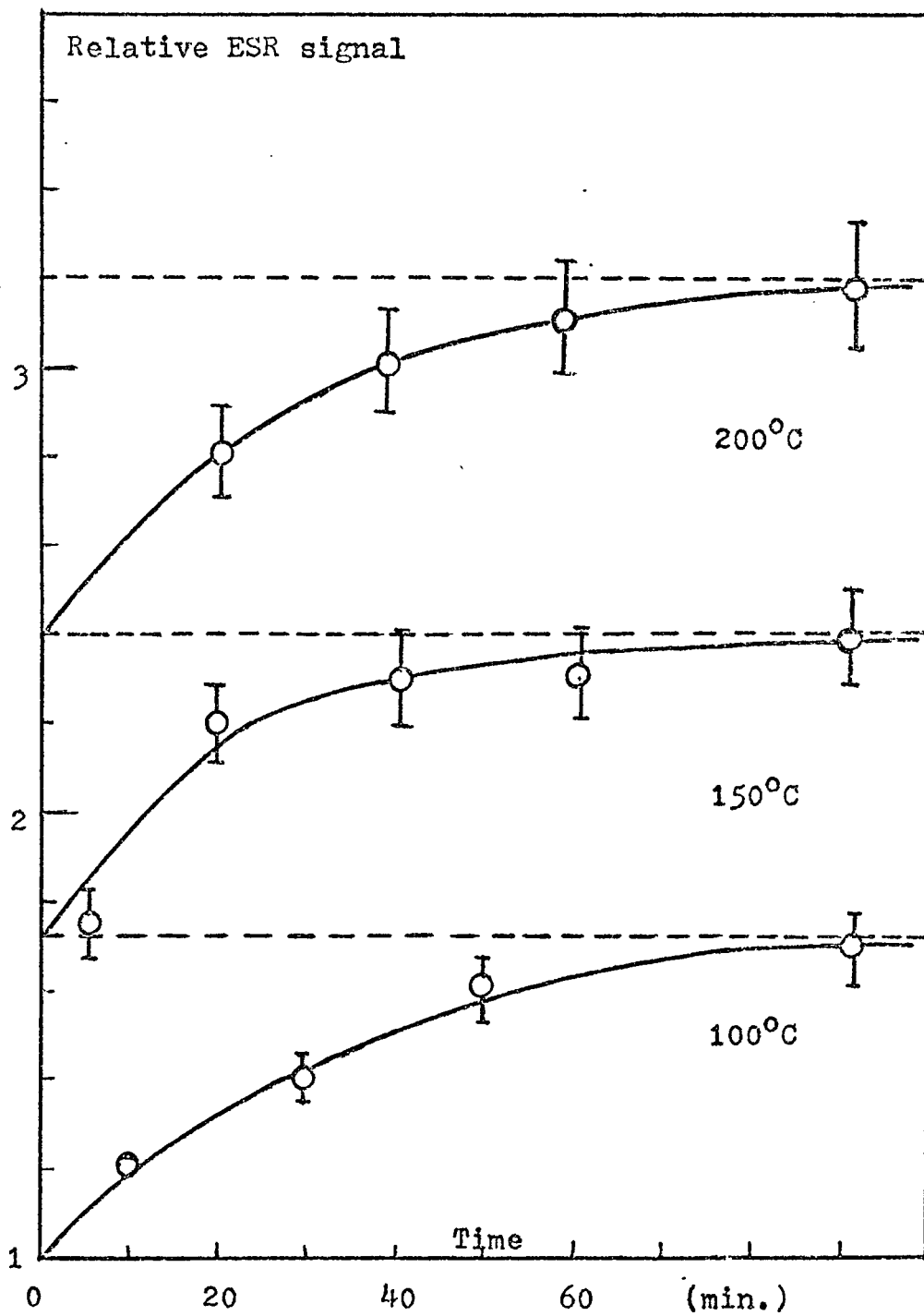


(Fig. 25-b) Room temperature ESR signal vs. total time of heating.

third branches of the curves in Fig. 25 give the results for this portion of the experiment. We conclude from the weight loss curves that a relatively long time is required to remove the water from a sample and that the water which requires the highest temperature for its removal also requires the longest incubation time for its removal. This last fraction of water we designate 'hard' water. We further conclude from the ESR curves that the ESR signal increase with the loss in weight (by heating) also needs a relatively long time, as that for the removal of water, to reach saturation. It is clear that the weight loss is strongly correlated with the increase in ESR signal. We assume that the weight loss is accounted for by the loss of adsorbed water from the sample and that the effects on the ESR signal are a direct result of the removal of this water. The fact that the ESR signal is observed to be restored to its original state when the sample is allowed to adsorb water gives us added confidence in the correctness of this assumption. We should note that the adsorption process is extremely slow (many days).

The spectrum parameters which are of interest in this study are line width, spin-lattice relaxation time, and spin density. The line width is easily observed, provided that one makes sure that the microwave power level is well below saturation level. The determination of T_1 and spin density are more complex and require establishing that the

signal is inhomogeneously broadened. A succession of spectra over a range of microwave powers in the saturation range is required. Analysis of these spectra and the calibration information, provided in this case by a standard free radical sample (DPPH), allow us to calculate both T_1 and spin density for our samples. The details of this method are presented in Appendix B. The results obtained are given in Table III.

The results in Table III indicate that drying the sample tends to increase both the spin density and line width, but to decrease the spin-lattice relaxation time. If the removal of water leads to an increase in spin density we might expect that the distance between spins would be decreased, provided that the spins are randomly distributed. Consequently, one might expect an increase in the spin-spin interactions simply because of the lowered inter-spin distance, and this in turn, would lead to a large increase in line width. No such large increase is noted. The small increase in line widths actually observed may indicate that the 'extra' spins produced by water removal are located in a restricted region and are not distributed throughout the entire sample volume. This suggests that the removed water was restricted to a surface or quasi-surface region of the melanin granule.

Table III

Line width, T_1 and Spin density of Wet and Dry Melanins

Type of Melanin	Line Width (gauss)		Spin-lattice relaxation time (μ sec)		Spin density ($\times 10^{18}$ spin/gm)	
	Wet	Dry	Wet	Dry	Wet	Dry
L-dopa	4.7 \pm 0.3	5.3 \pm 0.4	17 \pm 9	12 \pm 6	2.2	6.4
L-dopa with 0.25% DEA	4.6 \pm 0.3	5.2 \pm 0.4	20 \pm 10	17 \pm 9	2.2	4.8
L-dopa with ~20% DEA	4.6 \pm 0.3	5.3 \pm 0.4	23 \pm 12	13 \pm 7	0.7	5.6
L-dopa with ~10% HCTL	6.3 \pm 0.5	6.3 \pm 0.5	22 \pm 11	21 \pm 11	8.7	9.4
Tyrosine	8.0 \pm 1.0	8.0 \pm 0.5	---	---	0.1	1.0

The results obtained for the tyrosine melanin sample are in strong contrast to those obtained for the L-dopa melanin samples and are presumed to be a consequence of some basic morphological difference between the two types. The results of our X-ray studies on the two types of melanins indicate that they have similar local structure. According to the Raper-Mason scheme for formation of different melanins they both should be polymerization of the same monomer unit, so that the difference must be on a scale larger than the scale of local structure. A clue to the nature of the difference between the two types of melanins is obtained from our X-ray studies; the tyrosine melanin sample appeared to have a linear absorption coefficient for $\text{Cu}_{K\alpha}$ X-ray about twice that found for L-dopa melanin sample. This difference was interpreted as arising from the enhanced small angle scattering in the tyrosine melanin sample, on account of its smaller particle size. In general, the particle size for a given melanin seems to be related to its method preparation. Although particle size effects are important the observed differences of ESR spectral parameters between L-dopa melanin and tyrosine melanin cannot be completely resolved simply on the basis of differing particle size. For example, since the observed spin density in dry L-dopa is greater than that observed in dry tyrosine, we should

expect that the inter-spin distance would be less in L-dopa than in tyrosine melanin under an assumption that there is no local structure inhomogeneity in both samples and so free radicals are uniformly distributed, and therefore the line width should be larger for the L-dopa melanin compared with that of tyrosine melanin. This is not borne out by the experimental observations. Therefore, we suggest that there is yet another physical variable besides particle size, which can affect the measured ESR signal. An attractive 'candidate' for this variable might be found in the presence of a thin surface dead layer. We assume that there is a thin surface region which is devoid of active free radicals. The remaining non-surface free radicals are shielded from interacting with external oxidizers and are quite stable. However, those free radicals which lie close to the surface may be quenched by adsorbed water. A model explaining these features will be developed later and used to explain the difference between the L-dopa and tyrosine melanins.

When L-dopa melanin is doped with either DEA or HCTL it shows a large difference in line width and spin density in the wet state. Assuming that both DEA and HCTL melanin have the same intrinsic spin density and particle size, the difference are to be attributed to modification of the surface of the melanin granule by the dopants. The HCTL sample contains

less water than the DEA sample and has a shiny looking surface. This was assumed to be mostly due to different effects of these additions on the surface of a melanin granule.

4. Dependence of ESR signal on amount of water in sample

Although one could visualize recording the ESR spectrum while monitoring the weight loss during the drying process, this is not easily accomplished. For one thing, the total weight loss is but a small fraction of the total weight of the sample tube including the melanin, small changes in water content would be difficult to measure. Instead, an indirect method of measurement was used. Here, two identical samples, each with about 10 mg of melanin, were studied, one by ESR and the other by means of a thermogravimetric analyzer (TGA), a device which records the total sample weight as a function of furnace temperature. The temperature scan rate used for the TGA was 8° C/min. The ESR sample was heated in rough vacuum for a fixed time interval at a succession of temperatures ranging from 50° C to 250° C. After each heating interval, the sample was allowed to cool down to room temperature and an ESR spectrum was taken. The changes in ESR signal intensity as a function of heating temperature and the TGA result for weight loss as a function of temperature are both given in Fig. 26. We

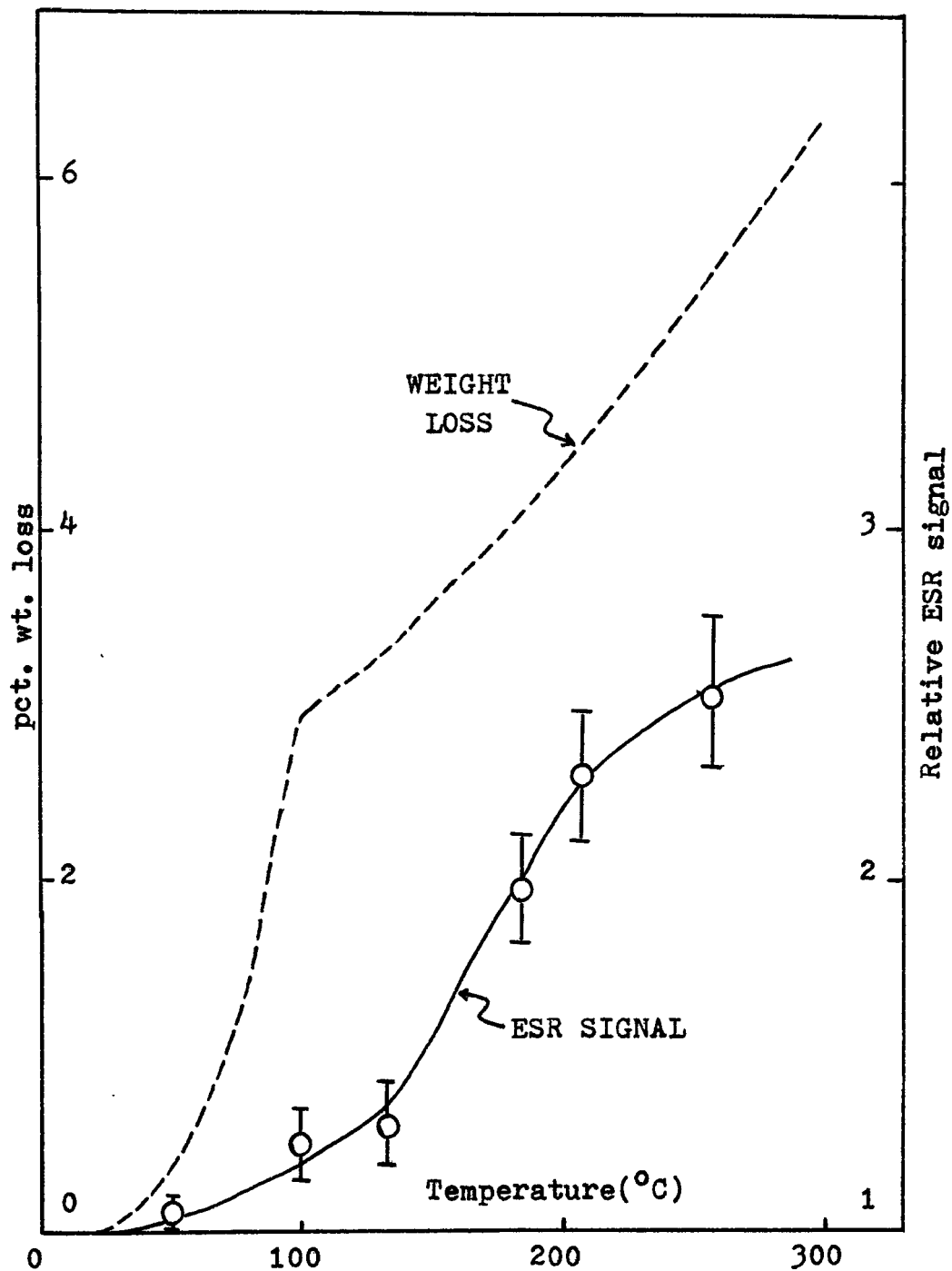


(Fig. 26) ESR signal(room temperature) and weight loss(TGA result) of L-dopa melanin vs. heating temperature.

note that much of the weight is lost at temperatures lower than 100°C, however, there is little change in the ESR signal accompanying this water loss. For temperatures higher than 100°C, the weight loss is correspondingly less, but the increase of ESR signal is large. For temperatures higher than 200°C the change in ESR signal tends to become small, but there is a continued weight loss. These results seem to indicate that the water which is released at low temperatures, the 'easy' water, that is lightly adsorbed, liquid-like water, has only a small effect on the ESR signal. The presence of this easy water are early detected in X-ray diffraction studies. In contrast to this the water released at high temperature, strongly adsorbed water, 'hard' water, which the X-ray analysis suggests may have an amorphous ice-like form, has the largest effect on the ESR signal. The continued weight loss observed at high temperature in the TGA may be associated with other process depolymerization or thermo-degradation of melanin. X-ray studies of samples heated to this temperature region suggest that this lost mass has a melanin-like structure, rather than any reasonable water-like structure.

5. Temperature dependence of ESR signal

Blois et. al.⁽⁵⁾ reported previously that the magnetization of the melanin free radical appeared to follow Curie's

Law over a wide range of temperature. Since we have shown that the number of spins contributing to the ESR signal vary with water content and that the water content varies with temperature it was thought to be of interest to check whether both wet and dry melanins obeyed the Curie Law.

ESR spectra were recorded for a wet sample using the variable temperature probe from a temperature of -100°C up to 200°C . The signal decreased with increasing temperature up to about 50°C . However for temperature between 50°C to 200°C the variations of ESR signals are dominated by variation in water content because of heating, rather than the temperature variation of the intrinsic magnetization. However, for the region of a temperature lower than room temperature, the water content in melanin can be taken as being constant. In order to have a dry sample, we held the sample at a temperature of 200°C for more than an hour, to ensure that its water content had equilibrated. The temperature dependence of the ESR signal of this dry sample was measured starting from 200°C and going down to -100°C . For this range the water content of this dry sample was constant.

The results obtained are plotted in Fig. 27, we see that both wet and dry samples follow a Curie law as long as the amount of water in sample is constant. The slope of

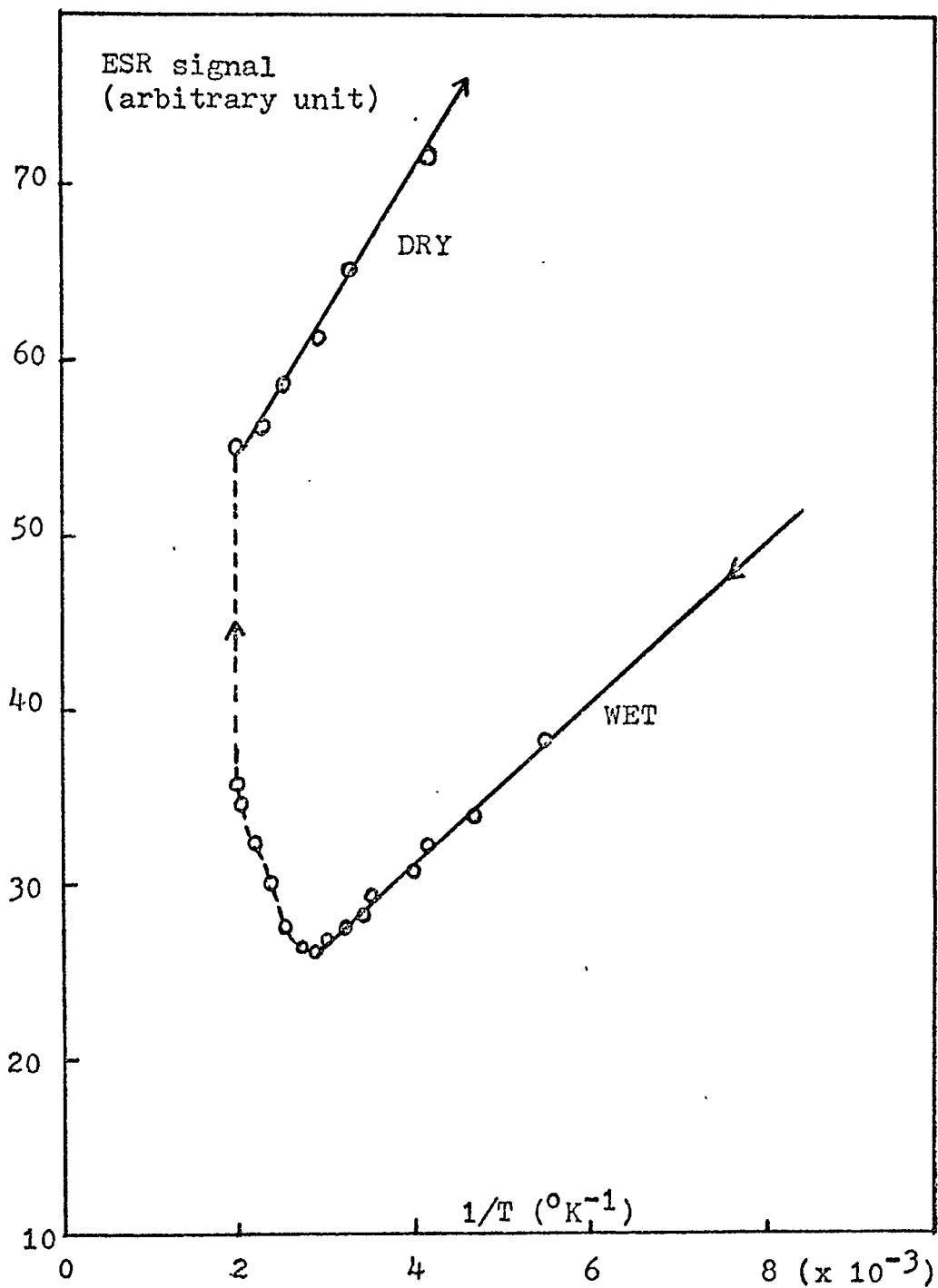


(Fig. 27) Temperature dependence of ESR signal of L-dopa melanin.

the wet portion sample is less than the slope of the dry portion in agreement with the observed quenching of spins by water. We conclude that a sample with a given amount of water obeys Curie's law as long as the amount of water is held fixed.

6. Kinetics of water readsorption Process

Although most of our studies started with wet samples and concentrated on the changes found when water was removed, we noted that samples stored in a water vapor atmosphere would recover the original wet sample properties. The time required for this recovery depends on the concentration of water vapor, but in any event the rehydration process is quite slow. Rather than study the time required to reach equilibrium, we chose to study the rate of quenching of the enhanced fraction of the ESR, signal induced by the removal of water, when water was reintroduced into the sample.

A piece of cotton saturated with water was placed in the top section of a sealed sample tube containing dry melanin and the changes in ESR spectrum of this sample were followed for several hours. In an additional experiment, methanol was used instead of water to quench the signal. Using methanol is useful because it tells us whether other dipolar liquids quench the ESR signal in the same fashion as

does the water. The results obtained in this study are plotted in Fig. 28, where the total ESR signal normalized to its initial value is plotted against time. To study the kinetics of the rehydration rate process, we examined the change in the quenched signal (dry signal - original wet signal) as a function of time and found that it to be described best by a second order rate equation. A second order rate process implies that the reciprocal of the difference of the signal from its quenched value is a linear function of time. This relationship is plotted in Fig. 29, where we see that the results for methanol as well as those for water fit the predictions of a second order rate process.

A second order rate process indicates that spins are quenched in pairs, and that a reaction of the following sort seems to be occurring in the quenching.



where, P = polar molecule

R = free radical

N_1, N_2 = non-radical species

This result seems to us to be very important and to be somewhat unexpected. The fact that the quenching rate is faster (larger slope) for methanol than for water is easily attributable to their different vapor pressures.

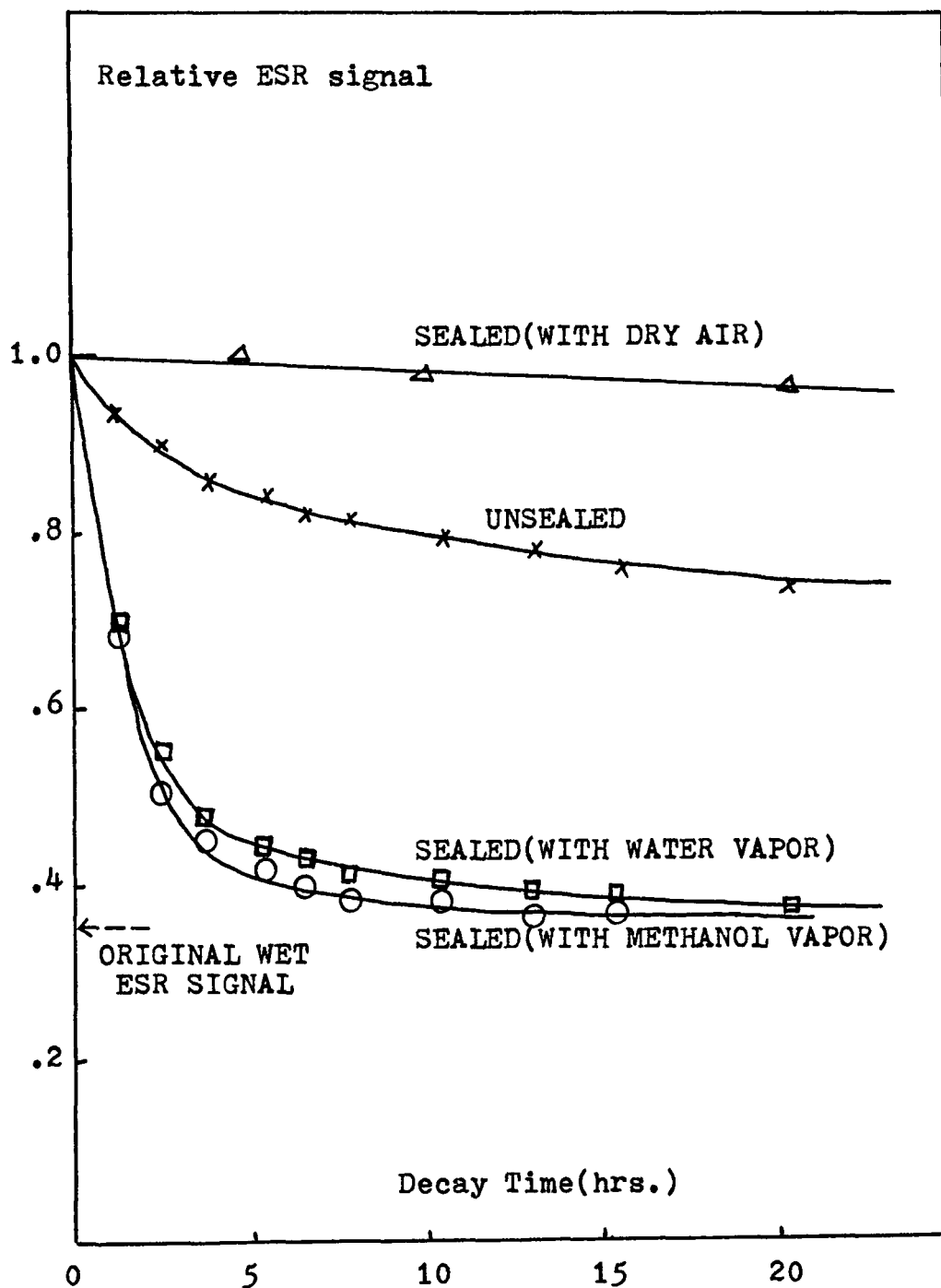


(Fig. 28) Decay of ESR signal of L-dopa melanin with different surroundings.

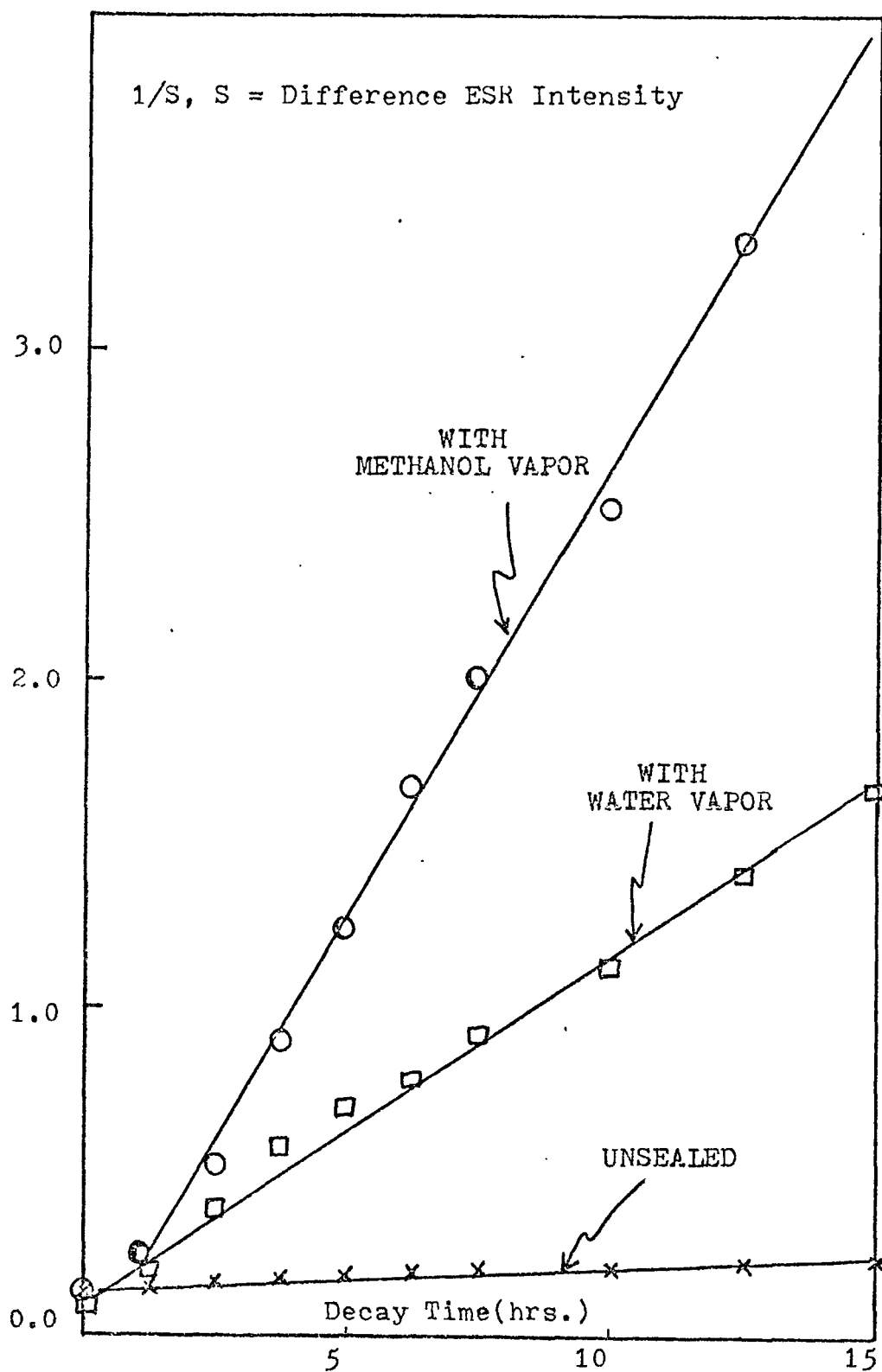


(Fig. 29) Reciprocal of the difference ESR intensity (total decay ESR signal - original wet signal) vs. time.

7. Summary of Results

The principal results of this ESR study on the effect of water on properties of the melanin free radical are summarized below:

(1) Only 'hard' water quenches the ESR signal:

This conclusion is based on the observation that only after removing the 'tightly bound' water has a significant increase of ESR signal observed.

(2) Water quenches the free radicals in pairs:

This follows from the fact that the decay of the enhanced ESR signal obeys a second order rate equation

(3) Only a fraction of the total radicals can be quenched by water:

Melanins suspended in aqueous solution still show an appreciable spin signal. This suggests that not all the free radicals can be quenched by water. There may be two or more distinct types of radicals or there may be those which are close to the surface and those which are deeper. In any case, not all the radicals can be quenched by water.

(4) The line width of the unquenched free radicals is not strongly affected by the quenching process:

This suggests that the quenched and unquenched spin sites are not randomly distributed but are more likely to be spatially separated.

(5) Free radicals can be quenched by a variety of polar solvents:

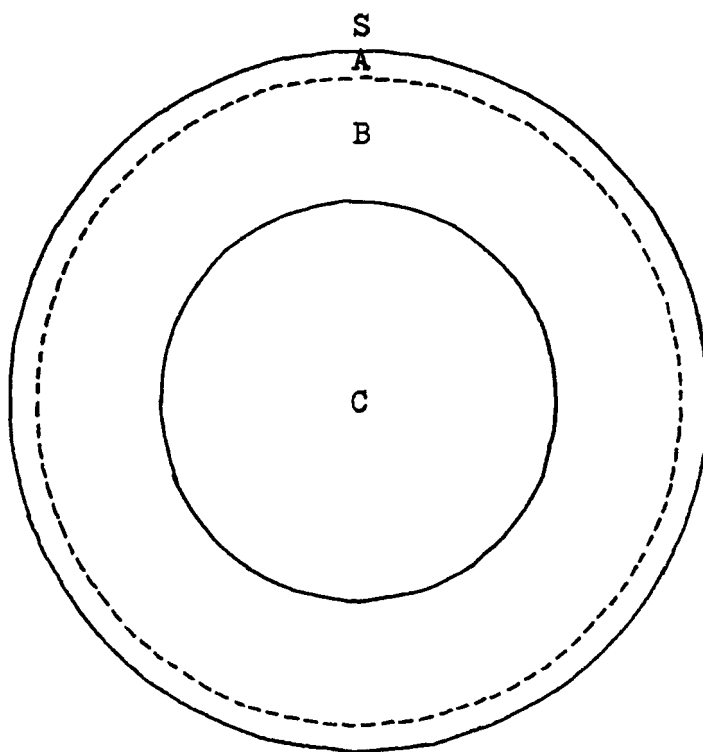
For example, methanol was shown to quench the spins, obeying the same kinetics as water. We note here the results of our experiments which showed that non-polar solvents, such as benzene, did not quench the melanin free radicals.

(6) The size, shape and surface morphology of the melanin granules all influence the available volume for absorption of 'hard' water:

We base this conclusion on the observation that melanins from different sources, with different preparations and either with or without dopants are found to have a variety of water contents, spin densities, and line widths. A model will be developed showing the relation of these factors to the ESR spin parameters.

8. Macrostructure model of a melanin granule

We now wish to construct a simple model which should help to provide both qualitative and quantitative understandings of some aspects of the water effect. The 'best' and the 'simplest' model we would like to propose for relevant characteristics of a melanin granule is shown in Fig. 30. Just beneath the surface is a dead zone, free of radicals. The depth of this layer ΔA is assumed to be the same for



S: SURFACE

A: FREE RADICAL DEAD AREA

B: FREE RADICAL QUENCHED AREA

C: FREE RADICAL UNQUENCHED AREA

(Fig. 30) Model of a macro-structure of melanin granule.

all melanins. This free radical 'dead' area might reasonably be expected to occur because of the ready availability of external oxidizers at the surface. We include the existence of such a layer in order to explain the much smaller spin density observed for the dry tyrosine melanin when compared with that observed for the dry L-dopa sample. Below the dead layer we suppose that there is a zone B of thickness ΔB in which the 'hard' water is absorbed. Water is held on the surface of channels which permeate this porous region. This water can quench spins which lie within zone B. The particle core zone C, is an intrinsic melanin zone, in which unquenched free radicals are randomly distributed. Although the boundaries between various regions are diffuse, there will be essentially no water absorbed in the core. The number of free radical per unit volume, ρ_0 , is the same in zones B when it is free of water, as is found in zone C.

According to this model, the measured ESR signal is simply proportional to the total number of melanin granules contained in the sample and the total number of unquenched free radicals in each granule. The volume of the C zone can be expressed as a function of the total granule radius R_0 and the thickness of the two outer zones. Namely

$$\frac{4}{3} \pi r_c^3 = \frac{4}{3} \pi (R_0 - \Delta A - \Delta B)^3 = \frac{4}{3} \pi R_0^3 \left[1 - \frac{(\Delta A + \Delta B)}{R_0} \right]^3$$

The total number of granules contained in a sample is inversely proportional to the volume of each granule.

Therefore the measured ESR signal strength S_m , is expressed in terms of ρ_0 , ΔA , ΔB and R_0 , by the equation.

$$S_m \sim \rho_0 \left[1 - \frac{(\Delta A + \Delta B)}{R_0} \right]^3$$

This model accounts for the following observations.

(1) Effect of particle size:

Since ρ_0 , ΔA and ΔB do not depend on the particle size, they are related to the intrinsic properties of melanin and water. Therefore if R_0 decreases the signal will decrease by a large factor if $(\Delta A + \Delta B)/R_0$ is comparable to 1. This shows why the smaller particle sized tyrosine melanin has a much smaller spin density than the L-dopa melanin.

(2) Effect of surface:

The ability of dopants to affect the surface, making it more or less porous is expressed by the variation of the parameters ΔA and ΔB . L-dopa melanin doped with HCTL has a very small value for ΔB while L-dopa melanin doped with DEA has a larger value for ΔB as compared to the ΔB value for undoped L-dopa melanin. Therefore the HCTL melanin

has a smaller water content and higher ESR signal, and the DEA melanin has larger water content and lower ESR signal as compared to corresponding values found for undoped L-dopa melanin.

(3) Effect of intrinsic spin density:

It may be that melanins prepared in different procedures or at different pH has different values for ρ_0 . The principal effect of differing ρ_0 would be found in the line width, arising from the dependence of spin-spin interaction on the average interspin distance (if our assumption of randomly and uniformly distributed free radicals in melanin granule is true).

(4) Effect of granule shape:

For simplicity we have assumed a spherical shape for a melanin granule. Although nothing specific is shown about the shape, it is most likely to be a complicated and irregular one. If the granule is very irregular the granule will have an increased surface to volume ratio and surface dependent effects should be greatly enhanced.

CHAPTER SIX

CONCLUSIONS

Based on the results of our X-ray diffraction study, we have concluded that the intrinsic melanin local atomic structure consists of an array of planar connected monomers of about 4-8 members per layer, with three layers stacked at about the graphite spacing of 3.4 Å. The layers have to be rotated about 5° with respect to each other about an axis perpendicular to the layer plane and the oxygen and nitrogen side atoms have to be given some random tilt. This supergroup or 'paracrystalline' array (there is no 2-D crystalline order in a layer) is then assumed to represent a well-correlated piece of the fully connected 3-D polymer. The melanin granule cannot be just a polycrystalline array of these units because melanin has neither been crystallized, nor does it dissolve in any known solvent, and it fractures like glass or other brittle solids.

X-ray analysis of the wet and dry melanins shows that the 'hard' or tightly bound water, which comes off at 150°C and higher, appears less mobile and has a structure similar to that of amorphous ice, while the 'easy' water which comes off at lower temperatures, has a structure more like that of bulk adsorbed liquid water.

In studying the influence of water on melanin free radical properties, we found that the reversible water effect has the following features: (1) only 'hard' water quenches the ESR signal; (2) water quenches the free radicals in pairs; (3) only a fraction of the total radicals can be quenched by water; (4) the line width of the unquenched free radicals is not strongly affected by the quenching process; (5) quenching of the free radicals can be obtained by absorbing a variety of polar solvents; and (6) the size, shape and surface morphology of the melanin granules all influence the available volume for absorption of 'hard' water.

Although these studies on melanin are far from definitive, we hope that some of these ideas may provide direction for further understanding of melanin structures, and that the water effect may be of some use for elucidating the nature of the free radicals as well as shedding some light on the biological functions of melanin.

References

1. Powell, M. R., et. al., *Bioenergetics*, 1, 493 (1970)
2. Rosenberg, J. C., et. al., in Experimental Methods in Biophysical Chemistry, ed. by C. Nicololaus, John Wiley and Sons (Interscience Pub.) London, New York (1973)
3. McGinness, J. E., private communication
4. Trukhan, E. M., et. al., *Biophysics*, 18, 413 (1973)
5. Blois, M. S., et. al., *Biophys. J.*, 4, 471 (1964)
6. Thathachari, Y. J., et. al., *Biophys. J.*, 9, 77 (1969)
7. Thathachari, Y. J., *Bull. Am. Crys. Asso.* 4, 56 (1976)
8. Thathachari, Y. J., private communication
9. Nicolaus, R. A., Melanins, Hermann, Paris (1968)
10. Raper, H. S., *Biochem. J.*, 17, 454 (1923)
11. Raper, H. S., et. al., *Biochem. J.*, 20, 69 (1926)
12. Raper, H. S., *Biochem. J.*, 21, 89 (1927)
13. Raper, H. S., *Physiol. Rev.*, 8, 245 (1928)
14. Raper, H. S., *Biochem. J.*, 26, 2000 (1932)
15. Mason, H. S., *Biochem. J.*, 192, 83 (1948)
16. Mason, H. S., *Adv. in Enzymol.*, 16, 105 (1955)
17. Blois, M. S., in Biology of Normal and Abnormal Melanocytes, T. Kawamura, et. al. eds., Univ. Park Press, Baltimore, London, Tokyo, (1971)
18. Wertz, J. E., et. al., in Free Radicals in Biological System, M. S. Blois Jr., et. al. eds., Academic Press, New York and London (1961)
19. Commoner, B., et. al., *Nature*, 174 689 (1954)

20. Mason, H. S., et. al., Arch. Biochem. and Biophys., 86, 225 (1960)
21. Longuet-Higgins, H. C., Arch. Biochem. and Biophys., 86, 231 (1960)
22. Sarna, T., et. al., Science, 192, 1132 (1976)
23. Leigh, J. S. Jr., J. Chem. Phys., 52, 2608 (1970)
24. Chio, S. S., et. al., Bull. Am. Phys. Soc., 20, 4241 (1975)
25. Grady, F. J., et. al., J. Am. Chem. Soc., 90, 2949 (1968)
26. Potts, A. M., et. al., Agnessologie, 9, 1 (1968)
27. McGinness, J. E., et. al., Science, 183, 853 (1974);
Filators, T., et. al., Biopolymers, 15, 2309 (1976)
28. Culp, C. H., et. al., to be published.
29. Spiegel-Adolf, M., et. al., J. Am. Chem. Soc., 61, 2178 (1939)
30. Ergun, S., Chemistry and Physics of Carbon, 3, 211 (1968)
31. Nicolaus, R. A., et. al., Tetrahedron, 20, 1163 (1964)
32. Piatelli, M., et. al., Tetrahedron, 15, 66 (1961)
33. Piatelli, M., et. al., Tetrahedron, 21, 3229 (1965)
34. Swan, G. A., et. al., Ann. N. Y. Acad. Sci., 100, 1005 (1963)
35. Warren, B. E., X-ray Diffraction, Addison-Wesley Pub. Co., Massachusetts (1969)
36. Macgillary, C. H., et. al., eds., International Tables for X-ray Crystallography, (Vol. III), The Kynoch Press, Birmingham England (1962)
37. Cohen, J. B., Diffraction Methods in Materials Science, The Macmillan Co., New York (1966)
38. Chipman, D. R., The Rev. of Sci. Instruments, 27, 164 (1956)

39. Warren, B. E., J. Appl. Phys., 25, 814 (1954)
40. Warren, B. E., in Ph.D. Thesis of R. L. Mozzi, M.I.T., (1967)
41. Milberg, M. E., J. Appl. Phys., 29, 64 (1958)
42. Warren, B. E., and R. L. Mozzi, Acta. Cryst., 21, 459 (1966)
43. Doyle, P. A., et. al., Acta. Cryst., A24, 390 (1968)
44. Norman, N., Acta. Cryst., 10, 370 (1957)
45. Renninger, A. L., et. al., J. Appl. Crystal, 9, 253 (1976)
46. Narten, A. H., et. al., in Water a Comprehensive Treatise, F. Franks, eds., Vol. I, Plenum Press, New York (1972)
47. Boutron, P., et. al., J. of Chem. Phys., 62, 4848 (1975); Boutron, P., et. al., Science, 187, 430 (1975)
48. Townsend, J. R., Acta. Cryst. 12, 806 (1959)
49. Chauffe, L., et. al., Biophys. J., 15, 565 (1975)
50. Castner, T. G. Jr., Phys. Rev. 115, 1506 (1959)

Appendix A

SCATTERING FACTORS

Scattering factors of C, N and O are calculated by using Doyle and Turner's formula:⁽⁴³⁾

$$f^0(k) = \sum_{i=1}^4 a_i \exp(-b_i k^2 / 16 \pi^2) + c$$

where $k = 4\pi \sin \theta / \lambda$, and a_i , b_i and c are nine parameters given in the following table.

Parameter	C	N	O
a_1	2.31	12.2126	3.0485
a_2	1.02	3.1322	2.2868
a_3	1.5886	2.0125	1.5463
a_4	.8650	1.1663	.8670
b_1	20.8439	.0057	13.2771
b_2	10.2075	9.8933	5.7011
b_3	.5687	28.9975	.3293
b_4	31.6512	.5826	32.9089
c	.2159	-11.5293	.2508

Further correction for the anomalous dispersion was considered for Cu data. Using the tabular values of $\Delta f'$ and $\Delta f''$, the final corrected scattering factors, $f = f^0 + \Delta f' + \Delta f''$, were obtained.

Appendix B T_2^* METHOD FOR DETERMINING SPIN-LATTICE RELAXATION TIME

It is known that homogeneous and inhomogeneous broadenings are the two principal types of resonant lines in solids. Homogeneous broadening occurs when the magnetic resonance signal results from a transition between two spin levels which are not sharply defined, but instead, are somewhat intrinsically broadened. Several sources of such broadening are: 1) dipolar interaction between like spins, 2) spin-lattice interaction 3) interaction with the radiation field, 4) diffusion of excitation throughout the sample, and 5) motionally narrowing fluctuations in the local field. Inhomogeneous broadening arises from interactions outside the spin system which varies slowly over the time required for spin-spin transitions to take place. The sources of inhomogeneous broadening are: 1) magnetic field inhomogeneities, 2) unresolved fine structure, 3) unresolved hyperfine structure, 4) crystal lattice irregularities (e.g. mosaic structure), and 5) dipolar broadening between unlike spins.

For inhomogeneous saturation, Castner derived the absorption susceptibility, the imaginary part of the rf susceptibility,

$$\chi'' = \frac{1}{2} \chi_0 \int_0^{\infty} \frac{\pi \omega' \rho(\omega - \omega') h(\omega' - \omega_0) d\omega'}{1 + \pi \gamma^2 H_1^2 T_1 \rho(\omega - \omega')}$$

by 1) considering the normalized line shape function $g(\omega - \omega')$ of the individual spin packet which is homogeneously broadened and very narrow, and the normalized envelope or distribution function $h(\omega' - \omega_0)$ of these spin packets, and 2) making use of the homogeneous result

$$\chi'' = \frac{1}{2} \chi_0 \omega_0 \frac{\pi \mathcal{L}(\omega - \omega_0)}{1 + \pi \gamma^2 H_1^2 \mathcal{L}(\omega - \omega_0) T_1}$$

where χ_0 is the Curie susceptibility, ω_0 is the microwave frequency at resonance, ω is the experimental microwave frequency, γ is the gyromagnetic ratio, and H_1 is the rotating component of the microwave magnetic field inducing transitions.

With further assumption of a Gaussian envelope of Lorentzian spin packets, i.e. to let

$$g(\omega - \omega') = \frac{T_2}{\pi} \frac{1}{1 + T_2^2 (\omega - \omega')^2}$$

and

$$h(\omega' - \omega_0) = \frac{1}{\pi^{1/2}} \frac{1}{\Delta\omega_G} \text{EXP} \left[- \left(\frac{\omega' - \omega_0}{\Delta\omega_G} \right)^2 \right]$$

(where $\Delta\omega_G$ is the Gaussian width of the inhomogeneous broadening and T_2 is the spin-spin relaxation time).

Castner solved the integral for $\omega = \omega_0$ and evaluated $\chi''(\omega_0)$ in terms of the error function integral,

$$\phi(at) = \frac{2}{\sqrt{\pi}} \int_0^{at} e^{-y^2} dy$$

$$\chi''(\omega_0) = \frac{1}{2} \chi_0 \pi^{\frac{1}{2}} \left(\frac{\omega_0}{\Delta\omega_G} \right) \frac{e^{-(a^2 t^2)}}{t} [1 - \phi(at)] \quad , \text{ as}$$

where $a = \Delta\omega_L / \Delta\omega_G$ is a parameter which measures the degree of inhomogeneous broadening, $\Delta\omega_L$ is the Lorentzian width of spin packets, and $t = (1 + \gamma^2 H_1^2 T_1 T_2)^{\frac{1}{2}}$ is a saturation factor.

The relative spectrometer absorption signal, Y_0 , is proportional to $\chi'' H_1$. By using notation $Z = \gamma H_1 (T_1 T_2)^{\frac{1}{2}}$, it can be written

$$Y_0 = \frac{Z}{\sqrt{1+Z^2}} e^{a^2 Z^2} \frac{\{1 + \phi[a(1+Z^2)^{\frac{1}{2}}]\}}{[1 - \phi(a)]}$$

Fig. A-1 shows the saturation behavior for various ratio of a , i.e. plots of Y_0 vs. Z at several a -values.

To determine the spin-lattice relaxation time, T_1 , Castner described an independent method called 'the T_2^* method' by considering the special case that $H_1 \gg H = 1/\gamma(T_1 T_2)^{\frac{1}{2}}$ and $a \ll 1$, then gave the approximation of the ratio of the saturated absorption susceptibility to the unsaturated one as

$$\frac{\chi_S''(\omega_0) H_1}{\chi_{US}''(\omega_0) H_1} = \left(\frac{2}{\pi} \right)^{\frac{1}{2}} \frac{1}{\gamma^2 H_1^2 T_1 T_2^*} + (\text{correction terms})$$

where $T_2^* = \sqrt{2}/\Delta\omega_G$.

Now, from the above equation, $\chi_S'' H_1$, $\chi_{US}'' H_1$, T_2^* and H_1 can be determined experimentally, and the correction terms are assumed to be small for $a \ll 1$, hence T_1 is the only unknown, which is easily calculated. The essential procedures to calculate T_1 are given below:

1) to estimate 'a': In order to ensure that 'a' is much less than one, we fitted our ESR saturation curve, Y_0 vs. $H_1/H_{1/2}$, to that of Fig. B-1. It turned out that all curves have $a < 0.1$, so it is possible to apply the T_2^* method.

Examples of this curve fitting of pure L-dopa melanin samples are given in Fig. B-1.

2) to calculate T_2^* : Since $\Delta H_{pp} = \sqrt{2}\Delta\omega_G/\gamma$, the experimentally observed peak-to-peak first derivative envelop line width, it implies that $T_2^* = 2/\gamma\Delta H_{pp}$. By knowing $\gamma = 0.87934 \times 10^7$ g.G⁻¹.sec⁻¹, one can easily calculate T_2^* .

3) to determine H_1 : We use the relationship given by Ingram, i.e.

$$(2H_1)^2 = Q \cdot P_w \frac{\sqrt{1 - \left(\frac{\lambda}{2x}\right)^2}}{30\pi \cdot x \cdot y}$$

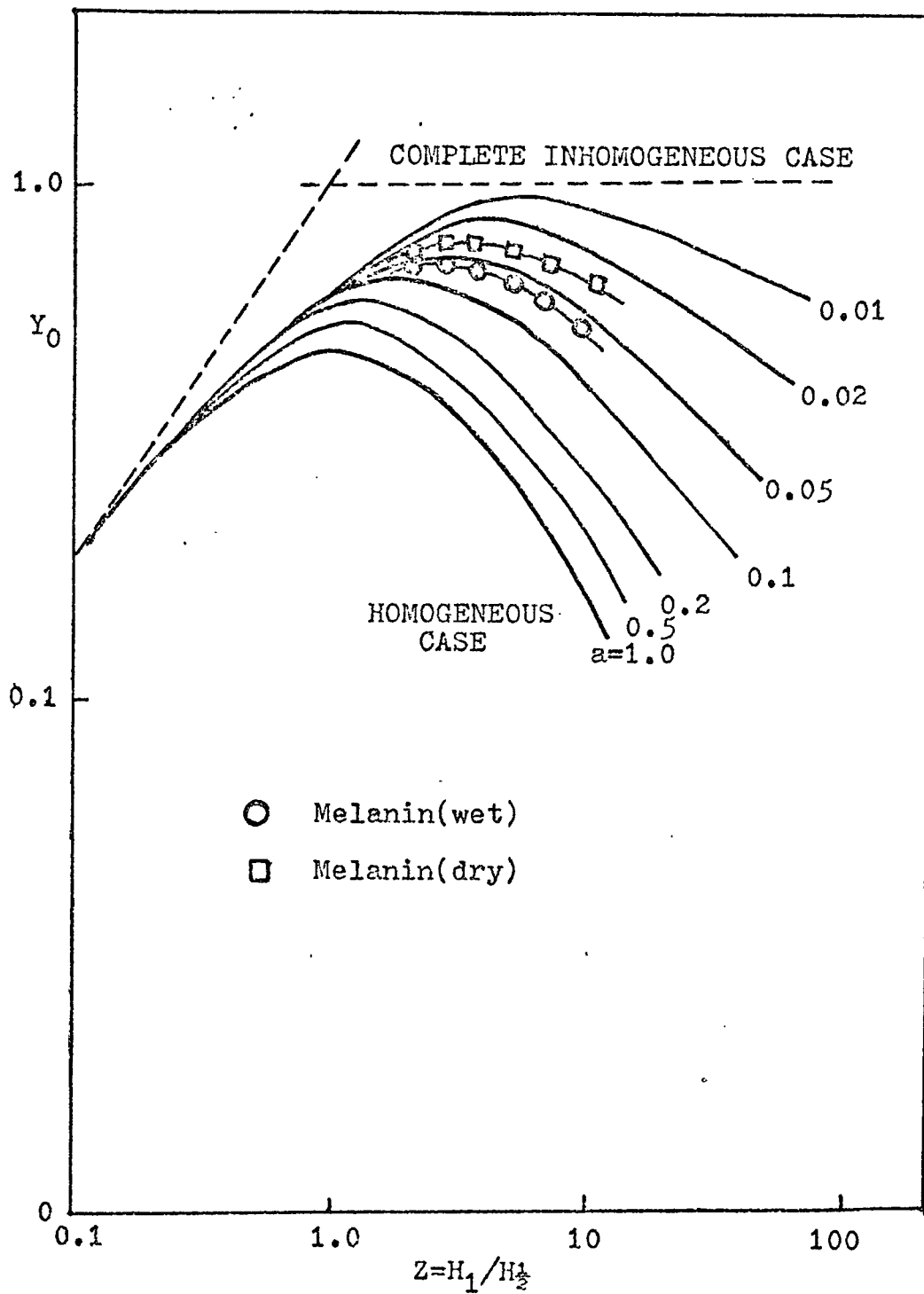


(Fig. B-1) ESR absorption signal Y_0 vs. reduced microwave field $H_1/H_{1/2}$ ($H_{1/2} = 1/\gamma(T_1 T_2)^{1/2}$)

and consider a standard X-band waveguide of dimensions 0.9 x 0.4 inches (2.29 x 1.02 cm) and a wavelength of 3.2 cm, it becomes

$$2H_1 = \frac{1}{17.5} \sqrt{Q \cdot P_w}$$

where H_1 is the value of microwave field at the specimen in gauss, Q is a factor that determines the degree to which a cavity is able to amplify the intensity of the microwave field, and is defined as

$$Q = \frac{2\pi (\text{maximum microwave energy stored in the cavity})}{(\text{energy lost per cycle})}$$

and P_w is the power in the waveguide in watts. In the estimation of T_1 , an average Q -value of 4500 ± 500 was assumed according to the manufactural given value 7000 of unloaded Q . The variation of Q , ± 500 , was assumed to give a maximum error in H_1 determination of about 30 percent according to Castner's measurement. Then the H_1 equation becomes

$$H_1 \approx 0.06 \sqrt{P_{mw}} \quad \text{Gauss}$$

where P_{mw} is the microwave power in milliwatt.

4) to obtain $\chi_S'' H_1 / \chi_{US}'' H_1$: A plot of the ESR signal Y_0 , integrated the derivative trace, versus H_1 , or \sqrt{P} (square root of the microwave power) was shown in Fig. B-2.

Which enable us to calculate the ratio of $\chi_S'' H_1$ to $\chi_{US}'' H_1$ at $H_1 \gg H_{1/2}$. From Fig. B-2, a ratio, χ_S'' / χ_{US}'' , at 1 mw microwave power was obtained to correct the ESR signal Y_0 (bring it back to unsaturate value) which was finally used for the spin density determination.

References

Castner, T. G., Jr., Phys. Rev. 115, 1506 (1959)

Ingram, D. J. E., Free Radicals as Studied by Electron Spin Resonance, Butterworths Scientific Publ, London (1958)

Poole, C. P. Jr., Electron Spin Resonance, Wiley (Interscience), New York (1967)

Poole, C. P. Jr., et. al., Relaxation in Magnetic Resonance, Academic Press, New York (1971)

Portis, A. M., Phys. Rev., 91, 1071 (1953)

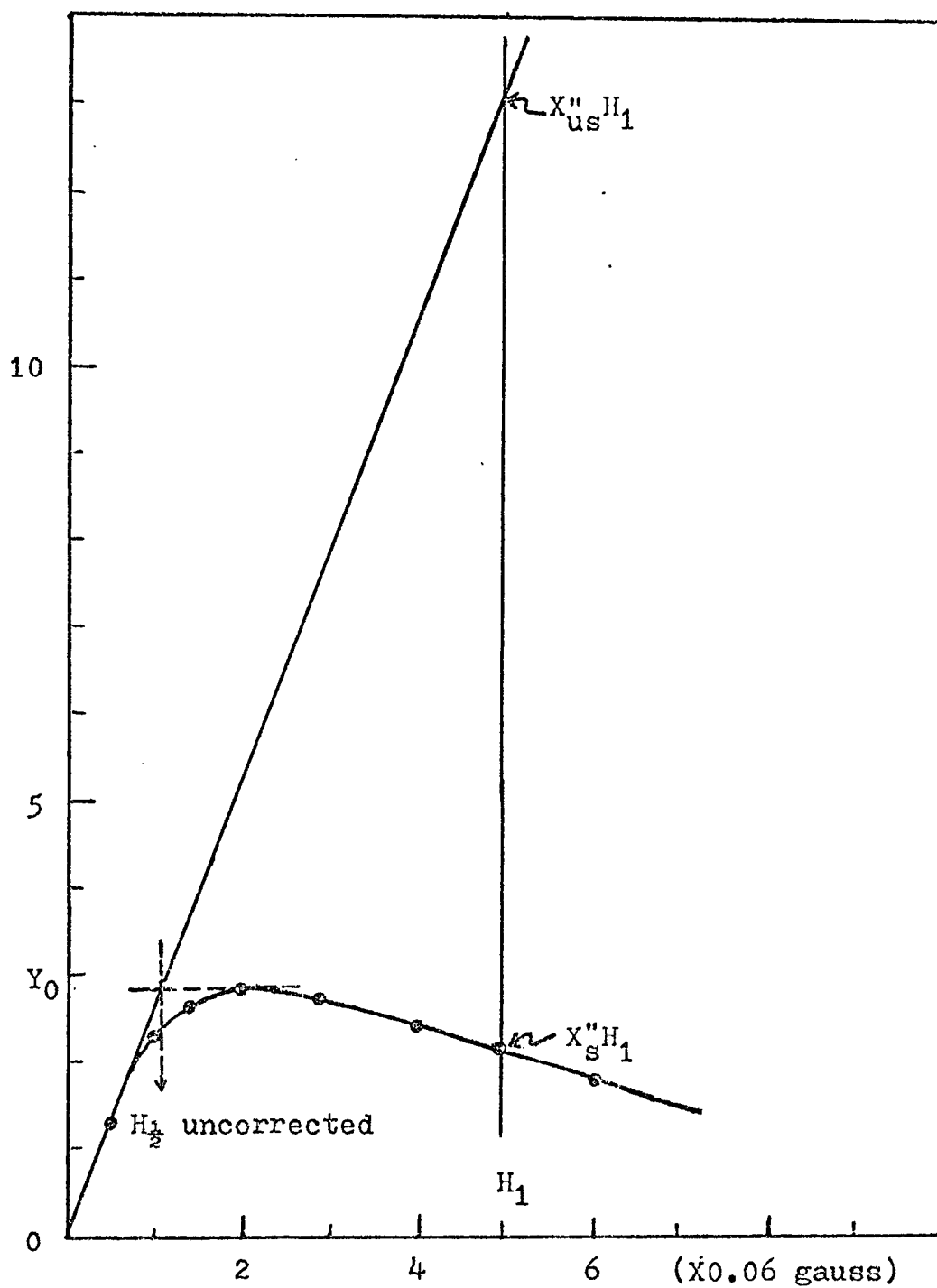


(Fig. B-2) Inhomogeneous saturation curve of L-dopa melanin.